TECHNICAL UNIVERSITY OF LIBEREC
Faculty of Mechatronics, Informatics
and Interdisciplinary Studies

Control of Continuous Casting Process Based on Two-Dimensional Flow Field Measurements

Dissertation Thesis

Study programme: P2612 – Electrical engineering and informatics
Study branch: 2612V045 – Technical Cybernetics

Author: **Shereen Abouelazayem**
Supervisor: doc. Dr. Mgr. Ing. Jaroslav Hlava

Liberec 2022

Declaration

I hereby certify that I have been informed that Act 121/2000, the Copyright Act of the Czech Republic, namely Section 60, Schoolwork, applies to my dissertation in full scope. I acknowledge that the Technical University of Liberec (TUL) does not infringe my copyrights by using my dissertation for TUL's internal purposes.

I am aware of my obligation to inform TUL on having used or licensed to use my dissertation in which event TUL may require compensation of costs incurred in creating the work at up to their actual amount.

I have written my dissertation myself using literature listed therein and consulting it with my supervisor and my tutor.

I hereby also declare that the hard copy of my dissertation is identical with its electronic form as saved at the IS STAG portal.

Date:

Signature:

Abstract

Two-dimensional flow field measurement allows us to obtain detailed information about the processes inside the continuous casting mould. This is very important because the flow phenomena in the mould are complex, and they significantly affect the steel quality. For this reason, control based on two-dimensional flow monitoring has a great potential to achieve substantial improvement over the conventional continuous casting control. This conventional control relies on single-point measurements of selected scalar variables; typically, it is limited to mould level control. Two-dimensional flow field measurement provides large amounts of measurement data distributed within the whole cross-section of the mould. Such data can be obtained using process tomography or other sensors with similar distributed measurement capacity.

An experimental setup of the continuous casting process called Mini-LIMMCAST located in Helmholtz-Zentrum Dresden-Rossendorf (HZDR), Dresden, Germany, is used for this thesis. The mini-LIMMCAST facility is a small-scale physical model of a continuous caster working with a eutectic GaInSn alloy at room temperature. This thesis examines two alternatives of flow measurement sensors: Ultrasound Doppler Velocimetry (UDV) and Contactless Inductive Flow Tomography (CIFT). Both sensor variants can obtain information on the velocity profile in the mould.

Available literature sporadically mentions the use of tomographic or similar sensors for real-time feedback control of various processes. However, the field of tomography-based control is still very young. Therefore, this thesis explores various approaches for utilizing the large amounts of data such sensors provide for automatic control. Generally, model-based approaches were preferred for the design of controllers whose objective is to achieve optimal flow patterns in the mould.

Two approaches were considered to create the process model needed for model-based control: a spatially discretized version of a model based on partial differential equations and computational fluid dynamics and a model obtained using system identification methods. In the end, system identification proved to be more fruitful for the aim of creating the model-based controller. Specific features of the flow were parametrized to obtain the needed controlled variables and outputs of identified models. These features are mainly related to the exiting jet angle and the meniscus velocity. The manipulated variables

considered are electromagnetic brake current and stopper rod position. Model predictive control in several versions was used as the main control approach, and the results of simulation experiments demonstrate that the model predictive controller can control the flow and achieve the optimum flow structures in the mould using UDV. CIFT measurements can provide similar velocity profiles. However, further technical developments in the CIFT sensor signal processing, such as compensating for the effects of the strong and time-varying magnetic field of the electromagnetic brake on CIFT measurements, are necessary if this sensor is to be used for closed-loop control.

Abstrakt

Za pomoci dvourozměrného měření pole proudění v krystalizátoru zařízení pro plynulé lití oceli lze získat podrobnou informaci o procesech, které tam probíhají. Tato informace je velmi důležitá, neboť složitá struktura proudění v krystalizátoru výrazným způsobem ovlivňuje kvalitu lité oceli. Z tohoto důvodu má zpětnovazební řízení založené na takovémto dvourozměrném měření velký potenciál k tomu, aby dosáhlo výrazného zlepšení oproti obvyklým postupům řízení procesu plynulého lití. Tyto postupy totiž vycházejí pouze z bodového měření vybraných skalárních veličin a základní regulační smyčkou je obvykle řízení výšky hladiny v krystalizátoru.

Dvourozměrné měření pole proudění v krystalizátoru poskytuje velké množství naměřených hodnot, které jsou rozloženy v celém průřezu krystalizátoru. Technicky může být takovéto měření realizováno pomocí průmyslové tomografie nebo jiných snímačů, které jsou podobně jako tomografie schopné snímat veličiny rozložené v rámci celého průřezu krystalizátoru. V práci je jako zdroj experimentálních dat použito zařízení Mini-LIMMCAST provozované v Helmholtz-Zentrum Dresden-Rossendorf (HZDR). Toto zařízení představuje malý model procesu plynulého lití pracující s eutektickou slitinou GaInSn, která umožňuje provádění experimentů za pokojové teploty. K měření dvourozměrného pole proudění v krystalizátoru jsou alternativně používány snímače založené na dvou různých principech: ultrazvuková dopplerovská velocimetrie (Ultrasound Doppler Velocimetry - UDV) a bezkontaktní induktivní průtoková tomografie (Contactless Inductive Flow Tomography - CIFT). Z obou variant snímačů lze získat informaci o rychlostním poli proudění v krystalizátoru.

V dostupné literatuře lze najít občasné zmínky o použití průmyslových tomografických a obdobných snímačů pro zpětnovazební řízení různých procesů. Vcelku se však jedná o problematiku, jejíž výzkum je teprve v počátcích. V rámci práce bylo nutné se zabývat volbou a výzkumem vhodných metod automatického řízení, které umožňují využít rozsáhlé množství dat, které tyto snímače poskytují. Při návrhu metod řízení schopných zabezpečit, že proudění v krystalizátoru bude optimální z hlediska kvality výsledného produktu, byly v zásadě preferovány přístupy založené na modelu.

Pro vytvoření modelu byly zvažovány dva základní přístupy: jednak prostorově diskretizovaná podoba modelu založeného na parciálních diferenciálních rovnicích a

výpočetní dynamice tekutin a jednak model získaný postupy identifikace systémů. Tento druhý přístup se ukázal pro realizaci řízení založeného na modelu jako výrazně vhodnější. Z dat byly extrahovány vhodné numerické charakteristiky proudění v krystalizátoru (úhel proudění z ponorné trysky, rychlost proudění na hladině krystalizátoru a další), které bylo možné použít jako regulované veličiny a výstupy modelů získaných identifikací. Jako akční veličiny byly použity proud elektromagnetické brzdy a poloha regulovatelné výpusti z mezipánve. Hlavním přístupem k řízení v práci jsou různé verze prediktivního řízení založeného na modelu. Ve spojení s UDV snímači byly navržené prediktivní regulátory schopné dosáhnout v simulačních experimentech stanoveného cíle řízení a zabezpečit optimální struktury proudění v krystalizátoru. CIFT snímače jsou v principu schopné poskytnout podobná data, nicméně pro jejich využití pro řízení v uzavřené smyčce bude nezbytný další výzkum v oblasti vyhodnocení signálu z těchto snímačů, kde je otevřeným problémem kompenzace vlivu silného proměnného magnetického pole elektromagnetické brzdy na signál z těchto snímačů.

Acknowledgments

I would like to thank my supervisor Dr Jaroslav Hlava for his endless support, knowledge, and kindness throughout the years.

I would like to thank my husband Nick for believing in me and helping me stay motivated till the very end.

I am also very grateful for all my family and friends for their patience and love throughout the years.

Abbreviations

API	Application Programming Interface
CFD	Computational Fluid Dynamics
CIFT	Contactless Inductive Flow Tomography
ECT	Electric Capacitance Tomography
EIT	Electrical Capacitance Tomography
EMBr	Electromagnetic Brake
EMT	Electromagnetic Induction
FDM	Finite Difference Method
FEM	Finite Element Method
FGM	Feasible Goals Method
FIR	Finite Impulse Response
GaInSn	Gallium-indium-tin
HZDR	Helmholtz-Zentrum Dresden-Rossendorf
IDM	Interactive Decision Maps
IMC	Internal Model Control
LDS	Lumped-Input/Distributed-Output System
LES	Large Eddy Simulation
LQG	Linear Quadratic Gaussian
MIMO	Multiple-Input Multiple-Output
MPC	Model Predictive Control
NARX	Nonlinear Autoregressive Model with Exogenous Inputs
NN	Neural Network
ODE	Ordinary Differential Equation
PCA	Principal Component Analysis
PDE	Partial Differential Equation
PI	Proportional-Integral
PID	Proportional-Integral-Derivative
PRBS	Pseudo-Random Binary Signals
PSO	Particle Swarm Optimization
SEN	Submerged Entry Nozzle
UDV	Ultrasound Doppler Velocimetry
VOF	Volume of Fluid

Table of Contents

List of Figures

List of Tables

1. Continuous Casting Process

Continuous casting is a vital process that accounts for approximately 95 percent of global steel production [2]. Figure 1.1 depicts the main operation of a continuous caster in which liquid steel flows from the ladle to the tundish and then into the mould through a submerged entry nozzle (SEN). A stopper rod or a sliding gate regulates the flow rate [3]. A solid steel shell is formed in the water-cooled mould, and the partially solidified strand is transported on rolls and cooled by water sprays until it is completely solidified. Additionally, argon gas is injected into the SEN for several steel grades to prevent nozzle clogging and to float inclusions. If argon is used, the flow field in the mould must not obstruct the rise of bubbles to the free surface[4], [10], [11].

The flow regime in the SEN and in the mould has a significant influence on the final product's quality. Issues such as clogging, turbulent flow, deep penetration of the jet, and slag entrapment have been shown to have a detrimental effect on the quality of the steel [4]–[7]. There is a preference for the double roll flow pattern in the mould as opposed to the single roll flow (see Figure 1.2) because it allows for both argon gas bubbles and impurities to rise up to the surface and avoid being trapped in the steel [7]. Electromagnetic actuators (electromagnetic brakes or stirrers) are often used to control this flow [8], [9].

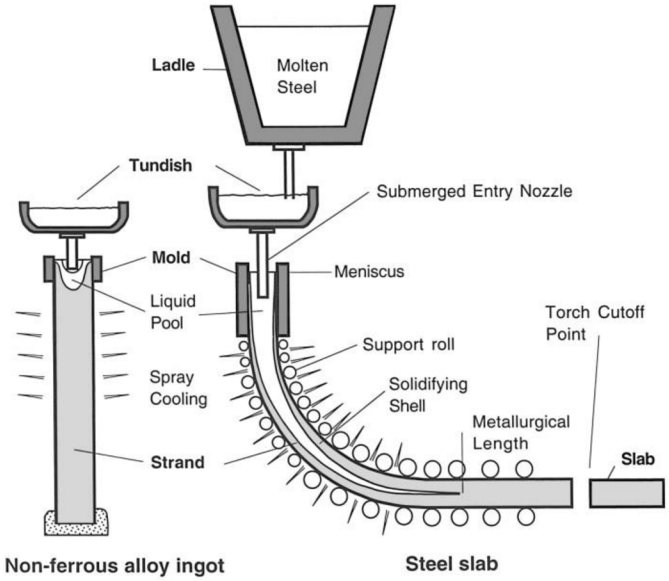

Figure 1.1. Schematic diagram of the continuous casting process [8]

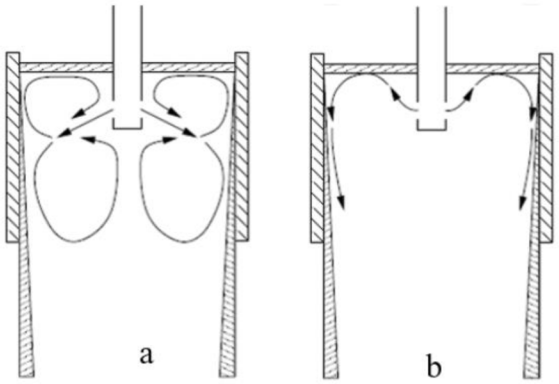

Figure 1.2. a) Double roll flow pattern, b) Single roll flow pattern

The continuous casting process is marked by several intricate phenomena that govern the process from beginning to end; these include turbulent fluid flow, electromagnetic effects, particle entrapment, and thermal-mechanical distortion [11], [12]. Creating mathematical models to describe the many coupled interactions that occur in the continuous casting process is one of the more difficult challenges when dealing with this process. Numerous advances have been made in the modelling of various aspects of the process; however, the topic remains open for further development. As more mathematical models are developed to describe the interactions in the process, the question of how to use these models to control the process arises. The following sections will demonstrate that the challenge of controlling the continuous casting process is limited not only by the need to accurately model the process, but also by the sensors used in the process. This is where two-dimensional flow monitoring comes into play as these sensors are able provide us with richer data that can be utilized for control.

1.1. Control of Continuous Caster

1.1.1. Mould Level

There is very little research on the use of two-dimensional flow field measurements in continuous caster control; most of the current research is based on conventional sensors and knowledge about the relationship between single measurable variables and product quality. The molten steel level in the mould has been shown to be one of the more important measurable variables [13]. To avoid potential defects, the fluctuation of this level must be

reduced. As a result, most of the published papers related to the continuous casting control are focused on mould level control. In many cases a reduced model is used to describe the fluctuations in the mould, and a simple mould level sensor is used for the control loop designed to control the mould level.

An example can be seen in [14] where a PI controller with a variable gain and dither signal was implemented to control the mould level. The quality of steel level stabilization is shown to be considerably better when compared to the referential steel stream and using correction vibrating signal (dithering) is significantly better. Comparison between different control strategies including PI with high frequency dither, linear cascade controller and non-linear cascaded controller was conducted in [15]. Similarly to [14], the authors also used a high frequency dither signal to deal with the non-smooth nonlinearities of the signal. It was concluded that the nonlinear controller had a better performance as it required less control action but was able to dampen the mould level oscillations more efficiently. Additionally, more advanced controllers such as H-infinity were designed and compared to the traditional PID controller in [13]. The H controller was created with four weight functions rather than the conventional two weight functions. This allowed for the controller to be designed based on disturbance rejection and robust stability at medium frequencies. In the end, it was shown that the proposed controller outperformed in both disturbance rejection and robust stability.

Fuzzy logic has also been implemented for the control of the mould level in the continuous caster [16], [17]. In [16] the authors discuss the issue of nozzle clogging and unclogging which affects the performance of conventional PID controllers. Therefore, they suggest the use of a fuzzy controller that would utilize the expert knowledge of operators to control the mould level in order to deal with disturbances such as clogging. Similar to the previous work, a robust nonlinear adaptive PI control based on fuzzy logic was used to deal with various slow disturbances including erosion, clogging, and tundish level variations [17].

1.1.2. Dynamic Bulging Disturbance

A common phenomenon that is being observed on the mould level is the bulging disturbance; bulging disturbance is mostly created by the supporting rollers that tend to push the liquid steel upward periodically [18]–[20]. Various control methodologies were proposed to compensate for this disturbance such as an adaptive sine estimator-based disturbance observer [21]. This observer was combined with a phase lead adaptive fuzzy controller as shown in Figure 1.3. Both simulation and experimental results proved that the controller was able to reduce the bulging disturbance effect on the mould level. A similar attempt at suppressing the disturbance was done using a basic PI controller with an additional adaptive compensation that adapts the gain and prediction time to compensate for the disturbance [22].

Further attempts include a global observer that compensates for both bulging and the clogging/unclogging of the SEN [23]. In this case an online estimator tracks the effect of both external signals on the mould level. The control loop also uses the mould level, stopper position, and the flow rate as measurement signals. This allows for the fluctuations generated by the bulging to be drastically reduced. A similar approach is found in [24] where an observer is combined with a feed forward loop to reduce the mould level fluctuations. The author also mentions that further improvement needs to be done to take into account variations of bulging frequencies caused by changes in casting conditions. Additional attempts at compensating for bulging disturbance include utilising Particle Swarm Optimization (PSO) [25], [26]. In [25] a fuzzy PID controller with nonlinear compensation term is used as shown in Equation 1.1 where the parameters of the fuzzy controller are optimized by using PSO algorithm. The nonlinear compensation term $N(e)$ compensates the output of the fuzzy PID controller, while in [26] a modified smith predictor based on PSO is developed to reject the bulging effect on the mould level.

$$p(t) = k_p e(t) + k_i \int_0^t e(\tau) d\tau + k_d \frac{de(t)}{dt} + N(e) \tag{1.1}$$

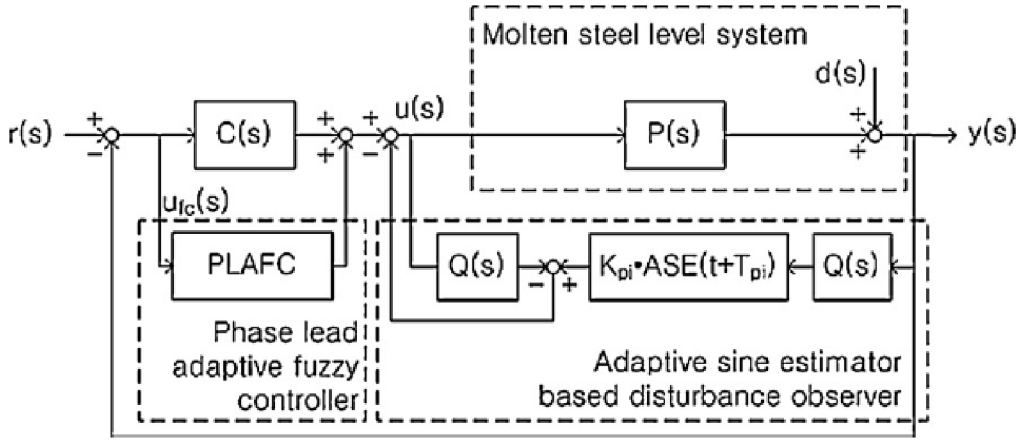

Figure 1.3. Disturbance observer combined with phase lead adaptive fuzzy controller [21]

1.1.3. Secondary Cooling

Secondary cooling that occurs during the rolling out phase plays a critical role in the quality of the steel. The steel strand is pulled out of the mould through the support rollers as shown in Figure 1.1. This is where the secondary cooling occurs. The flow rates of the cooling water significantly impact the heat exchange efficiency during the solidification process [27], [28]. The modelling of the secondary cooling zone is usually done using through Finite Element Method (FEM) or Finite Difference Method (FDM) where the particular space is discretized, resulting in a distributed parameter system that is later on used for designing the controller [29].

Various controller techniques have been implemented to control the secondary cooling zones. One of these techniques include Internal Model Control (IMC) [30] where the temperature fields are described using partial differential equations, and a finite element method is used to solve these equations and model the process. The author was able to create a lumped-input/distributed output (LDS) based on the FEM modelling for the purpose of creating the controller. The main concept behind LDS is the decomposition of the control synthesis into time and space control tasks. A robust control system for the LDS was created using an IMC structure as shown in Figure 1.4. A similar approach can be found in [31] where a model based on nonlinear partial differential equations is used for the control of secondary cooling in the continuous casting process. The control synthesis

was also designed using the lumped input/distributed output method. In this case a single-parameter constrained Model Predictive Control (MPC) was designed to generate the input signals into the secondary cooling zone.

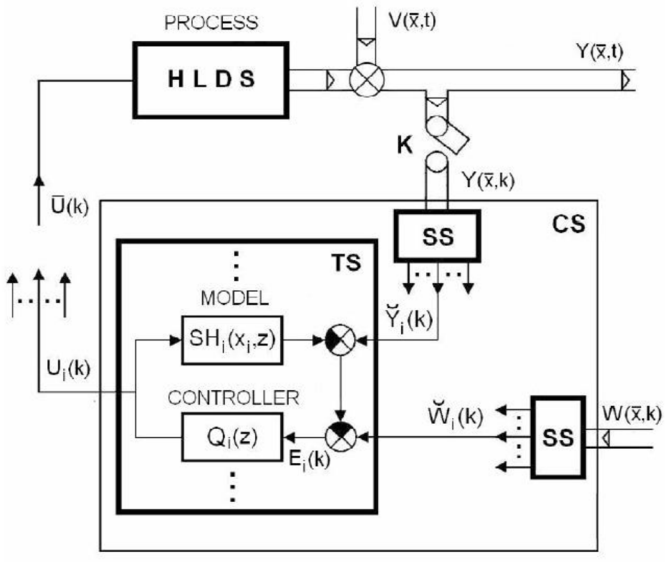

Figure 1.4. Robust control system for the LDS was created using an IMC structure [27]

Other techniques used to control in the secondary cooling process include decentralised PID controllers [32]; In this paper, the authors combine a one-dimensional FDM model in order to predict the slab temperature and solidification state. The model is updated in real-time using data from the caster, while a bank of decentralized PID controllers is used to achieve the optimum shell temperature and surface profile. Simulations show that this system can outperform the conventional control system already implemented on the caster. Additionally, fuzzy logic has been implemented for the optimal control of the secondary cooling process [33]. The control algorithm consisted of a 3D transient numerical model for the temperature distribution. FDM is used for the numerical solution of the model and various casting parameters are obtained such as the initial temperature distribution and the intensity of cooling. A fuzzy regulator operates as a supervision system and manipulated the casting parameters as seen in Figure 1.5. The fuzzy regulator can optimise the cooling intensities for different casting speed and casting temperature conditions. Furthermore, in [34] FEM is used for the discretisation, while the

control algorithm is done through a multi-criteria optimisation problem. In this case, the author uses a combination of Feasible Goals Method (FGM) and Interactive Decision Maps (IDM) to solve the optimisation problem. Lastly, neural networks have also been implemented for temperature control optimisation where a multimodal deep learning approach is utilised in the process [35].

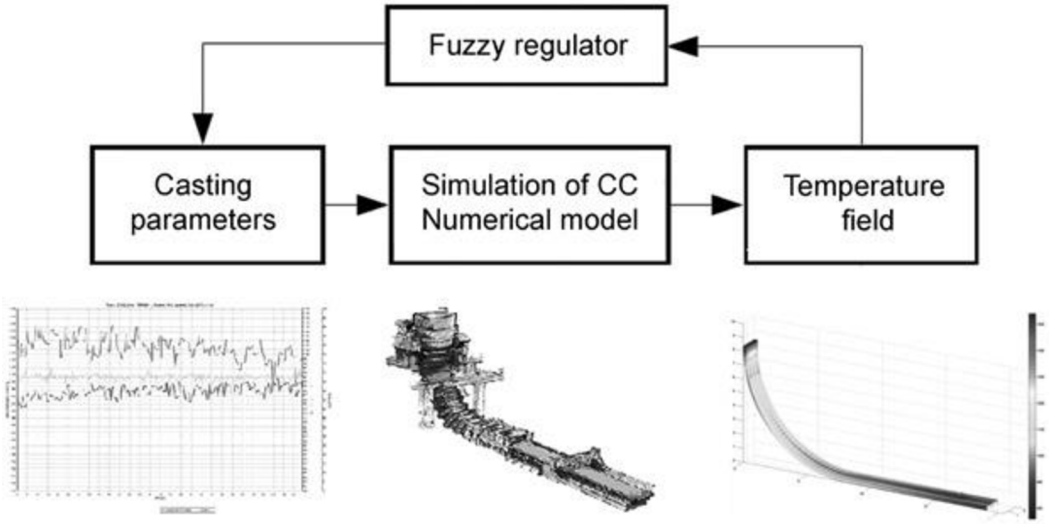

Figure 1.5. Fuzzy regulator used to optimise the cooling intensities for different casting speed and casting temperature conditions [30]

It becomes clear that the majority of the papers discussed above use variables measured at specific points of the process rather than taking into account what is going inside the process itself, especially when considering the flow structure inside the mould. Although the mould level provides some information on what is going on inside the mould, it provides limited information on the flow structures of the mould. Therefore, it becomes logically to consider sensors that would allow us to see into the mould and extract more information on the flow structures. A possible answer to this would be the use of two-dimensional flow monitoring sensors that would allow us to visualize the flow structure in the mould.

1.2. Control Based on Multidimensional Measurement Data

There is growing interest towards utilizing multidimensional measurement data in industrial control. The advantage of these sensors is that they can provide information on what is happening inside the process itself, allowing us to control variables that were previously not attainable. Many processes such as continuous casting lack control systems due to the inability of conventional sensors to be implemented. Non-invasive sensors, such as tomographic sensors, can be used to view into the opaque molten steel and collect information about the flow structure in the mould. This data can then be used to create the control loops that will improve the process' efficiency. Prospective sensors based on multidimensional measurement in process control is numerous and although they share certain common features they differ in many aspects.

As previously mentioned, control based on multidimensional measurement data in the process of continuous casting is extremely limited, mainly these sensors are used for monitoring of the process rather implementation in a control loop [36]–[39]. In this section we will be concentrating on the general application of sensors based on multidimensional measurement data in controlling various processes and applications. These sensors are well suited for treating the controlled process as a distributed parameter system. Therefore, in principle the control can be based on or designed using distributed parameters model. There are several articles that provide theoretical treatment of the control of distributed parameters systems described by partial differential equations [40]. However, the real attempts to design a controller in the context described above (distributed parameter model, distributed sensing, lumped actuation) are rare and at the end they mostly conclude with lumped parameter approximation even if they declare themselves as based on distributed parameter modelling.

An example for control based on distributed parameter model is reported in [41]. The objective was to control the moisture content in a batch fluidised bed dryer. An electric capacitance tomography (ECT) was used to measure the moisture content. Also, in this case most aspects of the controlled plant behaviour were modelled using lumped parameter models based on mass and energy balances. This is then used to feed the permittivity model with the required moisture content variable as seen in Figure 1.6. The permittivity model

is a distributed parameter model that will calculate the permittivity distribution. The controller is then designed to keep the distributed permittivity around a desired shape using optimal control tools. This approach, where distributed parameter modelling is used just to describe those aspects of the plant behaviour whose distributed parameter modelling is essential while the rest is modelled using lumped parameters, seems to be generally promising as such models can be tractable analytically and suitable for use in the context of model-based control.

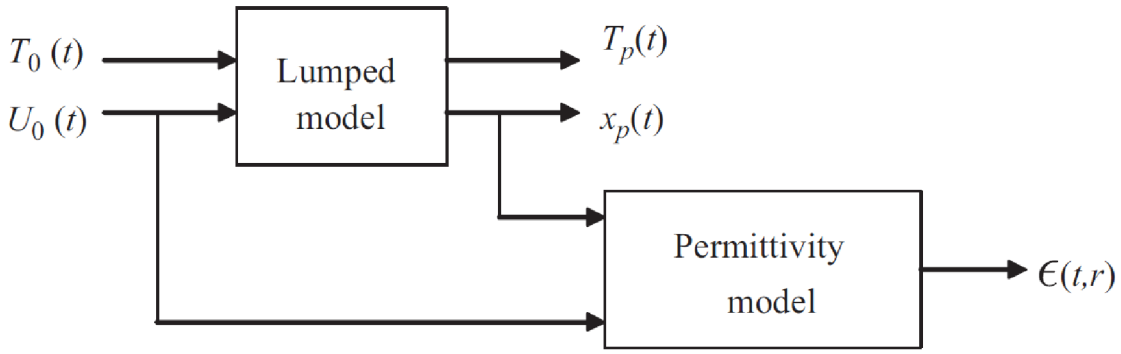

Figure 1.6. Moisture content is calculated by a lumped model and fed into the permittivity model to calculate the permittivity distribution [38]

In many cases, sensors based on multidimensional measurement data are used in highly nonlinear and complex processes. This adds further difficulty when it comes to modelling the process and designing model-based controllers. A possible solution to this is using Neural Networks (NN) as seen in [42] where a NN is used to model the pellet flow and the formation of dunes that occurs in the process using ECT sensor. The ECT sensor provides information on the permittivity density of the cross-sectional area of the pipe. Using the permittivity density, a feedforward NN with a single layer is used to predict the dune level using previous applied voltage values that controls the air velocity, and previous dune levels values. Based on this NN, an NN-based inverse controller is implemented where the output voltage is predicted using previous voltage levels and dune levels. Simulations showed that the controller is able to react to the dune build up and increase the voltage therefore increasing the air velocity in the pipe. It was also shown that the controller reacts well to disturbances in the mass flow. However, it should be noted the difficulty of assessing the stability of NN-based controllers using conventional control theory.

Furthermore, in [43] the author proposes a feedback control system based on Electrical Impedance Tomography (EIT) designed to regulate the concentration distribution of a substance in a fluid flowing through a pipe. The reconstruction algorithm allows for state predictions given by the evolution model, this is updated with the information provided by the measurements. The evolution model was described as a convection-diffusion model as seen in Equation 1.2 where both the velocity field and the conductivity distribution were reconstructed using an extended Kalman filter using measurements coming from the EIT sensor. Therefore, the EIT sensor does not measure the velocity field directly, instead it uses the concentration distribution of the liquid to estimate the velocity field.

$$\frac{\partial c}{\partial t} = -\bar{\mathbf{v}} \cdot \nabla c + \nabla \cdot \kappa \nabla c + q \tag{1.2}$$

A Linear Quadratic Gaussian (LQG) controller was applied using impedance tomographic measurements. The optimal values for the control input **u** are obtained by minimizing the quadratic cost function shown in Equation 1.3. Numerical simulations show that the control system was successful at obtaining the desired concentration on the output boundary. Furthermore, the state estimation and control strategies were shown to be relatively tolerant to misspecification of variables such as the velocity field which is important when it comes to more complex flows such as turbulent and multiphase flows.

$$J = E\left[\frac{1}{2}\bar{\mathbf{y}}_{t_f}^T \mathbf{H}\bar{\mathbf{y}}_{t_f} + \frac{1}{2}\sum_{t=0}^{t_f-1}\left(\bar{\mathbf{y}}_t^T \mathbf{Q}_y \bar{\mathbf{y}}_t + \bar{\mathbf{u}}_t^T \mathbf{R}\bar{\mathbf{u}}_t\right)\right] \tag{1.3}$$

A further approach using EIT is seen in [44] where the authors propose using EIT in a system that is highly nonlinear, high order and ill-posed. In this case, an EIT sensor is used to determine the positioning of an object inside a liquid tank. The control objective is to move the object from one position to another. The model of the system plus the sensor is represented using a state space model for the linear dynamic and a nonlinear output map. In the end, the controller will be mainly based on a linear state feedback controller and a nonlinear observer based on receding horizon principle. The state feedback linear controller will stabilize the linear dynamic while the nonlinear estimator will drive the estimation error to zero. By using the EIT sensor to measure the resistivity field the object's position is determined. Using this information, the controller is able to bring the object to the desired position.

A similar approach was implemented in [45] where state estimation is used to solve the inverse problem using both Electrical Capacitance Tomography (ECT) and Electromagnetic Induction (EMT). The linearized Kalman filter is applied to improve the temporal resolution of the reconstructed images. In the end, the state-estimation approach appears to be more suitable for the task of designing a controller as the state space model can be utilised in the mathematical derivation of the controller.

Another example of the use of sensors based on multidimensional measurement data in industrial control is shown in [46] where the author proposes a control system for an oil separator based on ECT sensors. ECT is used to distinguish between the different materials in the separator such as oil, water and air. The author uses PCA and cluster analysis to design their knowledge-based control strategy as shown in Figure 1.7. In the end, the concept relies on using the different pixels in the ECT image to get information on the distribution in the separator. Afterwards this distribution is compared to a knowledge database using Euclidean distance in order to determine the appropriate control action as each dataset in the knowledge-base is assigned a specific control action. In the end, we can see here a different approach for dealing with the images; instead of using specific measurements obtained from the sensors, the full image is used for the basis of the controller.

An interesting example of physical implementation of a multidimensional measurement based controller can be seen in [47] where a pilot-scale solid-liquid separation plant. The main purpose behind this setup was for teaching various control strategies and electronics design to undergraduate students. An EIT sensor is used to measure the air core size and position, therefore providing information on the separation status. Images from EIT show that the air core size can be measured and therefore a correlation can be determined with the angle of discharge and separation efficiency. The setup allows for multiple control strategies to be used for the control of the air core size. These range from PID controller, fuzzy logic and Kalman filters.

Reviewing the available literature on control based on multidimensional measurement data illustrates that there is no one-size-fits-all approach on how to deal with the data coming from these sensors; it relies heavily on both the process and the type of sensor used. Moreover, it becomes clear the challenge of creating a process model for

simulation testing and model-based control design. Due to the nature of these sensors, variables have both spatial and temporal dependence. This creates a challenge when modelling the process as the majority of modelling techniques in the field of control rely on lumped parameters rather than distributed parameters. This is the case both in models created by physical equations or system identification. The next section will go into depth on the various attempts of modelling the process when using multidimensional measurement data.

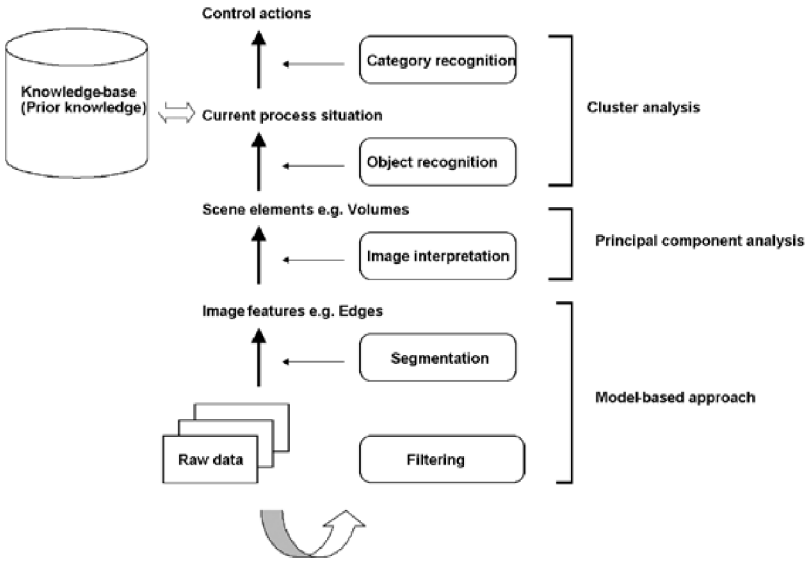

Figure 1.7. Knowledge-based control strategy using PCA and cluster analysis. The different pixels in the ECT image are used to obtain information on the distribution in the separator [44]

1.3. Modelling in Continuous Casting

Computational Fluid Dynamics (CFD) methods such as Finite-difference modelling has been proven to produce reliable mathematical models that are able to describe the interactions that occur in the continuous casting process. These models allow us to use model-based controllers such as Model Predictive Control (MPC) in order to achieve the necessary control objectives. However, due to the complexity of the whole process, it is not possible to model the entire process all together, instead the different phenomena are uncoupled, and assumptions are made to model them in isolation.

1.3.1. Electromagnetic Actuators

Due to the importance of the fluid flow in the mould in improving steel cleanliness, it has become common practice to use electromagnetic actuators to somewhat control the flow in the mould. These actuators can be classified under the terms electromagnetic stirrers and electromagnetic brakes (EMBr) [48]–[50]. The concept behind electromagnetic stirrers is creating a rotating magnetic induction field to eventually create an electromagnetic force that is applied to the steel liquid. Electromagnetic brakes on the other hand generate a static magnetic field which creates Lorentz forces in order to brake the fluid motion. This phenomenon has been modelled frequently in various research; in [51] where a finite-volume model was implemented using theory of computational fluid dynamics and magneto-hydrodynamics. It was shown that both the magnetic induction intensity and the position of brake region affect the fluid flow in the mould. As the magnetic field is increased, both the recirculating flow velocity and the impingement intensity become weak. Similar results were achieved with an electromagnetic stirrer [52] showing that the stirrer position effects both the fluid flow and solidification process in the mould. In [7] the authors investigated the effects of varying the depth of the submerged entry nozzle and the electromagnetic brake field intensity to see the combined effect. It became clear that increasing the EMBr field strength at a constant SEN depth reduced the downward velocity of the jet and decreased the top surface velocity along with other effects. Increasing the SEN depth without EMBr has a similar effect as increasing the EMBr field strength. However, increasing the SEN depth with EMBr had an opposite effect as above. The resulting flow structures can be seen in Figure 1.8 where the velocities of both upper and lower vortices vary.

Although various researchers have been conducted on the modelling and analysing the effect of electromagnetic actuators on the mould, it seems that there is gap when it comes to utilizing these actuators in a control loop. One of the few papers that attempt to incorporate an electromagnetic actuator [53] designed a control loop using an electromagnetic stirrer. The electromagnetic stirrer was used to both brake and accelerate the liquid steel in the mould to keep the flow speed at an optimal range. A sensor was used for the drag force to measure the flow at a certain point in the mould. System identification was used to model the process in which both a PI controller and a controller based on MPC

were designed for the control loop. In the end, it appeared that the MPC controller outperformed the PI controller, however, at a cost of much more aggressive control effort which may later lead to issues such as saturation and rate limiting.

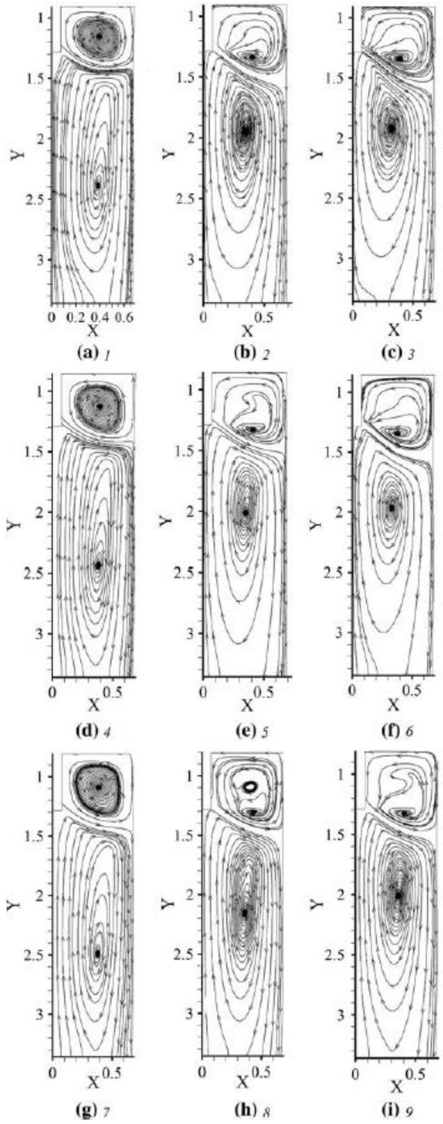

Figure 1.8. Various flow structures created varying the depth of the submerged entry nozzle and the electromagnetic brake field intensity in order to see the combined effect [50]

1.3.2. Temperature Field

There has been significant interest in modelling the heat transfer and solidification process that occurs in continuous casting; models are used to predict to temperature distribution and the solidifying steel shell [48] in order to control the secondary cooling and achieve the optimum steel product. Typically, a mathematical heat transfer model is used to simulate the solidification process in the continuous caster using technical conditions from a steelmaking plant. In [54] the mathematical model formulation is based mainly on a two dimensional unsteady state heat transfer equation as found in Equation 1.4. Several boundary conditions are applied, and the initial condition for the steel casting temperature is measured in the tundish from the steel plant. The model was verified by comparing the calculated slab surface temperatures with the measured temperature results which resulted in a relative error of less than 1.95%. In the end, the model concluded that the casting speed, pattern of spray cooling zone, and slab size have the largest influence on the temperature field of the slab. By lessening the water flow rate and increasing the casting speed, the solidification process can be improved

$$\rho C \frac{\partial T}{\partial t} = \frac{\partial}{\partial x}\left(\lambda \frac{\partial T}{\partial x}\right) + \frac{\partial}{\partial y}\left(\lambda \frac{\partial T}{\partial y}\right) \tag{1.4}$$

A further step was taken where a solidification model was combined with a model to analyse the bulging effect in the strand [19]. In this case the solidification analysis was performed by a one-dimensional finite difference model, while the building deformation was performed by two dimensional elasto-plastic and creep finite element model. The two models are combined by transferring the temperature field and shell thickness from the solidification model as an input to the bulging model. Similarly, to the previous paper, the result of this study showed the importance of casting speed and cooling conditions, but also considered the importance of roll pitch. Further research include the formulation of a three dimensional model for the temperature field and shell thickness [55]. The model was done using ANSYS where 29,000 8-node three dimensional elements were used. The authors noted that the numerical analysis can only be done in three-dimensional space as the y component of the health flux density is not equal to zero.

1.3.3. Argon Gas

To prevent nozzle clogging in continuous casting, argon gas is frequently injected in the SEN. However, due to the two-way coupling between the bubbles and the turbulent fluid flow, the gas injection often affects the flow pattern. Argon bubbles are carried by the turbulent flow into the mould after entering the SEN, where they affect the flow pattern mould level fluctuations, and slag entrapment. Larger bubbles in the mould tend to either go up to the surface and escape into the atmosphere or get stuck in the meniscus and cause surface defects. Furthermore, smaller bubbles tend to go deeper in the mould and cause internal defects [56]–[58].

Hence, modelling argon gas bubbles in the mould becomes vital to improving the quality of the steel. In [59] a Eulerian-Lagrangian approach is used to model the 3D turbulent flow in the mould with non-metallic inclusions and argon gas bubbles. Two methods were applied in this study: one-way coupling where only the melt flow impact on the dispersed phases was considered, and two-way coupling where both flow impact and the dispersed phases influenced one another. The conclusion was that the two-way coupling is essential to correctly model the movement of the inclusion and bubbles in the mould as the one-way coupling could not accurately predict the dispersion of the particles and velocity profile. Another study utilised a combination of Large Eddy Simulation model, Lagrangian Discrete Phase Model, and VOF multiphase model [60]. Using this 3D coupled model, the flow and bubble distribution in the mould was investigated. As can be seen in Figure 1.9, the argon gas flow rate has a significant impact on the flow pattern. Lower argon gas injection rate correlates with a double roll flow pattern, while higher argon gas rates correlate with a single roll flow pattern. A similar approach can be seen in [61] where a Discrete Phase Model and a Two-Phase Model are used to model the argon gas effect.

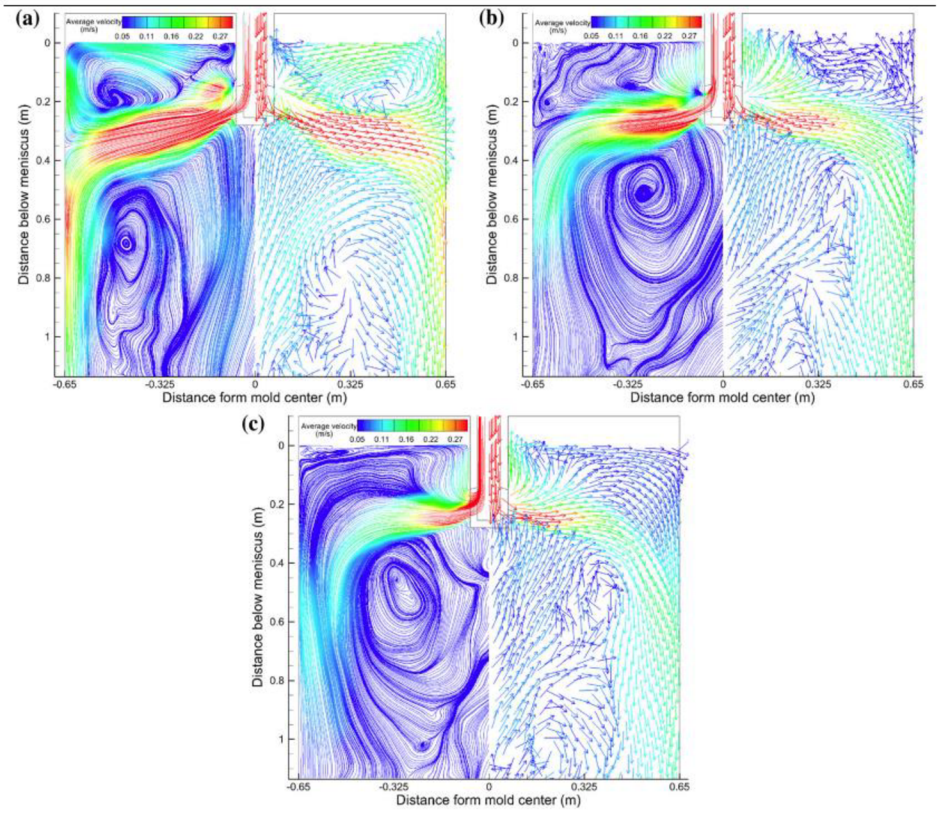

Figure 1.9. Flow and bubble distribution in mould investigated using Large Eddy Simulation mode coupled with, Lagrangian Discrete Phase Model, and VOF multiphase model [58]

However, in this study the casting speed was also changed to see the effect on argon gas flow. The study concluded that it is important to consider both argon gas flow rate and casting speed collectively when aiming for optimizing the steel product quality.

Additionally, studies have taken the further step of coupling the effects of both the electromagnetic brake and the argon gas injection on the flow in the mould. In [62] a 3D model using both finite element and finite volume was simulated to study the coupling between electromagnetic brake and the argon gas. The electromagnetic force was modelled using a one-way coupling where it is assumed that the induced magnetic field is much less than the external magnetic field from the brake. Equation 1.5 and 1.6 indicate the induced current density equation. Equation 1.7 is used to satisfy the conservation law for steady state. By substituting Equation 1.6 into Equation 1.7 and using Equation 1.8, we end up with the following Poisson Equation, where the resulting electromagnetic force equation is shown in Equation 1.9.

$$\vec{j} = \sigma\left(\vec{E} + \left(\vec{u} \times \vec{B}_0\right)\right) \tag{1.5}$$

$$\vec{E} = -\nabla\varphi \tag{1.6}$$

$$\nabla \cdot \vec{j} = 0 \tag{1.7}$$

$$\nabla^2\varphi = \nabla \cdot \left(\vec{u} \times \vec{B}_0\right) \tag{1.8}$$

$$\vec{F} = \vec{j} \times \vec{B}_0 \tag{1.9}$$

Simulations result show applying both the EMBr and argon gas can affect the upper re-circulating molten steel by increasing the upward movement. Furthermore, argon gas can improve the removal of the inclusion particles, while EMBr has little effect on this. Similar work can be seen in [63] where fluid flow in the mould is modelled using Navier-Stokes equations with electromagnetic force. The trajectories of the inclusion particles are calculated based on the computed velocity field. In the end, it was shown that the argon gas injection changes the trajectory of the inclusions resulting in re-entry into the upper recirculation zone and eventually floating out into the air. While the EMBr slows down the particles. The combination of the two improves the removal process of inclusions.

It should be noted that many of the CFD models shown in the literature were not necessarily created for the purpose of controller design, but rather to understand the physics behind the phenomena in more depth. The task of designing model-based controllers based on these complex CFD models is challenging due to the nature of distributed parameter models; converting these CFD models to state space models could result in extremely large matrices that are not feasible to use in real time control, therefore these challenges must be addressed. Furthermore, it is common practice in the field of control to obtain a quick estimate of specific phenomena for the development of online control [48]. Although it might seem counter-intuitive to not take advantage of both the spatial and temporal information obtained from the sensors, it might be interesting to see if a lumped parameter model will be sufficient in controlling the loop.

2. Doctoral Thesis Objectives

Based on the literature analysis, it becomes clear that the continuous casting process is a challenge when designing control systems due to the limitation of applying sensors. The existing control loops implemented in the continuous casting process are mainly limited to mould level control or temperature distribution control as these variables are currently readily available. However, many of the quality defects that occur in the end-product of the steel depend on the flow patterns in the liquid steel while in the mould. Issues such as slug entrapment, meniscus freezing, and other problems heavily determine the quality of the steel. Therefore, it is natural to look for solutions where we can try to 'see' inside the liquid steel before it is completely solidified. This is the point where two-dimensional flow monitoring comes into play. Sensors based on multidimensional measurement data provide two or three-dimensional measurements that are much richer in information than single-point measurements. They can also look inside the continuous casting process in a non-invasive way without penetrating it physically. The literature review has shown us that such sensors can bring many benefits not only for continuous casting but also for many other processes. However, it is also evident that their use in industrial control is limited as there are still many challenges in utilising the information and images provided by these sensors in a control loop.

The general objective of this doctoral thesis is to use two-dimensional flow monitoring sensors in a control loop to improve the control of a continuous caster. Two such flow monitoring sensors will be considered: Ultrasound Doppler Velocimetry (UDV) and Contactless Inductive Flow Tomography (CIFT). UDV will be mainly used in designing both the process models and controller structures in this thesis. The main reason for this is that the experimental data were obtained using a small-scale continuous caster Mini-LIMMCAST where the UDV sensors were finalised at the beginning of the research described in this thesis. On the contrary, CIFT sensors were and still are under development to some extent. It can be expected that it will be possible to extend the techniques developed with UDV and transfer them into CIFT as both sensors can reconstruct the velocity profile in the mould.

The general objective of improving the control of a continuous caster can be naturally split into several sub-objectives. Firstly, a process model is necessary to design and test any at least somewhat advanced controller. The mould of a continuous caster is a distributed parameter system. It may seem natural to use Computational Fluid Dynamics (CFD) approach to obtain a model of this process. However, an open question is whether building a CFD model and space-discretising it using a finite element or similar method is viable for getting a useful control-oriented model. This question will have to be answered in the thesis, and if the answer is negative, it will necessarily imply that the next objective is to find a more viable modelling alternative.

Secondly, the general statement that the quality of the final product depends on the flow patterns in the mould is true, but by itself, it is not a sufficient basis for control. For this reason, the next objective must be to identify appropriate quantitative flow characteristics that could be used as controlled variables for efficient closed-loop control based on distributed data inside the mould.

Thirdly, the central objective is to develop the controllers that will use these quantitative characteristics as controlled variables while stopper rod position and magnetic field of the electromagnetic brake will be manipulated variables. Since it is not clear in advance which control configurations and methods are the most promising ones, a part of this objective is to test different configurations (single-input, single-output, as well as multivariable control) and different control methods focusing mainly on model-based approaches. Since the availability of a model enables not only control but also other objectives like, e.g., fault detection, the thesis should also consider if control functionalities can be extended by additional functions like online detection of faults or operational issues.

Last but not least, the thesis should discuss the possibility of transferring the developed methods and techniques to CIFT sensors. In the end, there should be a clear analysis on what are the best approaches regarding processing the sensor data, modelling the process, and designing model-based controllers for the continuous casting process.

In accordance with these objectives, the thesis is divided into seven chapters, including this chapter with objectives and the preceding chapter describing the continuous casting process and the state-of-the-art of its control. Chapter 3 shows the Mini-LIMMCAST setup used to obtain experimental data for this thesis. Chapter 4 discusses

model-based control using computational fluid dynamics. In this chapter, Finite-Element Method is used to model the interaction between the fluid flow and the magnetic field from the EMBr. COMSOL is used for simulations, and the challenges of utilising this model for model-based control are discussed. Chapter 5 focuses on several different variants of model-based control using models obtained by system identification. It also treats the question of fault detection, particularly clogging detection. Chapter 6 investigates the use of CIFT in a control loop and the further improvements needed for the sensor. Chapter 7 discusses the summary of the thesis and the conclusions and challenges derived from the results.

The research done in this paper is a part of a European Training Network under the Marie Sklodowska-Curie Actions, under the name "Smart tomographic sensors for advanced industrial process control (TOMOCON)".

3. Experimental Setup: Mini-LIMMCAST Facility

The experiments included in this thesis were conducted on the Mini-LIMMCAST facility located at Helmholtz-Zentrum Dresden - Rossendorf (HZDR) which is shown in Figure 3.1. The setup consists of a small-scale model of the mould and strand of a continuous slab caster. Gallium-indium-tin (GaInSn) eutectic alloy is used in place of the liquid steel because it is a liquid at room temperature. GaInSn is poured from the 'tundish' into an acrylic glass mould via the SEN as shown in Figure 3.2. The flow rate in the SEN is controlled by a stopper rod. In order to run the experiments continuously, the melt flows from the bottom of the mould into the storage vessel, from which liquid is pumped back to the tundish to repeat the process. The physical properties and dimensions of the setup can be found in Tables 3.1 and 3.2. An electromagnetic brake is used to influence the flow in the mould as shown in Chapter 1.

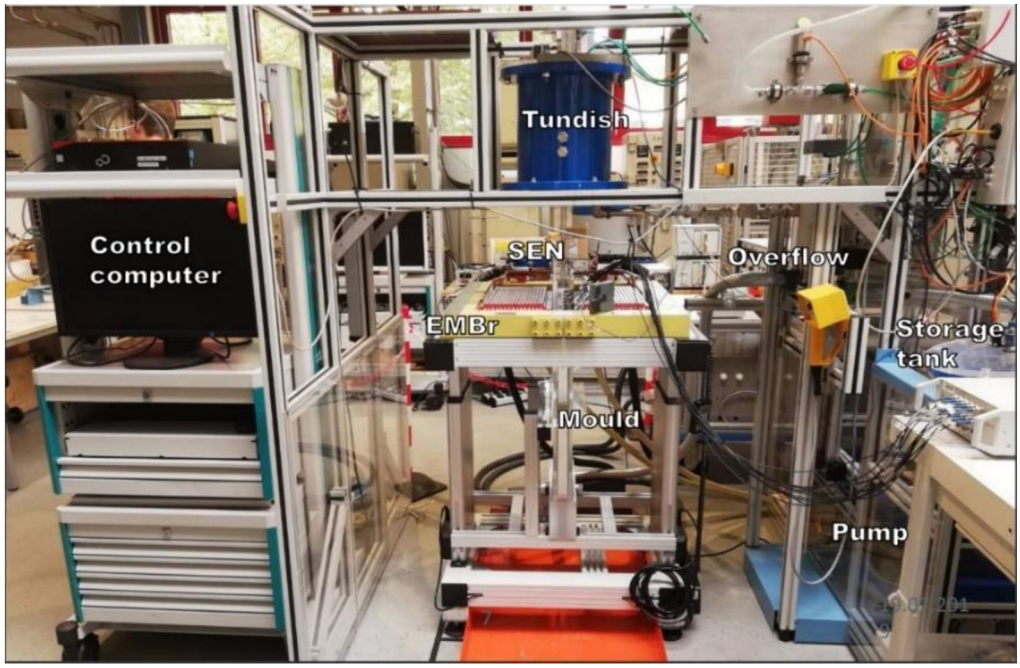

Figure 3.1. Mini-LIMMCAST Facility in HZDR.

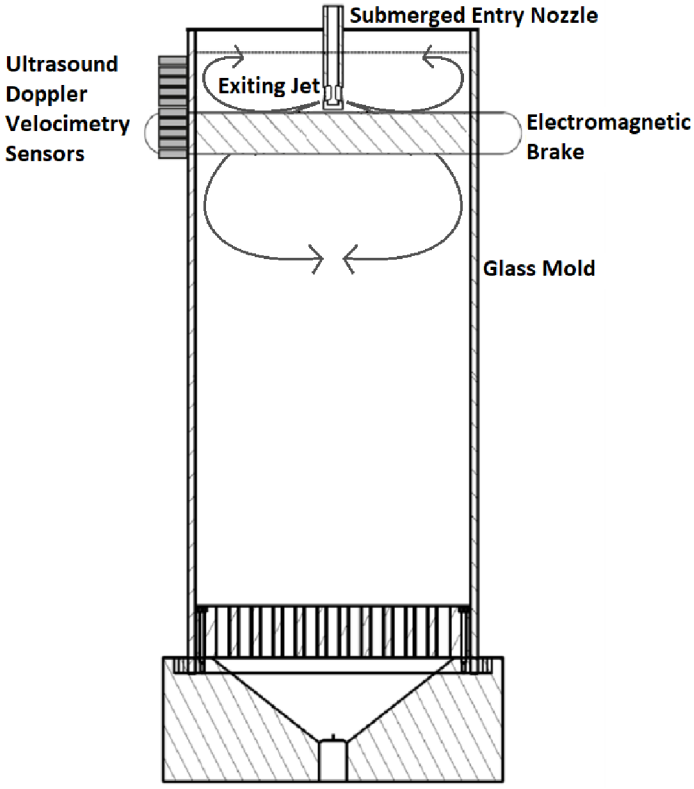

Figure 3.2. Schematic of mould illustrating the position of the sensors and electromagnetic brake.

Table 3.1. Physical properties of gallium-indium-tin [1].

	Values
Reference Temperature (°C)	20
Density (ρ)	6353
Kinematic Viscosity (υ)	3.44 × 10−7
Electrical Conductivity (σ)	3.29 × 10−7
Thermal Conductivity (λ)	23.98
Surface Tension	0.587

Table 3.2. Dimensions of the Mini-LIMMCAST setup [1].

	Dimensions
Mould Width (mm)	300
Mould Thickness (mm)	35
Mould Height (mm)	600
Submerged Entry Nozzle Immersion Depth (mm)	35 ± 10
Submerged Entry Nozzle Inner Diameter (mm)	12
Submerged Entry Nozzle Outer Diameter (mm)	21
Submerged Entry Nozzle Port Width (mm)	11
Submerged Entry Nozzle Port Height (mm)	13
Submerged Entry Nozzle Port Angle (deg)	−15
Electromagnetic Brake Windings per Coil	32
Electromagnetic Brake Max. Current (A)	600
Electromagnetic Brake Max. Magnetic Flux Density (mT)	404

The majority of experiments conducted on the Mini-LIMMSAST will be done using Ultrasound Doppler Velocimetry (UDV). The data from UDV will be used mainly in this thesis to create the process model and controller. The techniques used with UDV will then be later extended to CIFT to investigate the feasibility of using the sensor for the purpose of control. Using the velocity profile measured by UDV, we can visualize the flow structure in the mould. This will allow us to extract important features of the flow that will be utilized by the controller. It should be noted that the described techniques to design the control loop can be utilized for other sensors based on multidimensional measurement data as well, assuming that sufficient information on the velocity profile of the mould is obtained. The presented concepts will be extended to demonstrate that the flow structure obtained by UDV can be fully utilized for control. UDV is used during the experiments to reconstruct the flow in the mould by measuring the horizontal velocity component of the flow in the opaque liquid.

Figure 3.2 shows the 10 UDV sensors placed vertically on the narrow face of the mould with 10 mm spacing in between. Each UDV sensor measures the velocity of small moving

particles in GaInSn and returns the velocity profile along the horizontal ultrasound beam. The measurements were conducted using the DOP3000 which is able to operate 10 transducers [1]. The transmitters are activated sequentially, and this cycle is repeated so that the flow in the left half region of the mould is visualized.

The electromagnetic brake will be one out of two manipulated variables in the control loop. Generally, in continuous casting electromagnetic brakes and stirrers are used to stabilize the turbulent flow in the mould. However, due to the limitations of using conventional sensors during the process, the electromagnetic actuators are applied at specific pre-calculated strengths. In the Mini-LIMMCAST setup a static single ruler brake is used. Under the influence of the static magnetic field the velocity of the melt drives an electrical current in the melt. The current, in turn, generates the Lorentz force acting on the melt. It is assumed that the force is damping the velocities. The placement of the electromagnetic brake is critical for the control design as it has been shown that small variations in the vertical position of the brakes can significantly change the effects of the brake on the flow [1]. For the experiments, the optimal position for the electromagnetic brake is chosen where the pole shoes are right below the SEN.

By analysing the measured velocity fields gathered by UDV, it becomes clear that the brake moves the jet exiting the SEN upward so that it becomes more horizontal. In the experiments, the current of the brake is varied from 0 to 600 A. Chapter 5 concentrates on these experiments to create a model describing the relationship between the flow structure in the mould and the current using system identification.

Finally, CIFT will be applied to the Mini-LIMMCAST, where the reconstructed velocity profile will be used in the control loop. CIFT has already been successfully implemented on the Mini-LIMMCAST setup [64] and was used to reconstruct the velocity fields. The main concept of the CIFT technique relies on the flow of the conductive liquid going through a magnetic field created by the CIFT transmitter sensors. This creates electrical currents in the mould which results in an induced magnetic field. The induced magnetic field is measured by the receiver sensors and is used to reconstruct the velocity field in the mould.

4. Model-Based Control using Computational Fluid Dynamics

Two-dimensional flow monitoring can visualize what is occurring in the process in a manner that is non-invasive. In our case, both UDV and CIFT provide information on the velocity profile inside the mould of the continuous caster. This process is considered a distributed parameter system since the controlled variables (the velocity fields) rely both on spatial and temporal factors. Therefore, conventional physical modelling based on lumped input-lumped output cannot be applied in this situation. This poses a challenge when it comes to creating a model-based controller for these types of processes. The ideal case would be to build the model-based controllers using partial differential equations (PDEs). As seen in Chapter 1, the usual approach to dealing with PDE models is approximating the infinite dimensional PDE system to a set of finite-dimensional ordinary differential equations (ODEs) [65]. An important note is that although an ODE model can be derived using finite-dimensional modelling, it does not necessarily mean that the process will be controllable in the end. In this chapter we will discuss the idea of approximating the PDE model needed for the continuous casting process using FEM, and the feasibility of applying it in a model-based controller.

4.1. Governing Equations and Numerical Details

As our controlled variable is the velocity field in the mould, and our manipulated variable is the magnetic field from the EMBr, we need to model the effect of the EMBr on the liquid steel in the mould. Therefore, we need to model an incompressible electrically conductive fluid that is affected by the imposed external magnetic field through Lorentz force. This relationship will be described by the following Partial Differential Equations where the Lorentz force term is added to the Navier Stokes equations in order to model the effect of the magnetic field on the velocities in the liquid as shown below [66].

$$\nabla \cdot \boldsymbol{U} = 0 \tag{4.1}$$

$$\frac{\partial \boldsymbol{U}}{\partial t} + (\boldsymbol{U} \cdot \nabla)\boldsymbol{U} = -\frac{1}{\rho}\nabla\rho + v\nabla^2\boldsymbol{U} + \frac{1}{\rho}\boldsymbol{J} \times \mathbf{B} \tag{4.2}$$

$$\nabla^2\varphi = \nabla \cdot (\boldsymbol{U} \times \boldsymbol{B}) \tag{4.3}$$

where U is velocity, p is pressure, ν is the kinematic viscosity, ρ is density, J is the current density and B is the imposed magnetic field, which will be the manipulated variable used by the controller to influence the velocity field in the mould. In addition to the velocity and pressure, also the current density (J) needs to be calculated. In the case of continuous casting, we can use the one-way approach of magnetohydrodynamics instead of the two-way approach because the magnetic Reynolds number is much larger than 1 for the liquid metal flow.

4.2. Finite Element Modelling using COMSOL

Finite Element Method (FEM) is used to discretize the 3-D model so that later the discretized nodes can be converted to a state space model and utilized in a model-based controller. A similar approach was done in [65] where the concentration of a liquid in a pipe was modelled using the convection-diffusion equation. FEM was also used to obtain a state space model between the injectors in the pipe and the concentration in the liquid. The main goal for this step is to create a simplified model of the mould to decrease the number of nodes needed to accurately simulate the effect of the EMBr on the velocity fields. This is done to decrease the size of the matrices needed for the state space.

Model-based controllers such as MPC need to repeatedly solve an optimisation problem to calculate the values for the manipulated variable. Having a state-space model with matrices that are too large become unrealistic to use in this scenario. However, it is a challenge to decrease the nodes needed in the 3D model due to many factors such as the turbulent flow in the mould, and the complex geometry of the SEN. Although model-reductions methods can be applied, other steps can also be taken to simplify the complexity of the geometry. In our case, we will be modelling one half of the mould to avoid modelling the SEN. Therefore, instead of the SEN we will have a have a port opening where the liquid steel flows in. As the flow entering the SEN is constant, we can use experimental data to specify the velocity field at the port opening.

COMSOL Multiphysics is used for this step where toolboxes including the Magnetic and Electric fields and the Turbulent Flow toolboxes are utilised. For the turbulent flow, Large Eddy Simulation (LES) is used to resolve the three-dimensional unsteady eddies and model the effect of the smaller eddies. Figure 4.1 shows the results of the simulations where the double roll flow is visible in the mould with no applied magnetic

field from the EMBr. Figure 4.2 shows effect of applied magnetic field of 300 mT. The double roll flow is also visible, however now the exiting jet is now impinging higher on the narrow face wall. By using the EMBr we can manipulate the exiting jet and avoid a deeper impingement into the mould. This effect is confirmed with experimental data measured by UDV. These experimental data will be further discussed in Chapter 5.

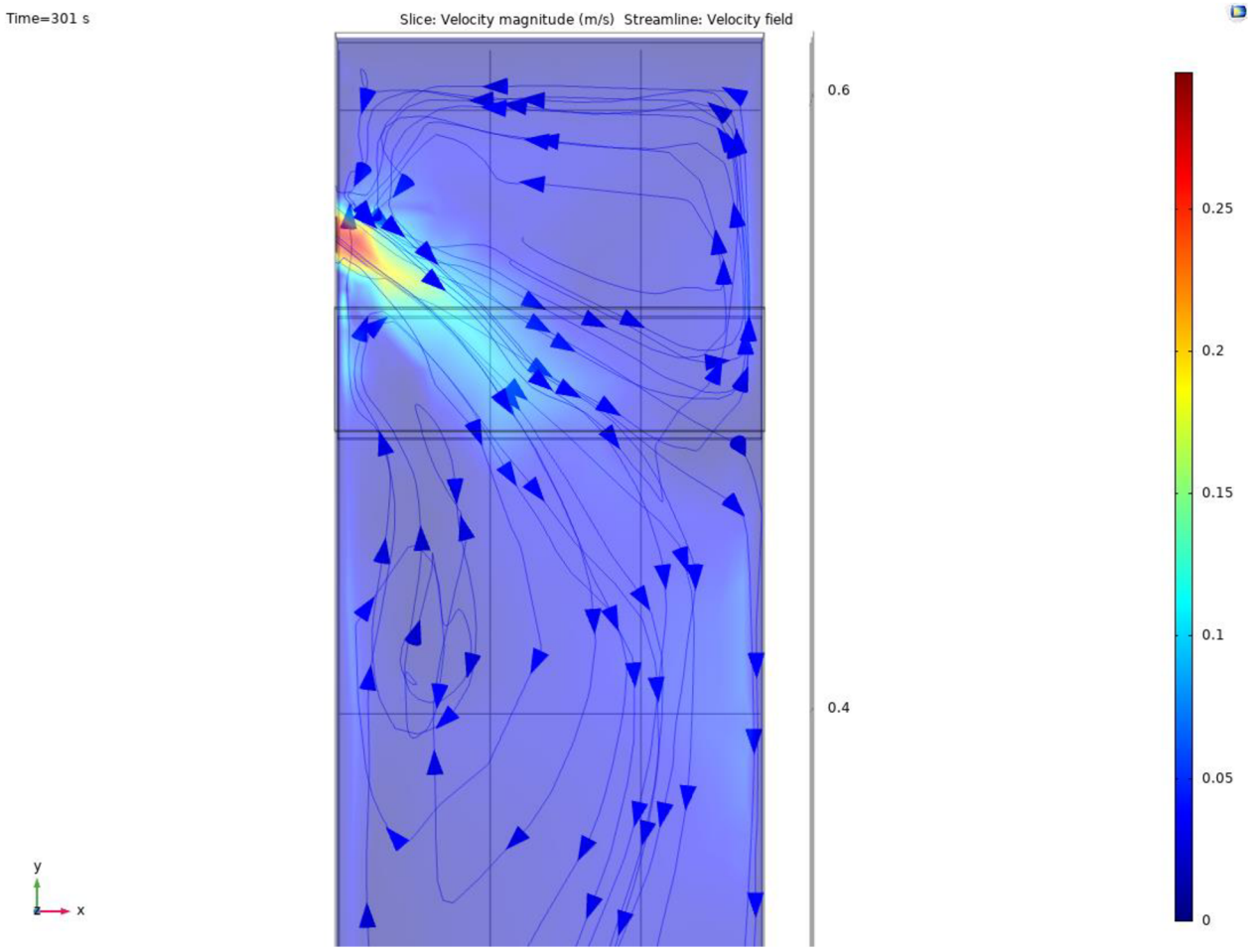

Figure 4.1. CFD simulation result with no applied magnetic field

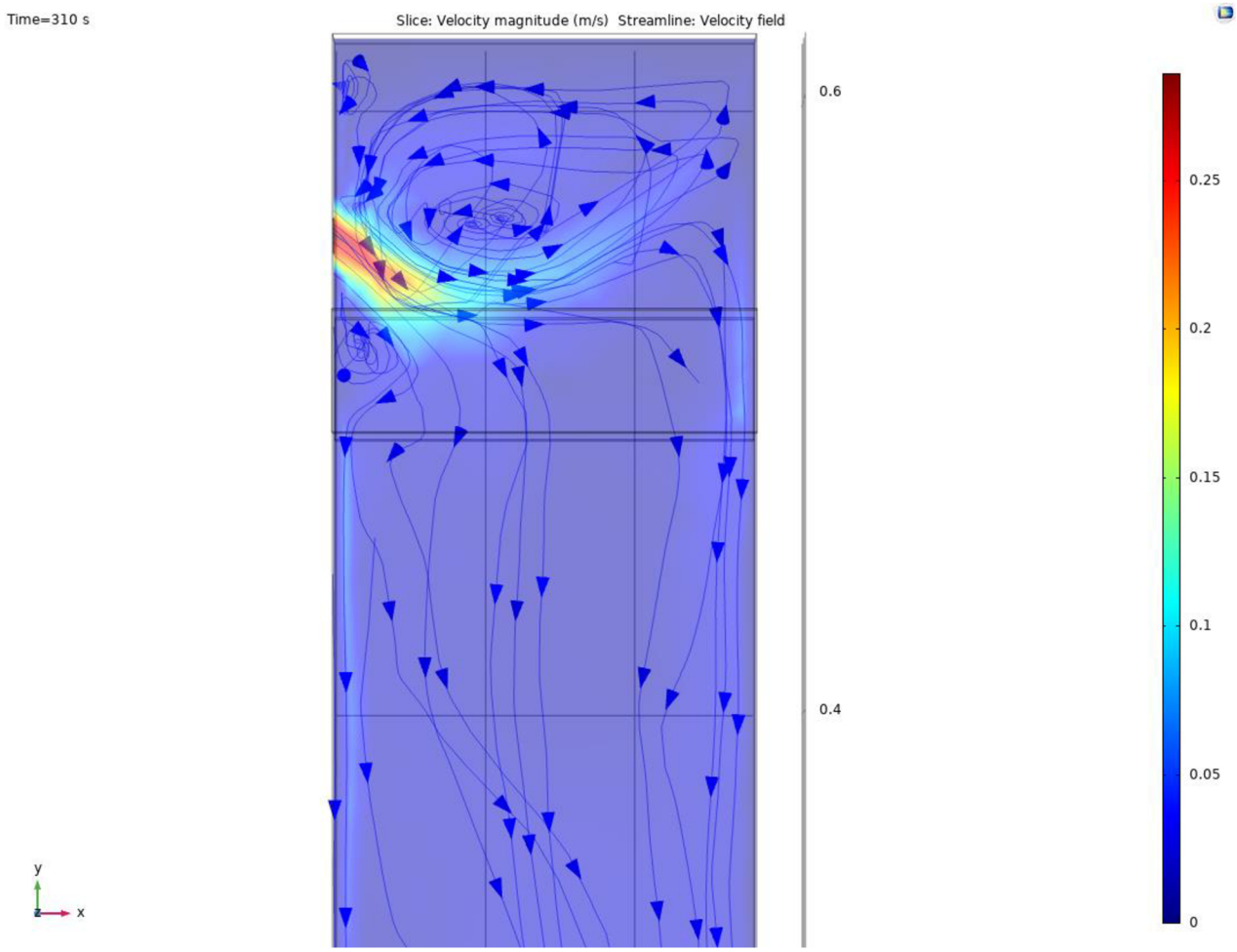

Figure 4.2. CFD simulation result with applied magnetic field of 300mT

4.3. Extracting State Space Matrices

The next step now is extracting the required state space matrices from this simulation so that we can develop our controller. A key feature of COMSOL is its interface with MATLAB using COMSOL's API called LiveLink for MATLAB. The feature of state space export allows us to create a linearized state-space model that corresponds to the COMSOL model. The following representation is used to extract the matrices of the dynamic system. This form is used as it more suitable for large systems because matrices Mc and McA become much more sparce than A.

$$M_c\dot{x} = M_cAx + M_cBu \tag{4.4}$$

$$y = Cx + Du \tag{4.4}$$

In the end, we are able to decrease the number of degrees of freedom of the model around 50,000 using the mesh shown in Figure 4.3. Less than this would not allow for the resolving of the PDE equations. Unfortunately, this would still result in matrices that were too large to be used for model-based control. Additionally, after analysing the matrices of the system it becomes clear that matrix Mc has a high condition number. Therefore, we are dealing with an ill-conditioned problem which adds even more complexity when trying to utilise these state space matrices for control. There are a few reasons that we can contribute to the ill-conditioned nature of the problem; they include the high turbulence in the mould and the limited number of actuators we have to influence the flow in the mould.

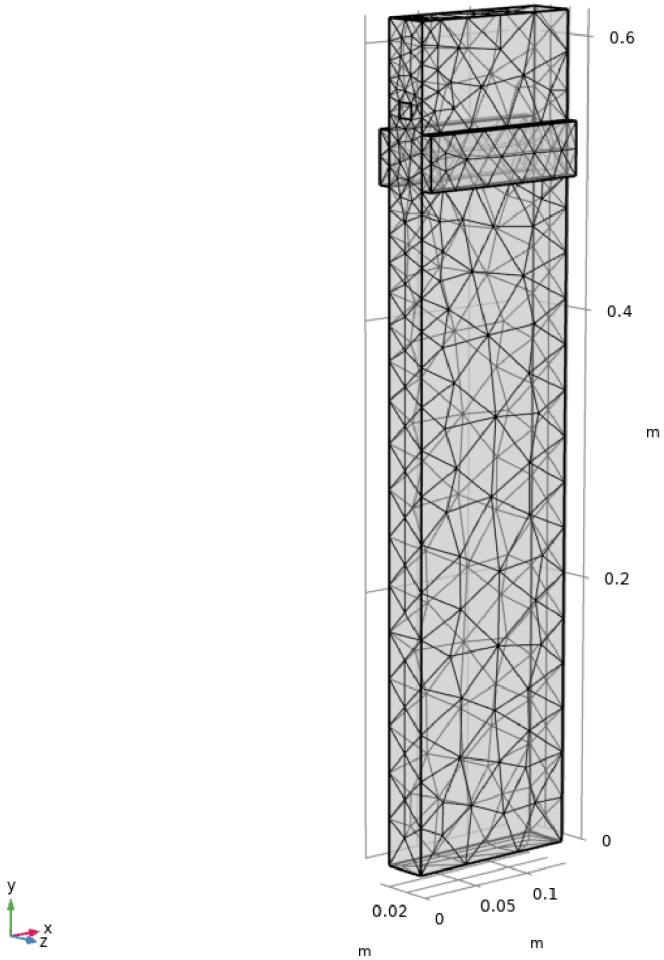

Figure 4.3. Three-dimensional mesh used to simulate the flow in half of the mould

It should be noted that using CFD simulation to create a distributed parameter model for the purpose of control is an option when it comes to more straightforward processes. An example is [65] where the author is simulating the laminar flow in a pipe and is controlling the concentration of the liquid. Additionally, the author has a much higher number of actuators than in the case of the continuous casting process. Therefore, making the process more controllable. Another example of a process that has been successfully simulated and controlled is shown in [67] where an LQR is designed to control the moisture distribution in an industrial microware drying process. The moisture is simulated using PDEs and FEM is then used to transform the PDEs into a system of ordinary differential equations. Similarly, to [65] the process is more straightforward and contains a higher number of actuators. In this case, six microwave sources with adjustable power levels were used to control the moisture in the foam. Additionally, these papers are examples of early-lumping methods that are used to approximate and reduce the PDE system into a finite dimensional system in order to utilize in controller design. Other reduction techniques include finite-difference, finite-volume, and modal approaches. It should be noted that the reduction of infinite dimensional models to finite dimensional models means that a part of the original dynamics of the system is lost. This might result in issues such as in inefficient control performance or closed loop instability.

In the end, although one of the advantages of sensors based on multidimensional measurement data is the combination of spatial and temporal information, another main advantage is the fact that they are non-intrusive. Therefore, these sensors are able to look inside the process without needing to penetrate them. This is an important advantage when it comes to processes that contain opaque fluids such as the continuous casting process. This means that even in cases where the full potential of the multidimensional data is not utilised in a control loop, extracting important quantitative characteristics that can then be implemented in classical feedback control is still very effective as will be seen in Chapter 5.

5. Model-Based Control Using System Identification

Chapter 4 shows the difficulty of using physical equations to create a model for our controller. The spatial dependence of the variables results in the need for PDEs to fully model the interaction between the liquid steel in the mould and the EMBr. Challenges such as solving the Navier Stokes equations make it very difficult to utilize these models in both simulation testing and control design. The needed time and complexity of the model means that the approach is not unfeasible for this purpose. In this chapter we aim to find quantitative characteristics of the flow that can be used to optimise the flow in the mould. System identification will mainly be used to create the process models needed for the control loop. The Mini-LIMMCAST setup allows us to obtain large amounts of experimental data from the sensors which is beneficial when coming to system identification as this methodology is data-dependent.

One of the main challenges in designing control loops for the continuous casting process is selecting the appropriate variables to achieve the optimum flow pattern needed in the mould. Now that sensors based on two-dimensional flow field measurements allows us to view into the mould and have an understanding on the flow structures, we need to decide on what are the optimum flow characteristics that would yield higher quality steel, and how to control it with our actuators. Section 5.1. introduces the exiting jet angle from the SEN as our controlled variable, and the EMBr as our manipulated variable. The exiting jet angle is crucial to the flow in the mould as it determines how easily impurities and slag are trapped in the mould, which significantly affects the quality of the steel. As shown in section 1.3.1, EMBr is frequently used in continuous casting to influence the flow in the mould and achieve higher quality steel. However, it is usually applied at pre-calculated values rather than being used in a feedback loop. In this section, we will be using the current going to the EMBr achieve the optimum exiting jet angle during the process. Section 5.2. concentrates on the meniscus velocity as our controlled variable. Keeping the meniscus velocity between optimum values is crucial as too low velocities will cause premature freezing, while too high velocities will increase the chances of slug entrapment [6]. The manipulated variable will be the current to the EMBr similarly to section 5.1. Lastly, section 5.3 extends the control loop in section 5.1. to a multiple input-multiple output by

using both EMBr and stopper rod to control the flow in the mould. The stopper rod allows us to control the flow rate in the SEN, therefore allowing us to influence the flow in the mould even further. In this section we are concentrating on the exiting jet angle rather than the meniscus velocity as there is a more direct effect on the exiting jet from our actuators; the reason for this is the proximity of the exiting jet to the position of the EMBr and the SEN port. This direct effect can also be seen in the models created for both controlled variables as will be shown in section 5.1. and 5.2. For this reason, we are basing our MIMO controller on features related to the exiting jet including the jet impingement point and the jet velocity.

5.1. Exiting Jet Angle

The exiting jet angle from the SEN plays an important role in improving the quality of the steel produced in continuous casting. The deeper the jet impinges into the mould, the higher the probability of slag entrapment in the mould as the particles are unable to float to surface and avoid getting trapped in the mould [68], [69]. Hence, avoiding a deeper jet impingement is linked to higher quality steel; this concept will be used to build our controller. Another question arises on the how to obtain information about the jet angle from the velocity profile in order to be used by the controller. One of the ways to achieve this is by parametrization of the two-dimensional flow field measurements rather than using entire velocity fields of the mould. This allows us to decrease the processing time by avoiding having the controller process large matrices in real-time. The results in this section are published in [70], [71].

5.1.1. Submerged Entry Noggle Clogging

Nozzle clogging contributes heavily to quality issues seen during the process of continuous casting. The presence of clogging in the Submerged Entry Nozzle (SEN) can significantly affect the exiting jet and therefore impact the quality of the steel product. Also, there is a high risk of inclusions due to parts of the clogging material breaking off and entering the mould [10], [72]. Therefore, it would be beneficial if our controller would be able to detect the occurrence of clogging in the SEN using information about the angle of the jet and adapt accordingly. Two sets of experimental data from the Mini-LIMMCAST

will be analyzed; the first set was performed with no apparent clogging in the SEN [67], while the second set of experiments was conducted with clogging in the SEN as shown in

In the following sections it will become clear that the clogging changes the dynamic response of the angle of the jet to the applied current to the EMBr, and therefore different models are needed to describe the dynamic response with SEN clogging and without SEN clogging. The next step will be to create an algorithm that allows us to detect clogging in the SEN by monitoring the angle of the exiting jet. Based on this clog detection setup, a switched MPC controller is used to keep the angle of the exiting jet between the optimum ranges using the EMBr. This allows the controller to keep the angle of the jet in the optimum range even when clogging occurs in the nozzle.

Figure 5.1. Clogging in the SEN near 'tundish' outlet

5.1.2. Parametrizing Jet Angle from Velocity Profile

This section discusses the parametrization of the exiting jet angle as a single variable to be used as the controlled variable to avoid deep jet impingement. The measured velocity fields in the mould are used to obtain the angle of the jet flow exiting from the SEN. In the end, the control objective will be to maintain the angle between the optimum ranges in order to prevent deep jet impingement during the process. Therefore, avoiding the entrapment of slugs and sustaining the double roll flow. The actuator used to change this angle is the varying magnetic field of the electromagnetic brake (EMBr).

As mentioned in Chapter 3, 10 UDV sensors are used to measure the horizontal velocities at the positions of the sensors. In our setup we will only concentrate on the left half of the region of the mould and assume that there is symmetry between the two regions. The direction of the velocity measured by the UDV sensors is identified by the sign of the velocity; negative velocities indicate that the flow is moving towards the sensors and mould wall, while positive velocities indicate that the flow is moving away from the sensors and mould wall (see Figure 5.3). Cubic spline interpolation is used to provide a finer resolution between the sensor positions. In order to track the movement of the jet, we compute the largest velocities with negative sign measured in the region surrounding the SEN outlet. During every frame captured by the sensors, the algorithm compares the interpolated velocities between the sensors and computes the y-axis position of the most negative velocities. After the most negative velocities have been computed, linear regression using least squares is used to fit a line that would represent the flow of the jet. The linear regression uses the quadratic loss function to calculate the error in the model (See Figure 5.2). Figure 5.3 and 5.4 illustrate the reconstructed angle responses and shows that the algorithm can track the movement of the jet successfully. Using this methodology, we avoid using the entire velocity fields measured by the UDV and instead use a single variable to represent the movement of the jet during the experiments.

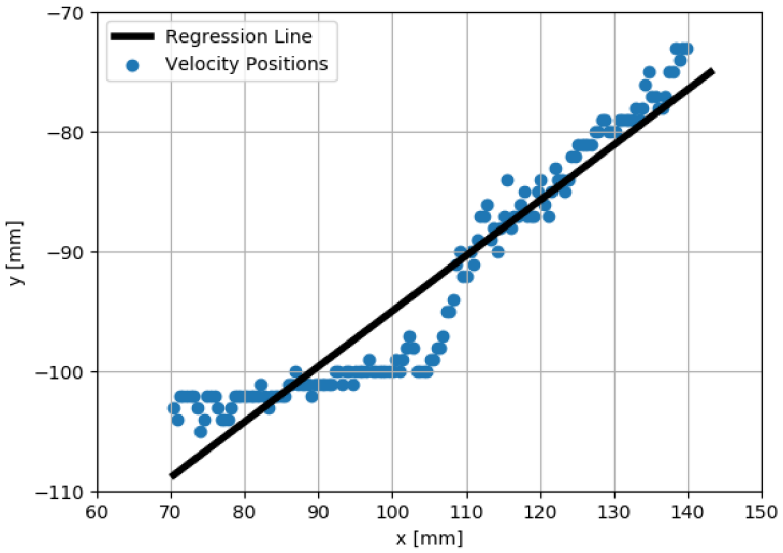

Figure 5.2. Linear regression line to fit positions of largest velocities with negative sign with EMBr turned off

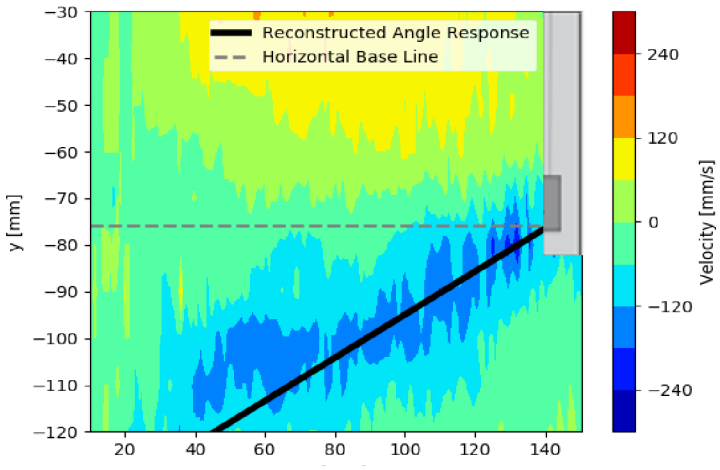

Figure 5.3. Reconstructed angle response with EMBr turned off

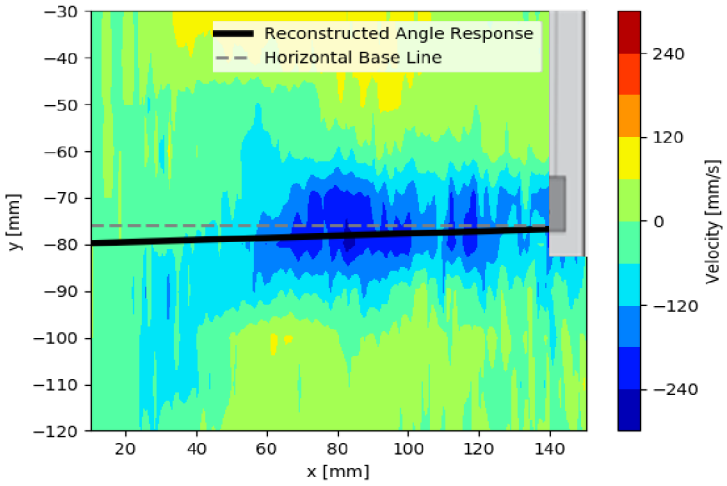

Figure 5.4. Reconstructed angle response with EMBr current of 450A

5.1.3. Process Modelling

A model is needed for both testing and designing the controller in the case of model-based control. System identification requires uniformly sampled time or frequency-domain data with the required inputs and outputs of the system. In our case our input will be the current to the EMBr, while the output if the angle of the exiting jet angle. For continuous time models, Pseudo-Random Binary Signals (PRBS) are commonly used to excite the dynamics of the system as they are easily generated and have a straightforward auto-correlation function. However, for non-linear systems, binary signals are not well suited as they are unable to identify the non-linearities of the system. The binary signal needs to be expanded to cover the full input range [73]. Returning back to our process, it is difficult to predict whether the relationship between the manipulated variable and controlled variable

will be linear or non-linear as there is limited research on the behaviour of the exiting jet in response to changes of EMBr current. Therefore, in our case, we will be varying our input range from 0 to 600A which is the full range of the EMBr and measure the angle of the jet as seen in Figure 5.5.

5.1.3.1.Linear Model

The first step will be to create a model for the process without any clogging present in the SEN. Process model estimation is used to create a transfer function describing the linear system dynamics. Through a process of trial and error where parameters including poles, zeros, and time delays are varied, the end result show that the relationship between EMBr current and jet angle can be described by a linear model in the form of a first order model [70].

$$G(s) = \frac{K_p}{1+sT_{p1}} \tag{5.1}$$

$$K_p = -0.0442 \tag{5.2}$$

$$T_{p1} = 1.44 \tag{5.3}$$

Where K_p represents the static gain and the T_{p1} represents the time constant.

$$Y(s) = G(s)U(s) + E(s) \tag{5.4}$$

Through Laplace transformation, *Y(s)*, *U(s)*, and *E(s)* represent the output, input, and output error of our system. The output error is modelled using a white Gaussian noise with variance λ [74].

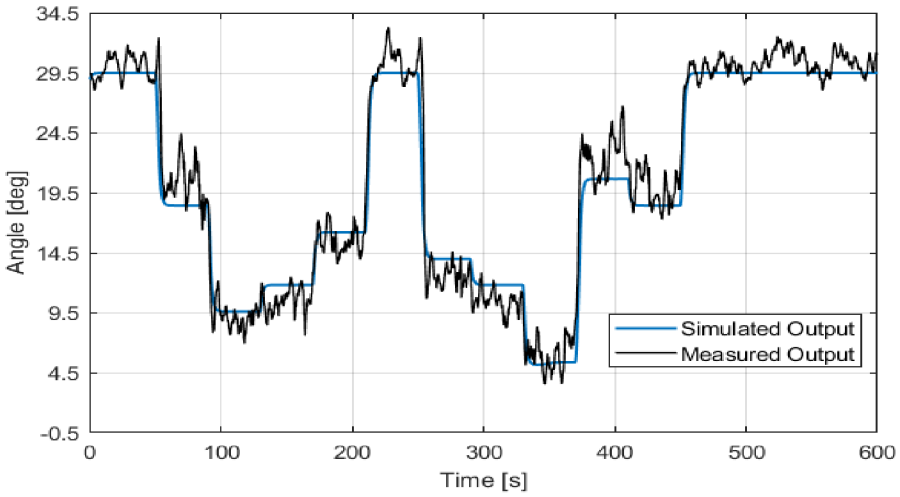

Figure 5.5. Comparison of simulated model output with measured output

Comparison of the first order model output with measurement (where the angle was calculated from the UDV data using the procedure described above) is shown in Figure 5.5. This figure gives the response to a series of random step changes of the EMBr current. It can be observed that there is a good fit between this first order model and measured data. Fast dynamics and relatively short time constant of model are due to the rapid responses of the velocity fields in the region of interest to the changes in the magnetic field produced by the brakes. It becomes clear that the relationship between brake current and jet angle can be described by a linear model in the form of the following first order model. Furthermore, second and third order models were created, and their performance were compared as shown in Table 5.1.

Table 5.1: Performance Comparison using Fit Percentage

Model	Fit Percent
1st Order Model	80.4%
2nd Order Model	82.2%
3rd Order Model	78.1%

Fit percent represents the normalized root mean squared error:

$$Fit\ Percent = 100\left(1 - \frac{\|y_{measured} - y_{model}\|}{\|y_{measured} - \overline{y_{measured}}\|}\right) \quad (5.5)$$

Although the second order model slightly outperforms the first order model, there should be a trade-off between the complexity of the model and its accuracy. In the end, the added complexity of the second order model does not improve the fit percentage significantly, which is why the first order model was selected.

5.1.3.2.Non-Linear Model

As seen in Figure 5.6, it becomes clear that the linear model from the previous section is no longer sufficient to describe the dynamic response if clogging occurs as the fit percentage goes down to 65.99%. There are two fundamental reasons for this; first, the oscillations of the angle are significantly higher with clogging. This is consistent with the results obtained by [75] where the author observed that flow turbulence increases with clogging very significantly. The turbulence kinetic energy may increase by 5 orders of

magnitude in the lower part of the nozzle. This increased turbulence is then the source of much increased jet angle oscillations and variance. Secondly, clogging evidently introduced some additional non-linearity to the response because some parts of the response are described well by linear model while the fit is unsatisfactory in other parts. This increased angle variance can be used to detect the appearance of clogging, and this will be discussed in a greater detail in the subsequent sections.

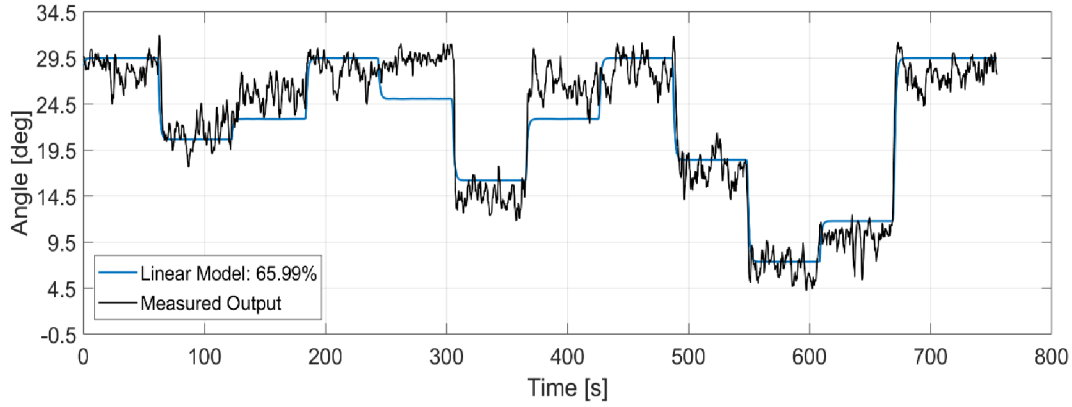

Figure 5.6. Comparison of Wiener model output with measured output

Therefore, non-linear models were investigated in order to improve the fit percentage. This led us to the Wiener model as we would like to keep the model as simple as possible while improving the fit percentage of the model. This approach is based on the concept of decoupling the linear behaviour from the non-linear behaviour. In a Wiener model the linear dynamic part is followed by a static non-linearity. In this case we are able to avoid expensive iterative optimisation methods which is an advantage of using this approach. The general Wiener model is represented as the following, where the linear difference equation is written with shift operator q^{-1}, where $y(k)q^{-i}=y(k-i)$ [73].

$$A_1(q^{-1})y(k) + A_2(q^{-1})y^2(k)+\ldots+A_l(q^{-1})y^l(k) = c_{00} + B(q^{-1})u(k-d) \tag{5.6}$$

The linear function and the static non-linearity are given as

$$A_1(q^{-1})x(k) = B(q^{-1})q^{-d}u(k) \tag{5.7}$$

$$y(k) = r_0 + r_1x(k) + r_2x^2(k)+\ldots+r_px^p(k) \tag{5.8}$$

Where the static non-linearity is given as a polynomial of order p. When both are connected in series, we obtain the simple Wiener model.

$$y(k) = r_0 + r_1 \frac{B(q^{-1})q^{-d}}{A(q^{-1})} u(k) + r_2 \left(\frac{B(q^{-1})q^{-d}}{A(q^{-1})}\right)^2 u^2(k) + \ldots \quad (5.9)$$

We will be utilizing the Wiener model for the second set of experiments; this set of experiments is used for modelling the dynamic response of the jet angle with clogging in the SEN as seen in Figure 5.8. The figure compares the response of the models to a series of random step changes to the EMBr current. The increased nonlinearity can be accounted for by adding a static nonlinearity to the linear model i.e. by using a Wiener model. The linear part of the Wiener model consists of a first order transfer function:

$$G(s) = \frac{K_p}{1+sT_{p1}} \quad (5.10)$$

$$K_p = 0.063 \quad (5.11)$$

$$T_{p1} = 1.7 \quad (5.12)$$

The output of the linear function is fed into a static nonlinear block in order to model the output nonlinearity. In this case, the Wiener model allows us to build on the linear transfer function and improve the fidelity of the model by adding a static non-linearity behaviour that has been introduced in the clogging state [71]. Both equations have similar absolute values for the time constant. The static nonlinear block in the Wiener model contains a piecewise linear function consisting of 2 breakpoints as seen in Figure 5.7. Figure 5.8 shows that the added nonlinear function improves the performance of the model by 14.74%.

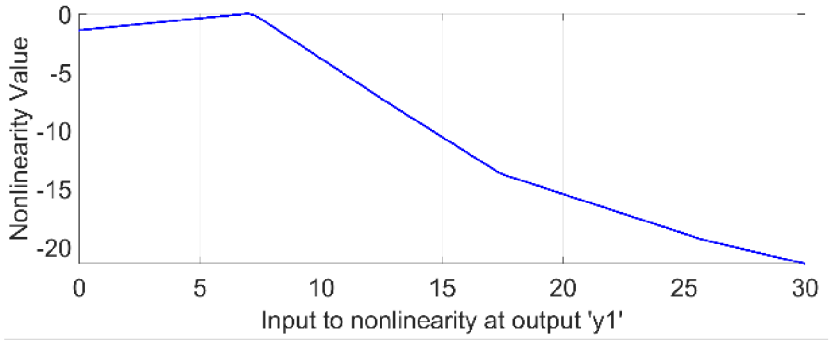

Figure 5.7. Piecewise linear function consisting of two breakpoints

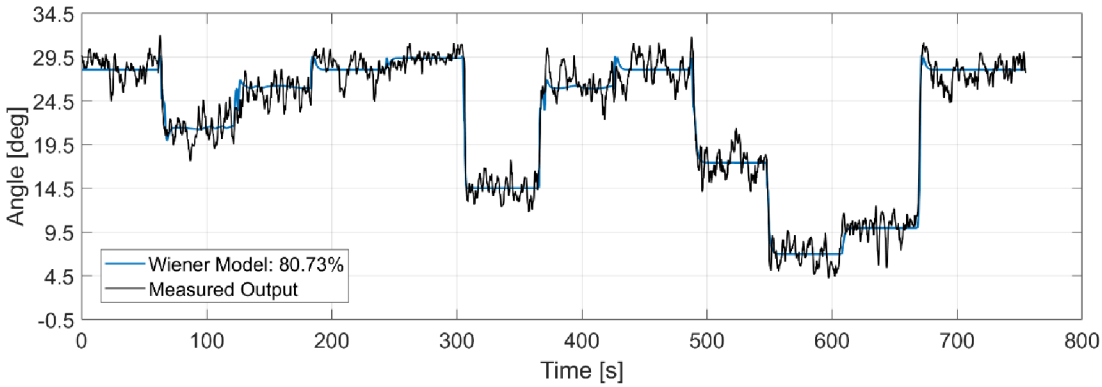

Figure 5.8. Comparison of Wiener model output with measured output

5.1.4. Controller Structure

5.1.4.1.Clogging Detection

The concept behind using the switched MPC is for the controller to modify its response depending on whether there is clogging or not in the SEN. SEN clogging changes the response of the jet angle to the changes to the current to EMBr as shown. The controller should be able to efficiently keep the angle of the jet between the optimum range in both cases of normal operation and during SEN clogging. In order to do so, the controller needs to detect if clogging has occurred during operation using information obtained from the angle of the jet. Figure 5.9 shows us the angle of the jet for two cases: Case 1 is taken from the first set of experiments where there was no SEN clogging during the measurements. Case 2 is taken from the second set of experiments where the SEN was partially clogged during the measurements. In both figures the EMBr is turned off. In the case of clogging, the angle of the jet oscillates more significantly than in the normal operation case. The signal contains higher frequencies. By taking advantage of this behaviour, we can detect the occurrence of clogging during operation by calculating the standard deviation of the signal along a moving window.

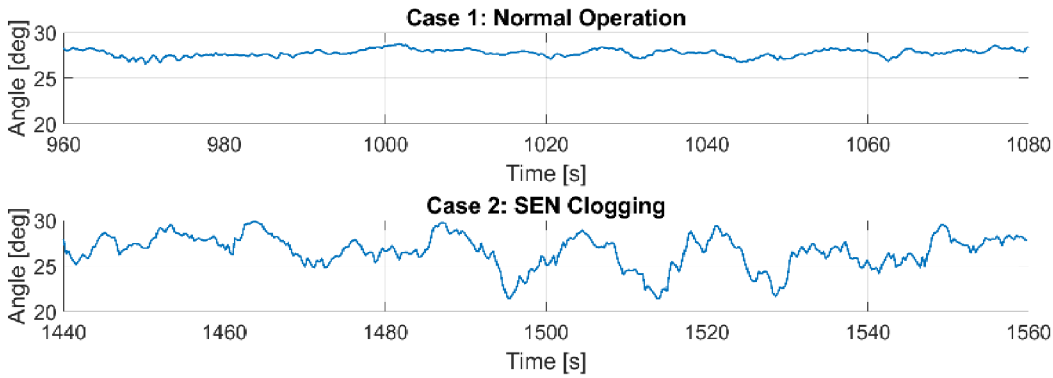

Figure 5.9. Comparison of jet angle with and without clogging

Varying the current to the EMBr results in sharp transitions in the angle of the jet. This can cause issues when calculating the standard deviation of the signal in periods where the current is changing. To tackle this issue a high pass filter is used to remove the low frequencies correlated to the changes in the current, so that the clog detection can be done while the EMBr is operational. A Finite Impulse Response (FIR) filter was used with a passband frequency of 0.1 radians/sample and stopband attenuation 60 dB. Figure 5.10 shows how the sharp changes in the angle due to current changes are filtered out while maintaining the original frequency of the signal.

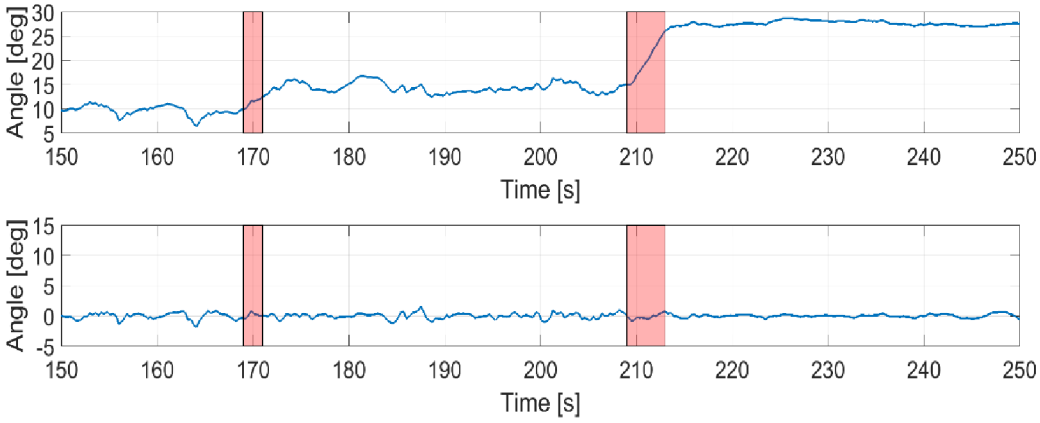

Figure 5.10. Before and after using high pass filter for jet angle. Highlighted sections show the periods where the current to the EMBr is changed.

By analysing the standard deviations of both experimental sets, we can see that in the case with clogging the filtered angle exhibited an average standard deviation above 0.6 degrees for 80% of the experimental data, while in the case with no clogging only 20% of

the experimental data exhibited this behaviour. Due to the fact that clogging in the SEN is a slow process, and that the signal from non-clogged system can exhibit a standard deviation of above 0.6 degrees at random moments, the decision on clogging should be done on multiple sequential windows to determine that the increase in standard deviation is constant, and thus confirming the presence of clogging. The controller will only confirm the presence of clogging after 10 sequential windows have been determined with a standard deviation of 0.6 degrees and above. Figure 5.11 shows clogging detection using the above algorithm. The clogging is detected after 830s from the beginning of the clogging. In the end, clogging is a slow building process that in most cases remains constant until the process is over and the SEN nozzle is replaced with a new one. This allows us to use a larger number of windows in determining the clogging so that it can be confirmed that the increase in standard deviation is due to a constant clogging, rather than random events that have affected the angle.

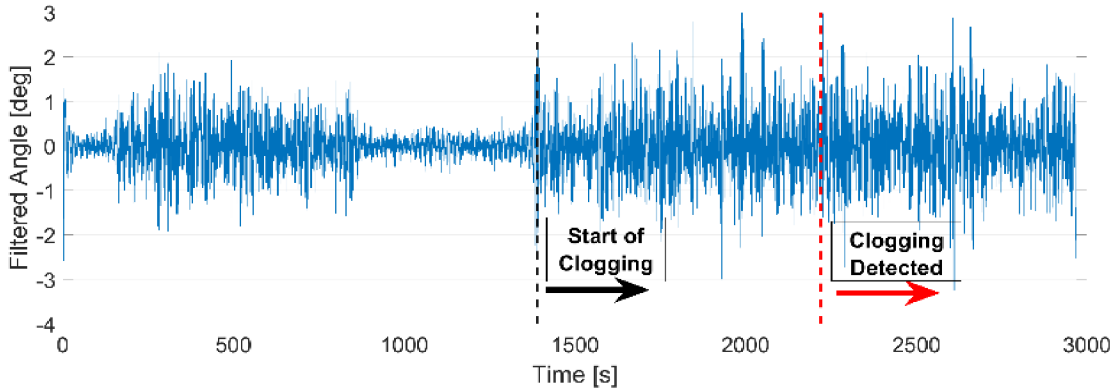

Figure 5.11. Clog detection using standard deviation of filtered angle

5.1.4.2.Model Predictive Control

Although Proportional-Integral-Derivative (PID) controllers are used in the majority of industrial applications, certain limitations make it unfavourable to apply PID controllers in specific processes. These include the difficulty of expanding the controller for MIMO processes due to interactions between loops. Also, PID controllers themselves are unable to incorporate constraints on manipulated variables and controlled variables. A possible solution for these issues is the use of Model Predictive Control (MPC). An

additional advantage of MPC is their ability to predict the future effect of control actions and optimize them in order to achieve the desired behaviour.

Model Predictive Control has been successfully implemented in many complex industrial applications due to its ability to incorporate constraints in its algorithm. Furthermore, Model Predictive Control algorithms can easily be expanded for multivariable control problems [76]–[78] which will be beneficial for this thesis in later sections. The main theory behind this control technique is the iterative, finite-horizon optimization of an internal plant model using a cost function *J* over the receding horizon. In this paper, the cost function consists of the sum of three terms:

$$J(z_k) = J_y(z_k) + J_{\Delta u}(z_k) + J_e(z_k) \tag{5.13}$$

where z_k is the vector of the quadratic program decision variables. $J_y(z_k)$ refers to the output reference tracking, $J_{\Delta u}(z_k)$ is for the manipulated variable move suppression, and $J_e(z_k)$ refers to constraint violations as seen below:

$$J_y(z_k) = \sum_{j=1}^{n_y} \sum_{i=1}^{p} \left\{ \frac{w^y{}_{i,j}}{s^y{}_j} [r_j(k+j|k) - y_j(k+j|k)] \right\}^2 \tag{5.14}$$

$$J_{\Delta u}(z_k) = \sum_{j=1}^{n_u} \sum_{i=0}^{p-1} \left\{ \frac{w^{\Delta u}{}_{i,j}}{s^u{}_j} [u_j(k+i|k) - u_j(k+j-1|k)] \right\}^2 \tag{5.15}$$

$$J_e(z_k) = \rho_\varepsilon \varepsilon_k^2 \tag{5.16}$$

where k is the current control interval, p is the prediction horizon, ny and nu are the number of plant output variables and number of manipulated variables. $y_j(k+j|k)$ and $r_j(k+j|k)$ are the predicted value and reference value of j-th plant output at i-th prediction horizon. $s^y{}_j$ and $s^u{}_j$ are the scale factor for j-th plant output and manipulated variable, respectively. $w^y{}_{i,j}$ and $w^{\Delta u}{}_{i,j}$ are the tunning weights for the j-th plant output and manipulated variable movement at ith prediction horizon. ε_k is the slack variable at control interval k. ρ_k is the constraint violation penalty weight [79]. The main control objective for the experiments conducted in this study is to maintain the jet angle in the range between optimum ranges during the operation of the casting process. The following constraints are applied on the manipulated variable to respect the limitations of the electromagnetic brake.

$$0 \leq u_1(k+i-1) \leq 600 \tag{5.17}$$

$$-100 \leq \Delta u_1(k+i-1) \leq 100 \tag{5.18}$$

5.1.4.3.Switched MPC

Following the formulation of the MPC, the next step will be to design the Switched MPC in order to deal with the two scenarios of clogged and unclogged states. Switched MPC has been successfully implemented in processes that exhibit multiple modes [80], [81]. The main concept is that the controller is able to transition between multiple MPC controllers in real time based on the operating conditions. This is usually done by designing each controller based on a specific region of the operating space. By using a switching signal, the current operating region is detected and based on this the appropriate active controller is selected.

Going back to our process; the control objective is to keep the jet angle in an optimum range. SEN clogging changes the response of the angle to the EMBr. Therefore, two different models are needed to describe the process with clogging and without clogging. By using switched MPC we can have our controller switch between two implicit MPC controllers. First MPC will be based on the model of the system without clogging, while the second MPC will be based on the model of the system with clogging. The switching signal will be the calculated standard deviation of the angle of the jet. This will allow us to select the suitable controller based on the state of the process. Each MPC will then solve a quadratic program to determine the optimal current steps for the current input signals. There are also constraints on the input current to the electromagnetic brake.

5.1.5. Testing and Results

Two sets of simulations were implemented; the first simulation included the MPC based on the linear model. In this simulation we are performing set point tracking in the case where there is no clogging and analysing the controller's response to various changes to the set point (see Figure 5.12 and 5.13). The controller is able to successfully track the set point with an average settling time of t=5s. In the end, the controller performance is shown to be sufficient for controlling the exiting jet angle. The response of the controller is fast enough for the dynamics of the system. In the second simulation we are testing the switched MPC and simulating the clogging affect to see how the controller will respond. Figure 5.14 shows that from t=0s to t=75s the model for normal operation is used, at t=75s the model is switched to the clogged model to simulate clogging in steel casters. We can

see that even without the clogging being detected by the controller, the MPC is able to perform the needed action to bring the angle of the jet to the required set point. At t=100s we simulate the clogging being detected and the switching to the second MPC that is designed for the clogging model. It is clear that the transition from the first MPC to the second occurs smoothly with the set point being tracked efficiently. At t=150s the controller is also able to effectively track the set point with the presence of clogging in the process. Figure 5.15 shows that the switched MPC is able to track the set point without exceeding the constraints on the manipulated variable which is the current in this case. However, it should be noted that the SEN clogging being analysed in this section is at a specific point between the tundish and SEN. Clogging can occur in other points in the SEN including the port nozzle. The next step should be to analyse the behaviour of the jet angle with clogging nearer to the nozzle port to see if it exhibits similar behaviour to the one in this paper.

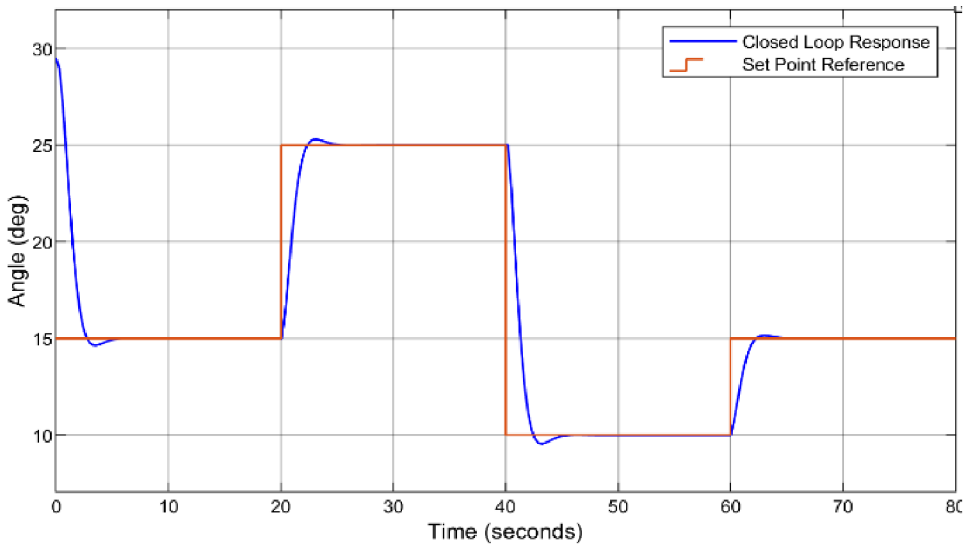

Figure 5.12. Closed loop response for set point tracking

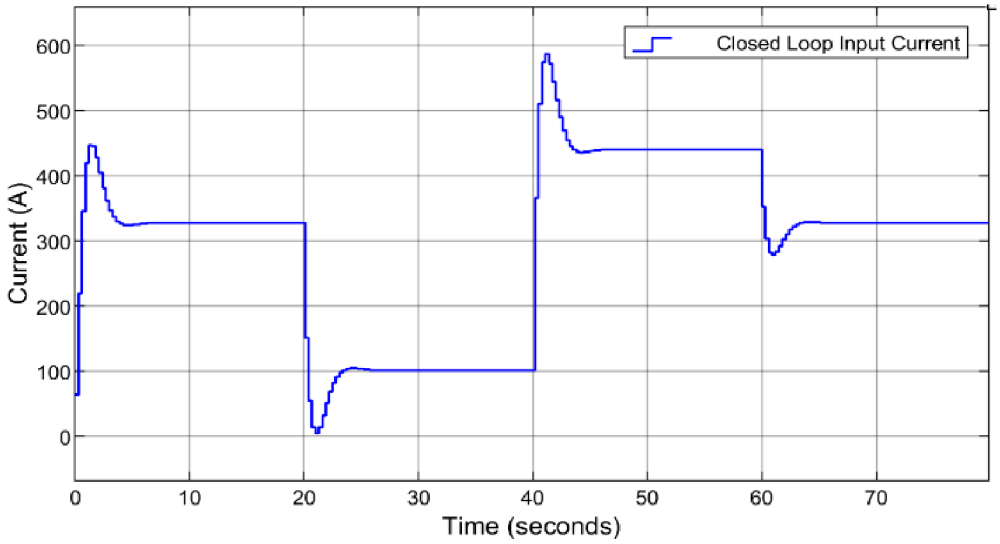

Figure 5.13. Input current for set point tracking

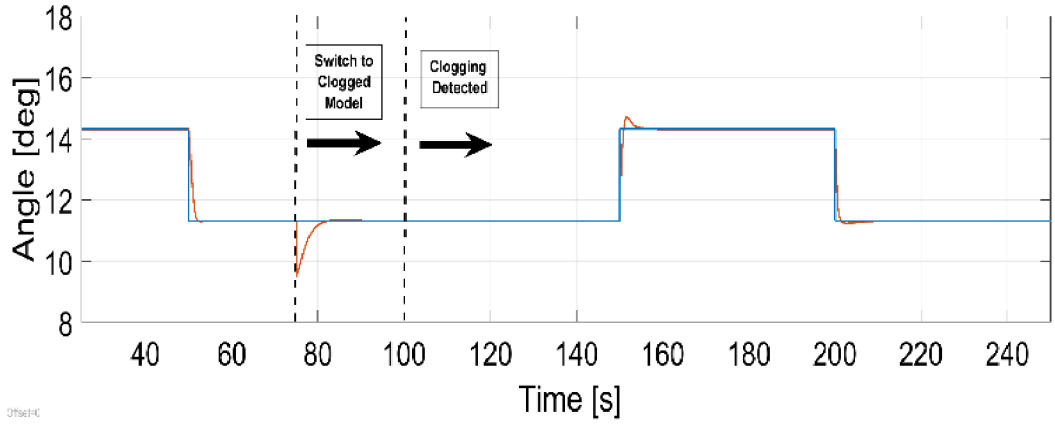

Figure 5.14. Comparison of model output with set-point reference

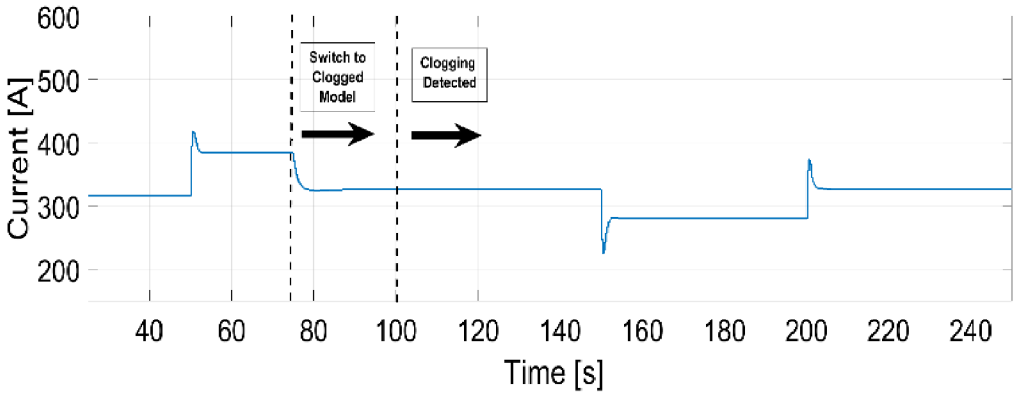

Figure 5.15. Input current for set-point tracking

5.2. Meniscus Velocity

In this section, we move away from the exiting jet to the meniscus velocity as our controlled variable. Meniscus velocity in continuous casting is critical in determining the quality of the steel, it needs to be kept between a specific range; too high velocities create excessive turbulences that can increase the potential of slug entrapment. On the other hand, too low meniscus velocities result in excessive cooling which can cause various surface defects as well [6]. Due to the complex nature of the various interacting phenomena in the process, designing model-based controllers proves to be a challenge. Therefore, a NARX neural network model is trained to describe the complex relationship between the applied current to an EMBr and the measured meniscus velocity. Adaptive Model Predictive Control (MPC) is used to deal with the non-linearity of the model by adapting the prediction model to the different operating conditions. The controller uses the EMBr as an actuator to keep the meniscus velocity within the optimum range and reject disturbances that occur during the casting process. The results in this section were published in [82].

5.2.1. NARX Neural Network Model

As mentioned in Chapter 3 UDV sensors are used to measure the horizontal velocities at the position of the sensors to provide the same information about the velocity fields. In this section, we will only concentrate on the top sensor near the surface of the mould to extract the meniscus velocity during the experiments. The measured velocities are first smoothed out using a median filter. A median filter is used in this case to maintain the fast transitions in velocity which are caused by the changes in the EMBr magnetic field.

The filtered velocities between 70 mm to 80 mm from the narrow mould wall will be averaged to provide a more accurate representation of the meniscus velocity in the midpoint between the mould wall and the SEN. Using this experimental data, a dynamic neural network with feedback connections was designed using a nonlinear autoregressive model with exogenous inputs (NARX). The NARX model is based on the linear ARX model but instead of using the weighted sum of its regressors to predict the current output, it uses a nonlinear mapping function *f* as can be seen in Equation 5.19. In our case the nonlinearity estimator will be done using the neural network in Figure 5.16. The neural network time series toolbox in MATLAB was used to design the model.

$$y(t) = f(y(t-1), y(t-2), \dots, y(t-n_y), u(t-1), u(t-2), \dots, u(t-n_u)) \tag{5.19}$$

The NARX network consists of a two-layered feedforward network. A sigmoid function is used in the hidden layer, while a linear transfer function is used in the output layer. The tapped delay line allows for previous input and output values to be stored. The input x(t) represents the current going to the EMBr, while the output y(t) represents the meniscus velocity. It is clear that a feedback connection is needed for the network to take in previous values of the meniscus velocity in order to create the dynamic model. In our case 10 hidden neurons were used, with the number of delays of 2.

$$y(t) = f(y(t-1), y(t-2), u(t-1), u(t-2)) \tag{5.20}$$

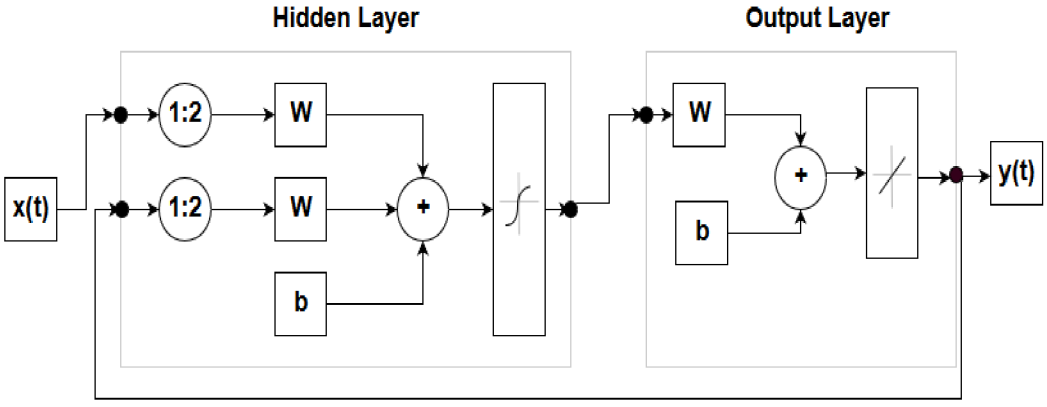

Figure 5.16. Neural Network NARX model

5.2.1.1.Testing and Validation

The data set used to train the network was obtained through experiments using the Mini-LIMMCAST setup where the current going to the EMBr was changed per time step and the meniscus velocity was recorded using the UDV sensor. The experiment consisted of random current step inputs to the EMBr between 0 to 600A. This was done in order to cover the full dynamics of the system. The data set consisted of 2750 time steps for both the input and output; 70% of the data set was used for training, 15% for validation and 15% for testing. It is important to note that the network is trained in the open loop form rather than closed loop; it is more efficient to train the network with the accurate past output values rather than the feedback from the closed loop form. The training algorithm used for the network was Levenberg-Marquardt.

Figure 5.17 illustrates the error autocorrelation which is typically used to validate the performance of the network. The best-case scenario should be that the only one nonzero value is at lag 0; this means that the prediction errors are completely uncorrelated with each other. However, in most cases it is expected that the error falls within the confidence limits of 95% around zero. Furthermore, Figure 5.18 shows another performance validation which is to check the cross correlation of the errors with the input x(t). It is clear from Figure 6 that some lags do exceed the confidence limit, which shows that the network can be further improved. The number of hidden neurons and the number of delays were increased during the simulations, however it showed that the more complex structure did not significantly improve the performance of the model, and in some cases resulted in overfitting of the data. The better option for improving the performance is to use a larger data set, however in our case the data set was restricted to the size of the experimental data obtained from the Mini-LIMMCAST. On the other hand, Figure 5.18 shows that the correlation between the error and the input lie within the confidence limit.

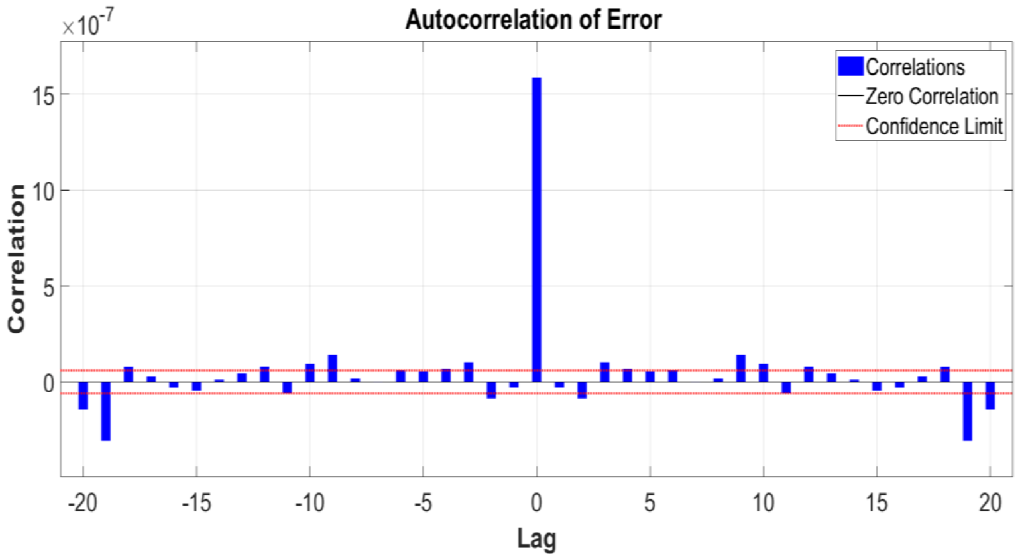

Figure 5.17. Autocorrelation of error

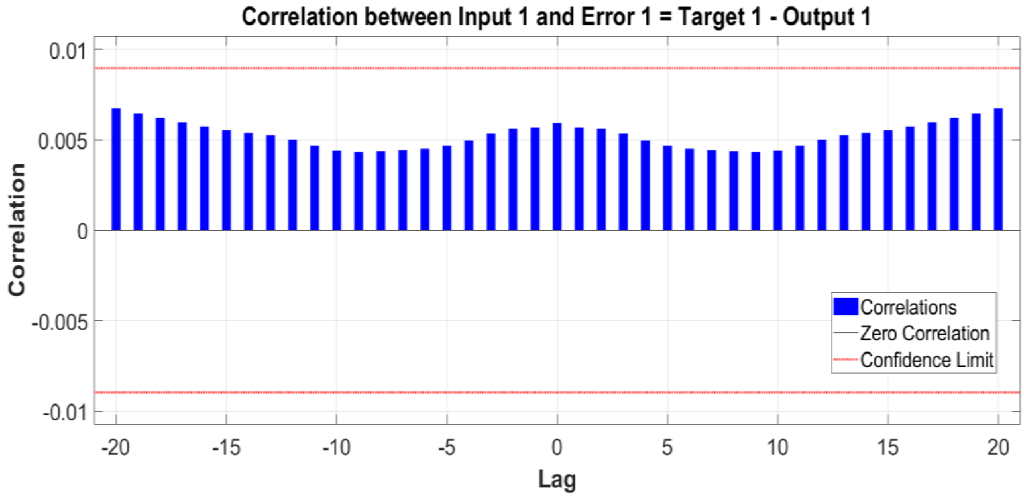

Figure 5.18. Correlation between input and error

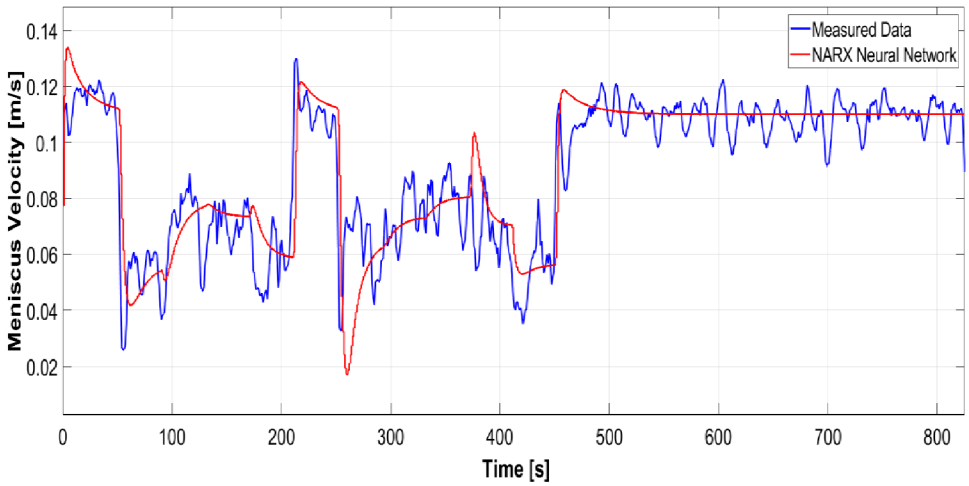

Figure 5.19. Comparison of neural network output with experimental data for random current input

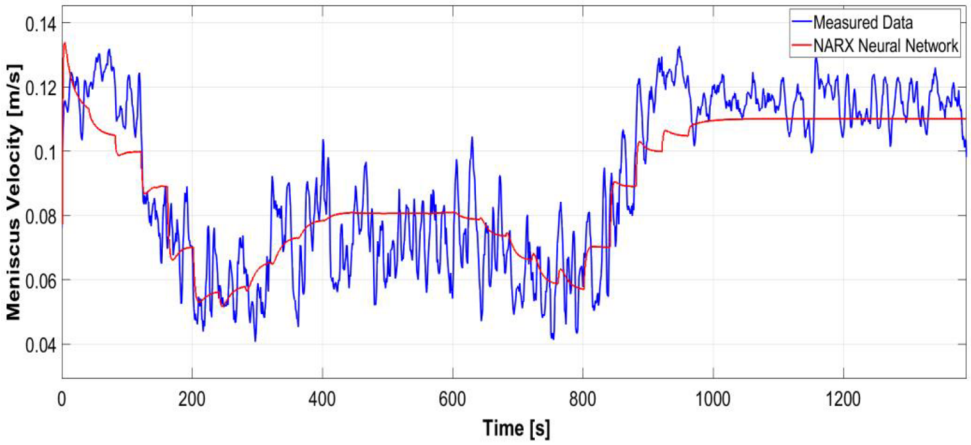

Figure 5.20. Comparison of neural network output with experimental data for step-wise current input

Figure 5.19 compares the output of the NARX neural network model with the measured velocities from the random current input experiment. The model is able to track the changes in meniscus velocity without overfitting the data, however it can be seen that the performance of the network can further be improved. In the end, the model was validated using a separate experimental dataset from the Mini-LIMMCAST as can be seen in Figure 5.20. In this experiment the current going to the EMBr was changed in steps of 50A from 0 to 600A and back to 0A. The model output is compared to the measured meniscus velocity, where it shows that it is able to track the changes in the velocity efficiently and is able to describe the nonlinearity in the relationship between the current to the EMBr and the meniscus velocity.

5.2.2. Adaptive MPC

The main objective of the control loop is to maintain the meniscus velocity within the optimum range and to reject disturbances during the process. Besides minimum and maximum limits related to the optimum range of the meniscus velocity, there is also the maximum limit on the current of the EMBr. As it is evident from the previous section, the controlled plant is not only nonlinear but there are other issues as well. This nonlinearity is not well amenable to analytic description and it may be time varying. This would complicate the use of nonlinear MPC. We also regarded it as desirable to keep the beneficial features of MPC based on linear models and quadratic programming. For all of these reasons our approach of choice is to implement adaptive MPC where online model estimation is used to update the internal plant model in order to achieve a reasonable level of control performance with this nonlinear plant. This adaptive MPC is based on continuously updated linearized model. For this purpose, NARX Neural network is linearized and converted to the discrete time state space.

A recursive polynomial model estimator is used for the online model estimation. This is used to update the internal model of the MPC by linearizing the NARX model. An ARX model is estimated as the following:

$$A(q)y(t) = B(q)u(t - n_k) + e(t) \tag{5.21}$$

Where q is the time-shift operator x, u(t) is the input, y(t) is the output, e(t) is the error, and nk is the input delay. The values of u, y, na, nb, and nk are known beforehand so that the algorithm is able to estimate A and B at every time step. A Kalman filter is used for the recursive estimation algorithms, the general form of the infinite-history recursive estimation algorithm can be found below [83]:

$$\hat{\theta}(t) = \hat{\theta}(t - 1) + K(t)(y(t) - \hat{y}(t)) \tag{5.22}$$

Where θ(t) is the parameter estimate at t, and ˆy(t) is the prediction of y(t) based on observations until time t-1. y(t) is the observed output at time t, while the gain K(t) defines how much the prediction error y(t)−ˆy(t) affects the update of the parameter estimate. Figure 5.22 shows the overall structure of the adaptive MPC; the recursive polynomial estimator model linearizes the NARX model per time step and updates the internal model of the MPC. By using this linearized model, we can avoid using a nonlinear MPC and use the quadratic cost function shown in Equation 5.13 in the optimizer.

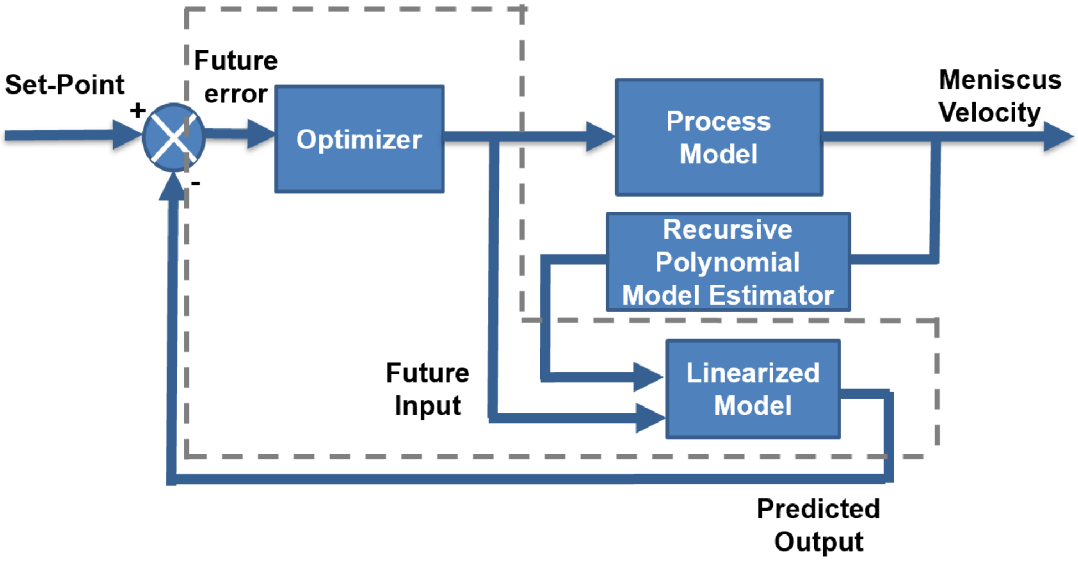

Figure 5.21. Adaptive MPC connected with process model (NARX model)

5.2.3. Testing and Results

The first control experiments concentrate on set-point tracking where the controller's response to various changes to the set point is analysed (see Figure 5.22 and 5.23), four different set points were used. Constraints on both the manipulated variable and the manipulated variable rate were implemented in the optimization problem, while the tuning weight for manipulated variable tracking was set to 0 to omit the term from the cost function. The controller was able to successfully track the set point with the settling time ranging from 50 to 100s. It is important to note that at the beginning of the simulation the Recursive Polynomial Model Estimator needs time to reach an adequate model. This explains the oscillatory behavior from 0 to 400s. In this case the constraints on the manipulated variable are applied after this period to allow the model estimator to reach an adequate model.

The second set of control experiments concentrate on disturbance rejection (see Figure 5.24 and 5.25) which is the main objective of this study. One of the main disturbances in the continuous casting process is the changing of the casting speed. The casting speed is changed sporadically throughout the process; it would be valuable to see if an automatic control loop can keep the meniscus velocity in the optimum range and reject

the effect that might occur from changing the casting speed. The disturbance from changing the casting speed will be applied at the output of the model; increasing the casting speed results in an increase in the meniscus velocity.

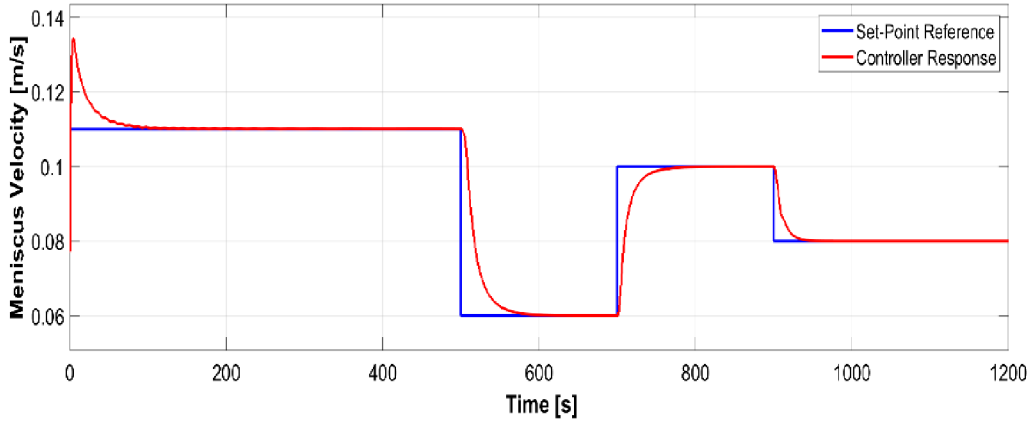

Figure 5.22. Closed loop response for set point tracking

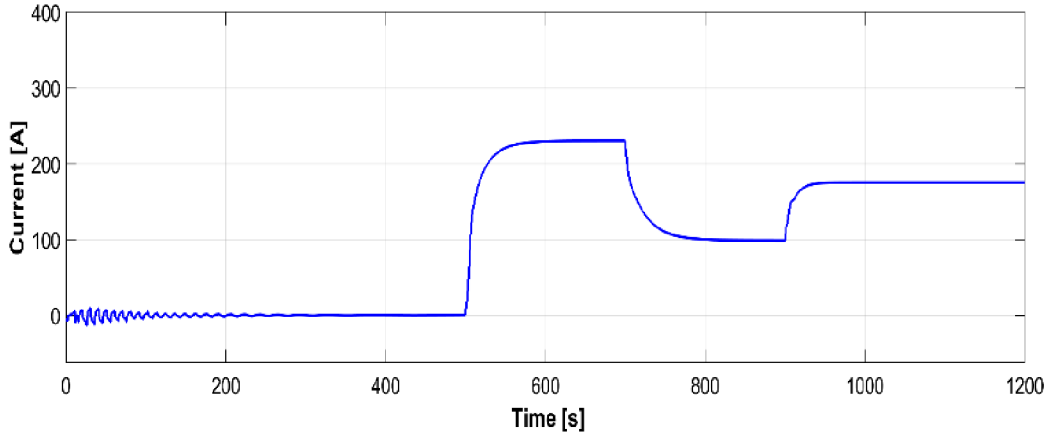

Figure 5.23. Input current for set point tracking

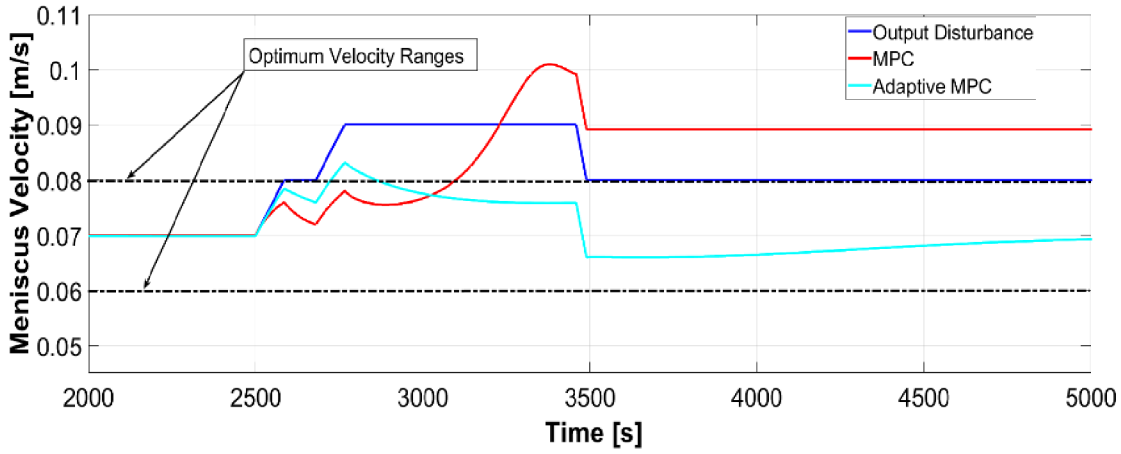

Figure 5.24. Closed loop response for disturbance rejection

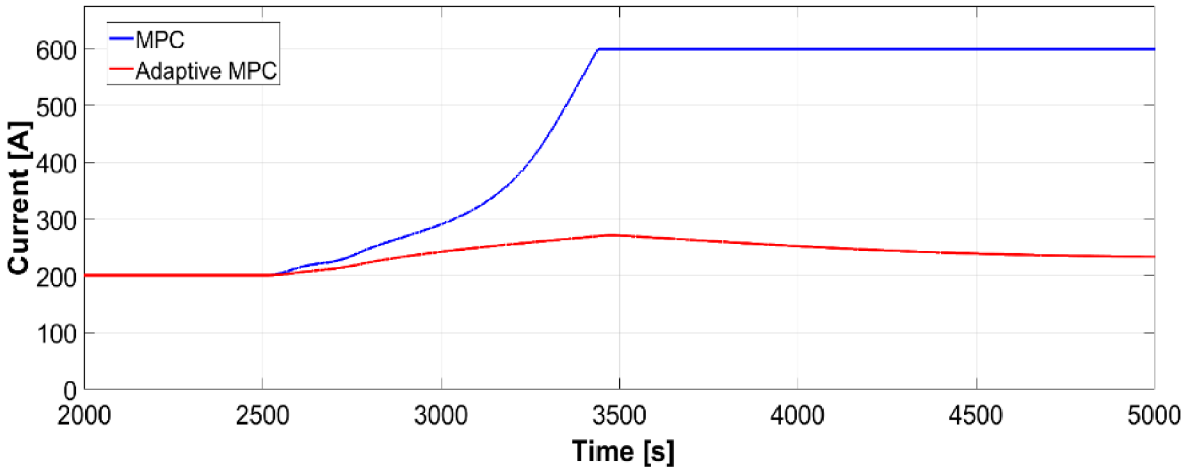

Figure 5.25. Input current for disturbance rejection

In Figure 5.24 we compare the performance of a conventional MPC with the adaptive MPC. The disturbance on the output was taken from [6]. Both the MPC and adaptive MPC respond to this disturbance in order to keep the meniscus velocity between the optimum ranges. In the case of the adaptive MPC, the velocity slightly goes beyond the range at T=2725s but it is then brought back to the optimum range at T=2860s. On the other hand, the conventional MPC goes beyond the optimum range at T=3100s and is unable to bring the velocity back to the optimum range for the remainder of the experiment. This is due to the saturation that occurs in the manipulated variable as shown in Figure

5.25. We can clearly see here that the adaptive MPC outperforms the conventional MPC due to its ability to deal with the nonlinearity of the system, especially at the higher current ranges of the EMBr where this non-linearity is even more present. It is important to note that the problem faced by the conventional MPC can be resolved by increasing the weight for the manipulated variable rate, therefore forcing the controller to use smaller increments. However, this results in a poorer controller response compared to the adaptive MPC.

5.3. MIMO Control Loop

Previous experiments have included only the EMBr as the manipulated variable; the next step will be to extend the control loop to multiple input-multiple output by using both EMBr and stopper rod to control the flow in the mould. In this section, we are moving away from the meniscus velocity and concentrating once again on the exiting jet. Although section 5.2 shows that the meniscus velocity can be controlled and kept within optimum ranges using the EMBr, there is a more direct effect on the exiting jet from our actuators. For this reason, we are basing our MIMO controller on features related to the exiting jet including the jet impingement point and the jet velocity. The results in this section were published in [84].

5.3.1. Extracting Controllable Features

In order to avoid using all velocity fields in the region, the concept of feature extraction is used to isolate the specific features of the flow that are the most useful for indicating whether the flow is optimal or not. For the case of the continuous caster, we need to determine the specific features of the flow in the mould that can help improve the quality of the steel, and at the same time can be controlled using our manipulated variables. The two features chosen in this paper for control are the jet impingement point on the narrow wall, and the velocity of the exiting jet.

5.3.1.1. Jet Impingement

The importance of the jet impingement point is analysed in [10] where a deeper impingement into the mould correlated with higher slag entrapment and argon bubbles being trapped deep in the mould. Furthermore, the importance of the velocity of the exiting jet is shown by Thomas [11] where the strength of the jet can affect the steel shell at the

impingement point on the narrow face wall where it impinges. Additionally, the strength of the jet influences the shape of the meniscus. The jet impingement point defines how deep or shallow the jet impinges into the mould. The optimum case is to keep the jet as close to the horizontal baseline as possible to ensure a shallow impingement. As shown in Figure 5.26, this feature can be quantified by calculating the mean value of the velocity field between UDV sensors 5 to 7 (−0.07 m to −0.09 m from the surface level). If the value increases, it is more likely that the exiting jet is oscillating in this region. The value of the mean velocity will be used as the controlled variable.

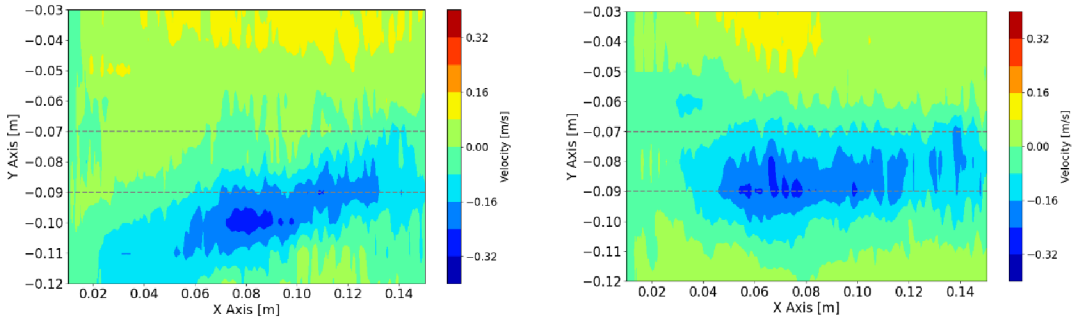

Figure 5.26. Reconstruction of velocity profile with identified shallow region to quantify jet impingement (a) t = 300 s, (b) t = 800 s.

5.3.1.2.Jet Velocity

The idea of using the velocity of the exiting jet is based on section 5.1 where a straight line is used to represent the exiting jet. The shape of the jet can be identified by scanning for every vertical line in the velocity map for the largest negative velocity and fitting a line using linear regression which would then represent the exiting jet. In this section, we will be extending this concept to include a more realistic shape of the jet, which has sometimes a more 'banana' like shape. In order to model this adequately, a third-degree polynomial is used to fit the shape of the jet during each captured frame as shown in Figure 5.27. It is clear that the polynomial can track the movement and shape of the jet efficiently. The controlled variable is the overall velocity of the jet and is the mean of the velocities along the polynomial.

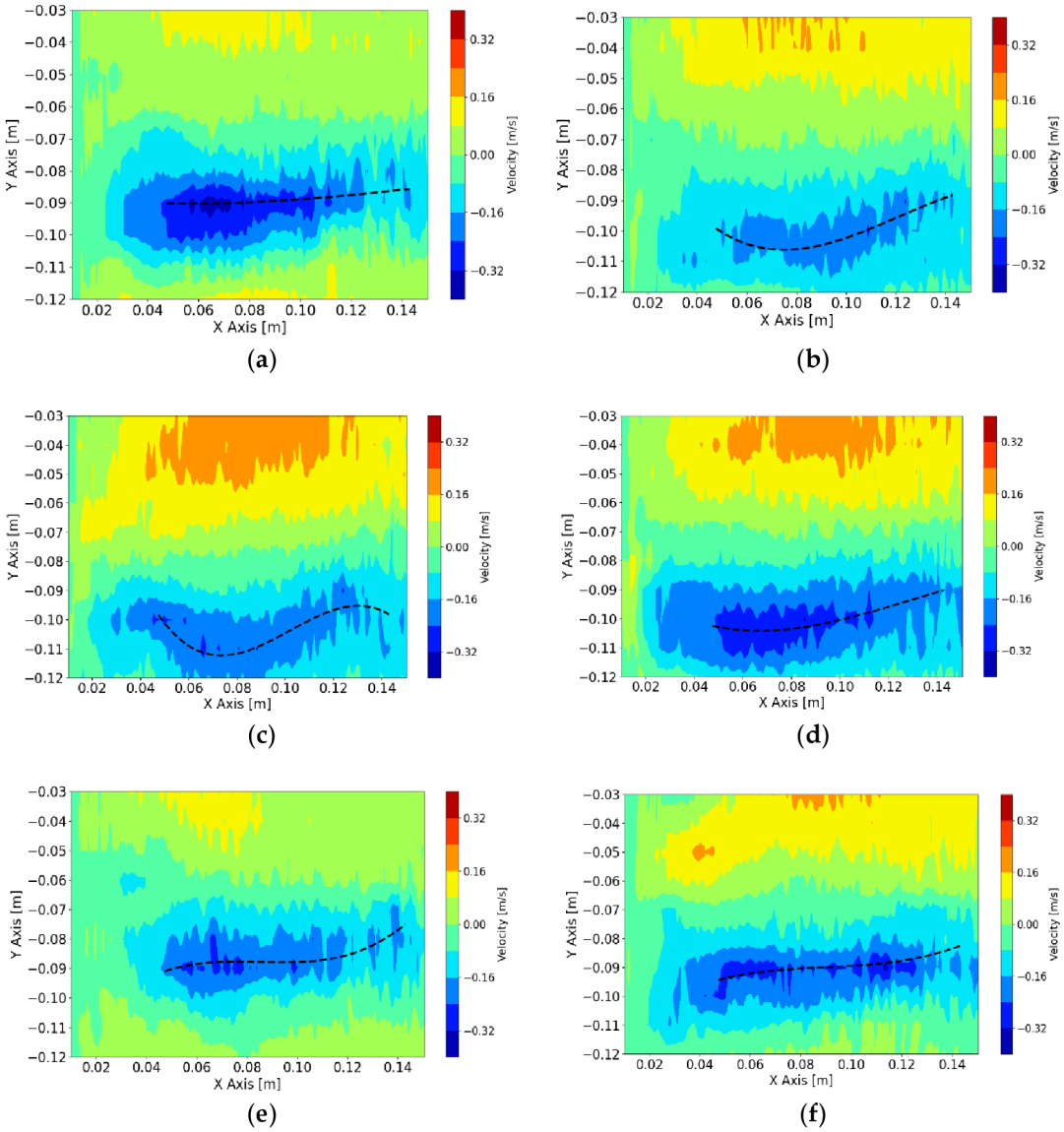

Figure 5.27. Reconstruction of velocity profile with tracking of jet shape to quantify jet velocity, (a) t = 200 s, (b) t = 400 s, (c) t = 500 s, (d) t = 600 s, (e) t = 800 s, (f) t = 1050 s.

5.3.2. State Space Estimation

A black-box model is created based on both extracted features from the UDV measurements and applying system identification to determine the dynamic relationship between the inputs and outputs. A 2-input, 2-output model is created where the inputs are the current of electromagnetic brake and the stopper rod position, while the outputs are the jet impingement point and the jet velocity. The current of the brake was varied from 0 to 600 A, while the lifting of the stopper rod position was between 5–10 mm.

As seen in Fig 5.28 and 5.29, random input steps are applied to both the electromagnetic brake and stopper rod position to excite the full dynamics of the process. It becomes clear that both features have fast dynamic responses to the manipulated variables. Figure 5.28a shows that increasing the current of the brake significantly increases the jet impingement value which correlates to a shallow impingement point. Furthermore, increasing the current of the brake increases the jet velocity. However, this effect is less significant. On the other side, increasing the stopper rod position also lifts the impingement point, as shown in Figure 5.28b, but the effect is less significant in comparison with the strength of the brake, while the effect is more pronounced for the jet velocity.

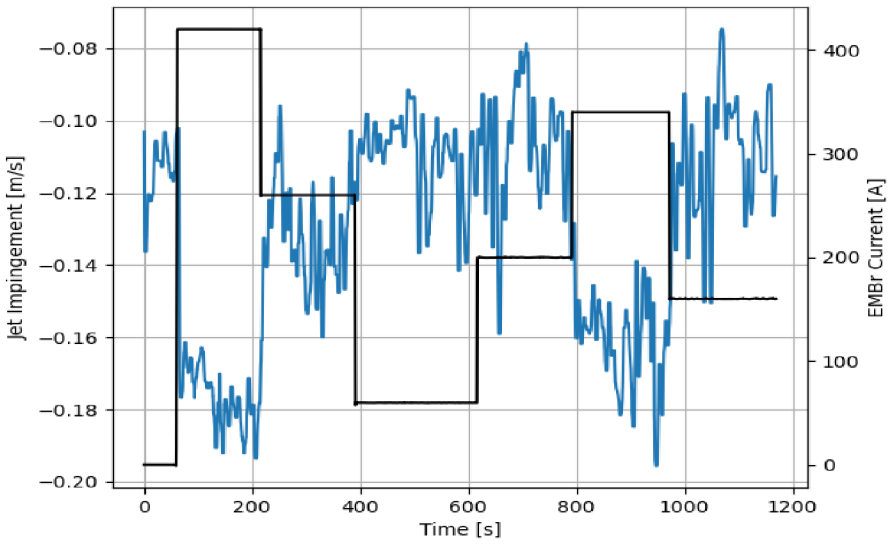

(a)

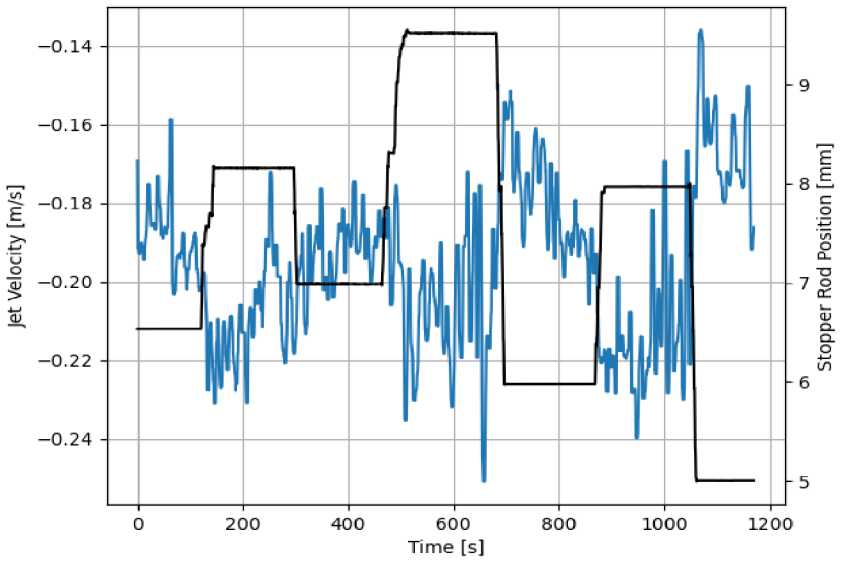

(b)

Figure 5.28. Measured response of jet impingement to manipulated variables, (a) Electromagnetic brake current, (b) Stopper rod position.

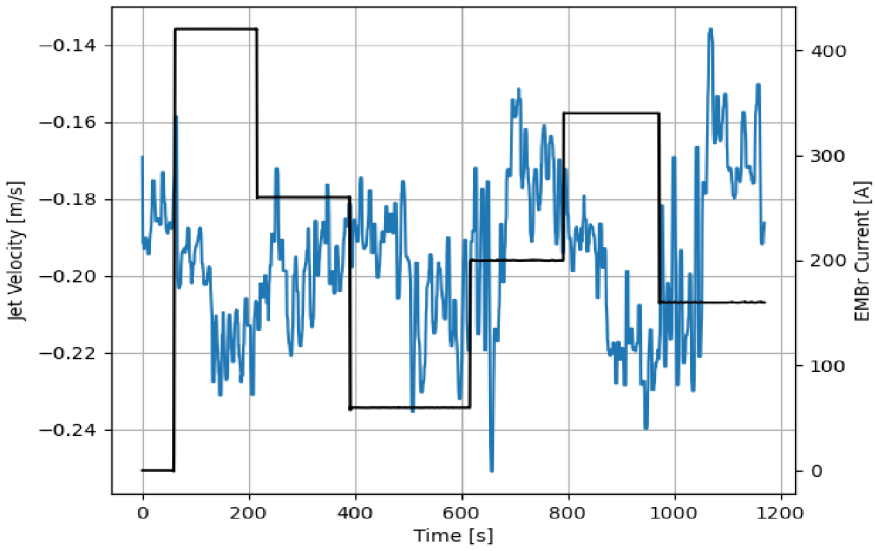

(a)

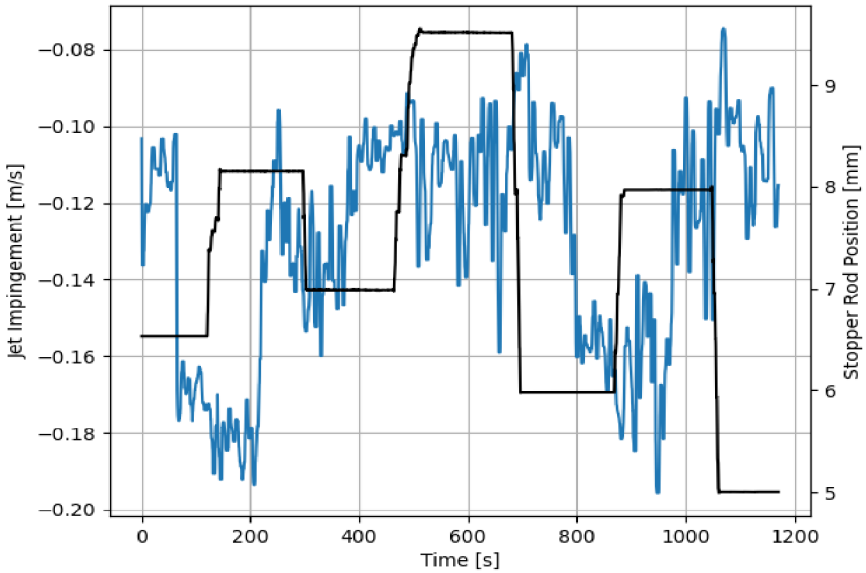

(b)

Figure 5.29. Measured response of jet velocity to both manipulated variables, (a) Electromagnetic brake current, (b) Stopper rod position.

State space estimation using subspace method was applied to create a 4th order discrete state space model using subspace method in the form:

$$\dot{x}(kT+T) = Ax(kT) + Bu(kT) + Ke(kT) \tag{5.23}$$

$$y(kT) = Cx(kT) + Du(kT) + e(kT) \tag{5.24}$$

where A, B, C, D and K are the state-space matrices. Disturbance component K is set to 0, while the sample time T = 0.3 s. u(kT) represents the input to the system which are the current of the electromagnetic brake and position of the stopper rod, while y(kT) represents the output which are the jet impingement and velocity. The output of the state space model was compared with the measurement output in Figure 5.30 and 5.31. The model is able to track the deterministic part of the signal which is the dynamic response due to the changes to the manipulated variables. The stochastic part of the signal that is due to the turbulent nature of the flow [4] is not described by the model. However, it turned out that we do not need to describe this part of the signal to build the model-based controller.

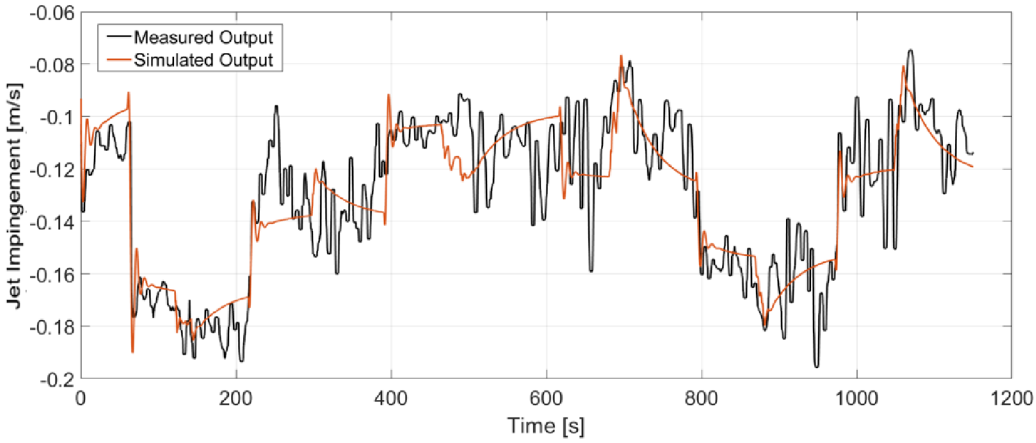

Figure 5.30. Comparison of the output of identified model with the measured output for jet impingement. The deterministic part of the output relevant for model-based control is captured sufficiently by the model.

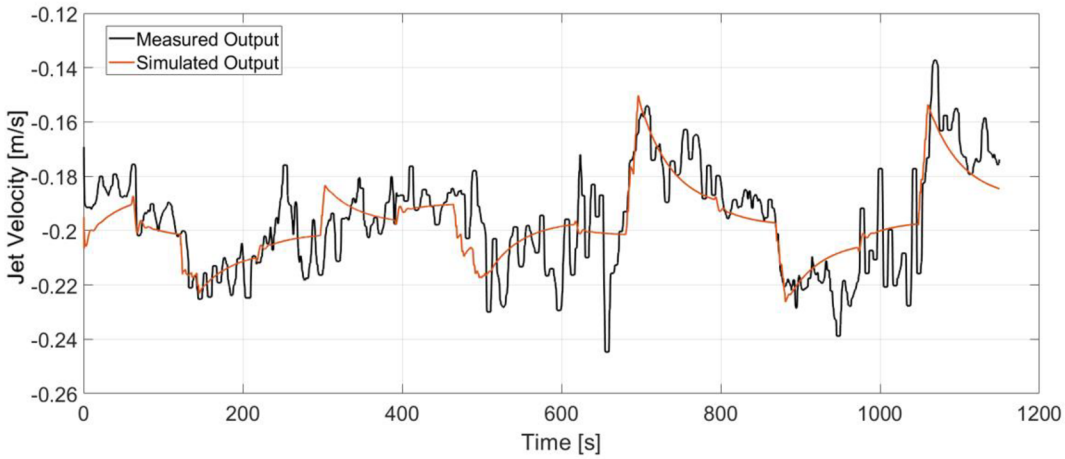

Figure 5.31. Comparison of the output of identified model with the measured output for jet velocity. The deterministic part of the output relevant for model-based control is captured sufficiently by the model.

By analyzing the pole-zero plot of the discrete system it becomes clear that we are dealing with a non-minimum phase system due to zeros outside the unit circle as seen in Figure 5.32. Although unstable zeros do not always result in inverse response in the case of discrete time systems, this system features inverse response and this poses an additional difficulty for control. One way to tackle this issue is to use predictive control such as Model

Predictive Control. In this way the controller can predict the future changes in the output and anticipate this initial change in direction before settling to the steady state value.

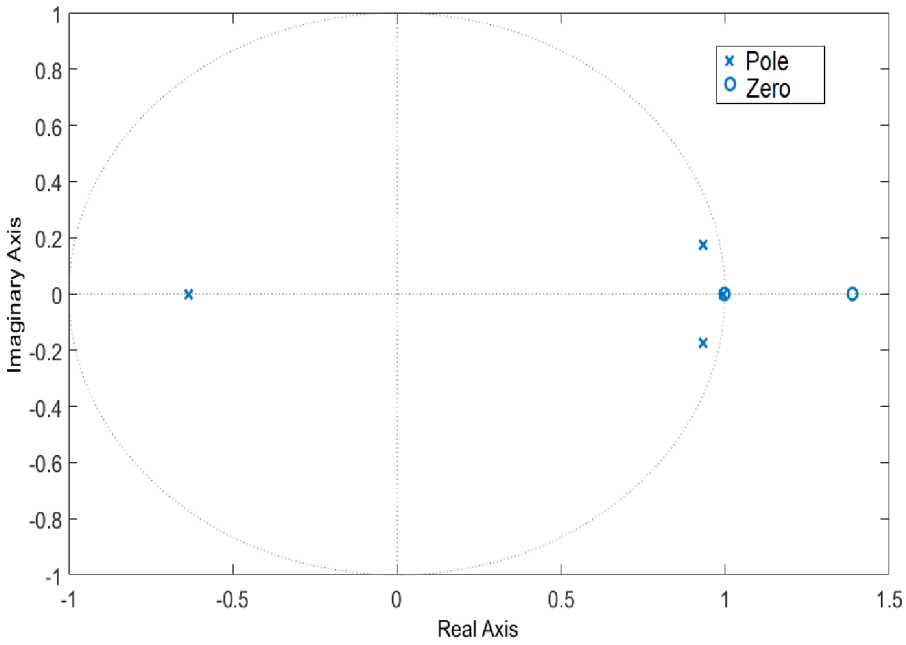

Figure 5.32. Pole-Zero plot for identified discrete model indicating a non-minimum phase system.

5.3.3. MPC Based on MIMO Model

As mentioned before, MPC algorithms can easily be expanded for multivariable control problems. The cost function J can be expanded to include multiple controlled and manipulated variables. Therefore, we will be using the cost function shown in section 5.1.4 and expanding it to our MIMO system. The main control objectives for the experiments conducted in this section are to achieve a shallow jet impingement and maintain the jet velocity within an optimum range. The first controlled variable $y_1(k+i-1)$ is the jet impingement, while the second controlled variable $y_2(k+i-1)$ is the jet velocity. The following constraints are applied on the manipulated variables to respect the limitations of both the electromagnetic brake and stopper rod:

$$0 \leq u_1(k+i-1) \leq 600 \tag{5.25}$$

$$5 \leq u_2(k+i-1) \leq 10 \tag{5.26}$$

$$-100 \leq \Delta u_1(k+i-1) \leq 100 \tag{5.27}$$

$$-1 \leq \Delta u_1(k+i-1) \leq 1 \tag{5.28}$$

where the first manipulated variable $u_1(k+i-1)$ is the current of the electromagnetic brake, while the second manipulated variable $u_2(k+i-1)$ is the position of the stopper rod. The proposed controller parameters for the MPC are listed in Table 5.2. In this case, avoiding large increments in the manipulated variables is desirable in order to create a more robust performance from the controller. Although this will compromise the reference tracking, increasing the manipulated variable rate weights will help compensate for the changes in the velocities due to the turbulent flow that is not fully described by the internal model of the controller.

Table 5.2. Model predictive control design parameters.

	Values
Sample Time (T_s)	0.50
Prediction Horizon (p)	10
Control Horizon (m)	4
Output Variable Reference Tracking Weight (w^y)1	0.06
MV1 Reference Tracking Weight	0
Manipulated Variable Increment Suppression Weight ($w^{\Delta u}$)1	1.68
Output Variable Reference Tracking Weight (w^y)2	0.06
Manipulated Variable Increment Suppression Weight ($w^{\Delta u}$)2	1.68

5.3.4. Testing and Results

Figure 5.33 illustrates the control loop implemented in the following experiments. The algorithm starts by processing the raw data from the UDV and constructing the velocity profile in the desired region of the mould. The next step is to extract the necessary features from the velocity profile including the jet impingement and jet velocity. These features can then be processed by the controller where a set-point reference for both controlled variables are implemented. Lastly, based on the error between the set-points and

the controlled variables, the controller decides how to change both actuators utilizing the internal prediction model and cost function.

In Figure 5.34 and 5.35 the dynamic response of the system to the changes in the set-points is presented. A stochastic signal is superimposed at the output to emulate the effect of turbulence seen in Figure 5.28 and 5.29. At t = 100 s a negative step input is applied to both set-points, while at t = 250 s a positive step input is applied. The figures show that the controller can track both set-points in the positive and negative step changes. Both dynamic responses have a settling time of ~20 s, although the jet velocity overshoots the set-point before settling down. Furthermore, Figure 5.36 and 5.37 show the manipulated variables during the experiments. The controller can achieve the control objectives without exceeding the constraints on the manipulated variables. In the end, these optimal conditions promote the optimal double roll pattern by avoiding a deeper impingement into the mould. This allows for the formation of sufficient upper flow circulations as seen in Figure 2 that prevents the entrapment of impurities. Furthermore, it should be noted that the inputs and outputs of this system are coupled as shown in Figure 5.28 and 5.29. Both manipulated variables influence both controlled variables. This should be taken in consideration when deciding the values for the set-points for the controller. Moreover, the optimal values for the jet impingement and jet velocity chosen for these experiments have been selected after a careful literature review and detailed analysis of the measured velocity fields from Mini-LIMMCAST. In the future, the ideal way to select these values for industrial application would be to observe the quality of the steel product after solidification to identify the optimum values needed to avoid defects in the steel.

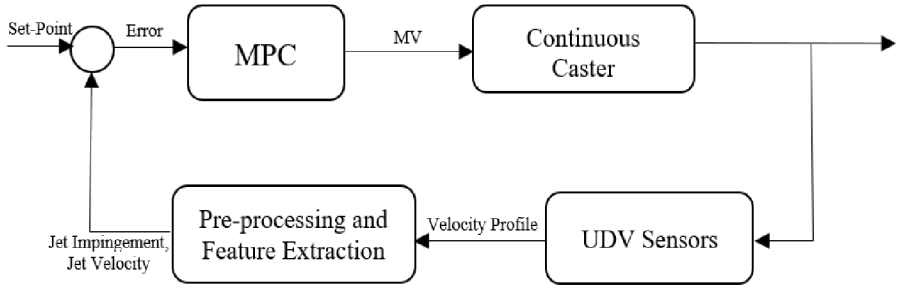

Figure 5.33. Control loop based on measured velocity profile from ultrasound Doppler velocimetry.

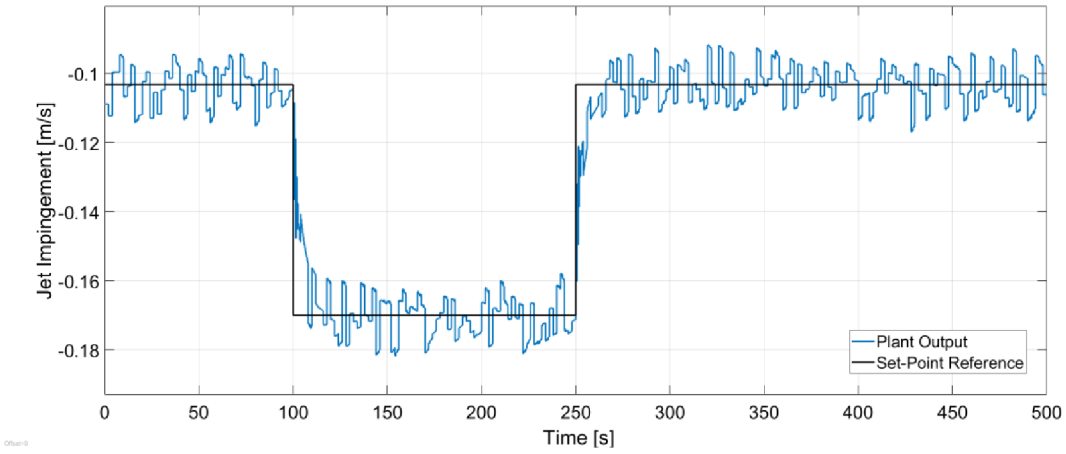

Figure 5.34. Closed loop response of jet impingement for set-point tracking.

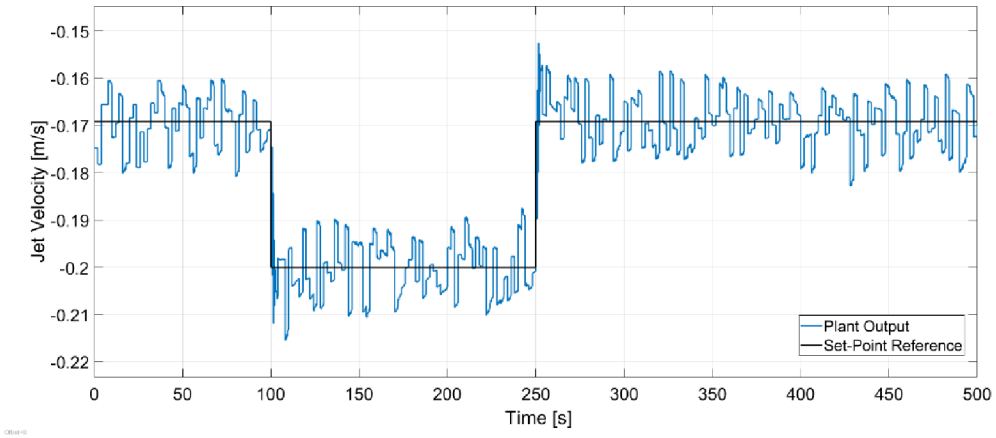

Figure 5.35. Closed loop response of jet velocity for set-point tracking.

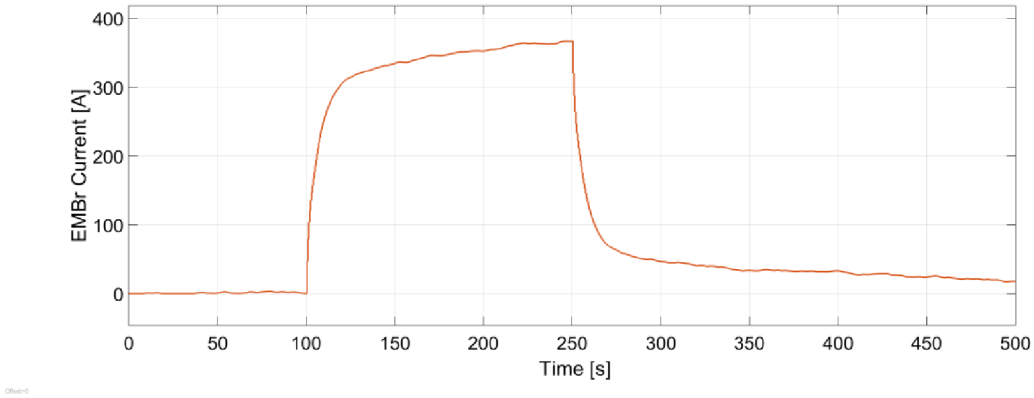

Figure 5.36. Changes of electromagnetic brake current generated by the controller to track the jet impingement. The manipulated variable does not exceed the constraints of the brake.

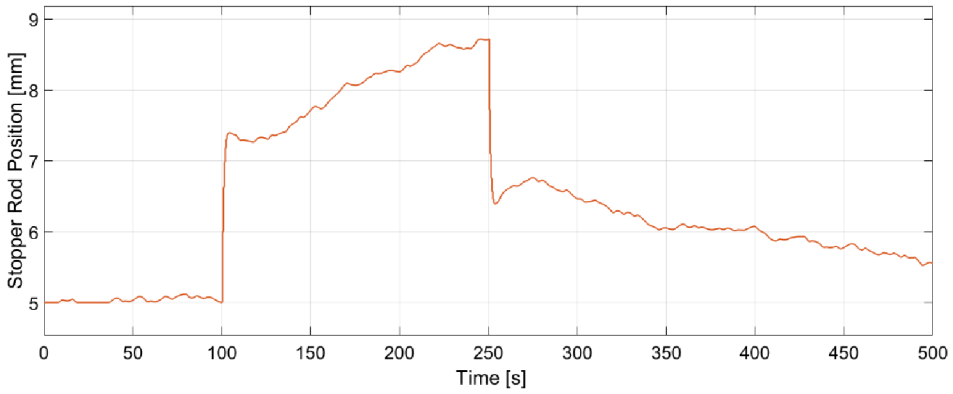

Figure 5.37. Changes of the stopper rod position generated by the controller to track the jet velocity. The manipulated variable does not exceed the constraints of the stopper rod.

6. Control Loop Structure Based on CIFT

CIFT is a tomographic sensor that is able to measure the multi-dimensional velocity fields of conductive fluids; this is done by measuring the perturbations of an applied magnetic field caused by the flow of the conductive fluid. Similarly, to UDV, this sensor can be applied to the mould of the continuous caster in order to provide two-dimensional flow field measurements. While UDV is able to obtain velocity component in one direction of the ultrasound beam, CIFT is able to measure the three-dimensional velocity fields.

The main concept of the CIFT technique relies on the flow of the conductive liquid going through a magnetic field created by the CIFT transmitter sensors. This creates electrical currents in the mould which results in an induced magnetic field. The induced magnetic field is measured by the receiver sensors and is used to reconstruct the velocity field in the mould. As shown in Figure 6.1, two excitation coils are placed, one above and one below the poles of the EMBr. To measure the flow-induced magnetic field, fourteen coils were placed, seven on each narrow side of the mould. The velocity field reconstruction depends on the inversion of the linearized integral equations shown in Equation 5.29 and 5.30 [85].

$$b(r) = \frac{\mu_0 \sigma}{4\pi} \iiint_V \frac{\left(v(r') \times B_0(r')\right) \times (r - r')}{|r - r'|^3} dV' - \frac{\mu_0 \sigma}{4\pi} \oiint_S \frac{\varphi(r) n(r') \times (r - r')}{|r - r'|^3} dS' \tag{5.29}$$

$$\varphi(r) = \frac{1}{4\pi p(r)} \iiint_V \frac{\left(v(r') \times B_0(r')\right) \cdot (r - r')}{|r - r'|^3} dV' - \frac{1}{4\pi} \oiint_S \frac{\varphi(r) n(r') \cdot (r - r')}{|r - r'|^3} dS' \tag{5.30}$$

From these set of equations, the flow induced field b(r) is computed outside of volume V of the fluid under the influence of the primary field B_0 (r'). It is assumed that the boundary S= dv is insulating, and the conductivity rho of the liquid is homogenous. Phi represents the electric scalar potential, while v(r') is the velocity of the liquid. r and r' are vectors in the 3-D Euclidian space. While p(r) is a factor determined by the shape of the boundary surface [86]. The equations are solved by discretising the volume of the liquid, which leads to a system of linear equations containing the magnetic flux density and the

velocity field in the discretized volume. In the end, we are left with a linear inverse problem which is resolved in order to reconstruct the velocity field from the measured magnetic field. Figure 6.2 shows the reconstructed velocity profile from an experiment conducted on the Mini-LIMMCAST setup. The figure shows that we are able to reconstruct both sides of the mould, in this case we can see a clear double roll flow in the mould.

In this chapter, we will extend the techniques used for UDV measurements to CIFT measurements for the purpose of control. The exiting jet angle will be obtained from the 3-D velocity fields from the CIFT data. The feasibility of using CIFT in a control loop similarly to UDV will be analysed.

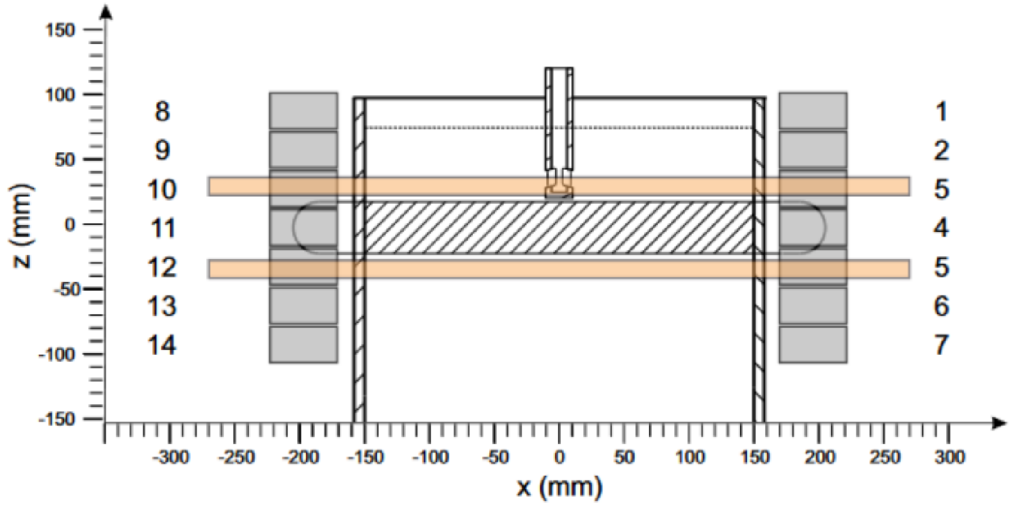

Figure 6.1. Mini-LIMMCAST setup showing the placement of CIFT sensors and the two excitation coils of the EMBr

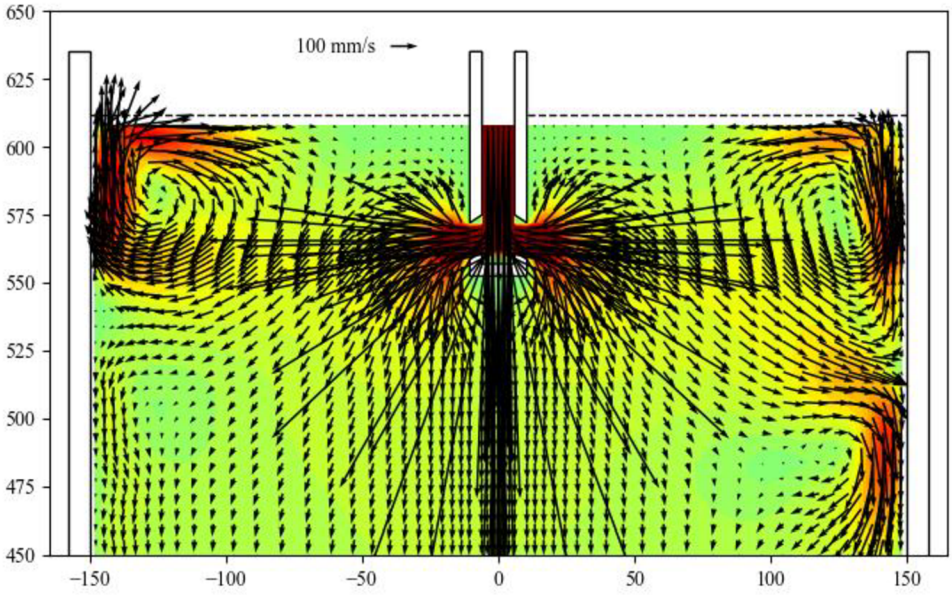

Figure 6.2. Reconstructed velocity profile from CIFT showing a double roll flow in the mould

6.1. Parametrization of Jet Angle from Velocity Profile

The previous section illustrates how we are able to obtain similar velocity profiles to the UDV measurements in Chapter 5. The next step is to investigate whether we are able to obtain the exiting jet angle from the velocity profile in order to use it as our controlled variable for our control loop. Again, we are using the jet angle for our controller to avoid deep jet impingement into the mould. Therefore, avoiding the entrapment of slugs and impurities. The actuator used to change the jet angle is the varying magnetic field of the electromagnetic brake (EMBr).

In the case of UDV measurements, we concentrated on the mid-region between the SEN and the narrow face wall. Velocities near the narrow face wall were avoided due to the turbulence affecting the accuracy near the wall. In the case of CIFT, we instead concentrate on the velocities near the narrow phase wall because it is more accurate than the velocities in the mid-region. This is due to the fact that velocities closer to the receiver sensors have a higher accuracy compared to the velocities in the mid-region. By concentrating on the narrow face wall, we are able to identify the impingement point of the jet and correlate this with the jet angle.

The first step of the algorithm is to average the z-axis velocities near the narrow face wall. The change in the sign of the z-axis velocity correlates to the impingement point as we can see in Figure 6.2, the exiting jet impinges upon the wall and splits into two vortexes, one above and one below. Therefore, the change in the sign of the velocity will indicate where the jet has split against the wall. Cubic spline interpolation is used to provide a finer resolution between the sensor positions. In order to track the movement of the jet, we need to track the change in position of the impingement point. During every frame captured by the sensors, the algorithm scans through the velocities near the narrow wall to find the change in impingement point. Based on this the exiting jet angle is calculated by connecting the impingement point with the SEN nozzle. Using this methodology, we avoid using the entire velocity fields measured and instead use a single variable to represent the movement of the jet during the experiments.

6.2. Preliminary Results from CIFT

Figures 6.3 and 6.4 depict the angle of the jet in response to random changes to the EMBr current. Similarly, to section 5.1 the Mini-LIMMCAST setup is run in a continuous experiment. Random current steps are applied to the EMBr to record the full dynamics of the process, while the CIFT sensors measure the induced magnetic field. This induced magnetic field is used to reconstruct the velocity fields, where the angle of the jet is obtained from the impingement point on the narrow face wall. The figures show that it is difficult to conclude a clear relationship between the angle of the jet and the EMBr current. It is expected that the CIFT sensors would not produce equally clear results as UDV because UDV relies on the direct measurements of the ultrasound beams, while CIFT requires an added step of the linear inverse problem to reconstruct. Although the potential of using CIFT for control of the continuous caster is there as we can see in Figure 6.2, the double roll flow can clearly be seen; the accuracy of the reconstruction algorithm requires further improvement due to the effect of the EMBr applied magnetic field. This will be further discussed in section 6.3.

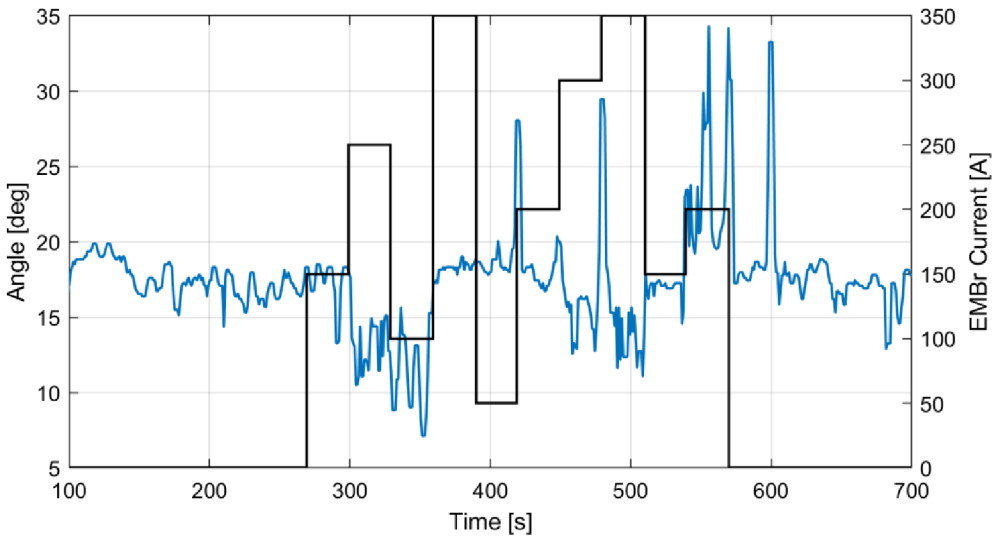

Figure 6.3. Response of jet angle to current changes to the EMBr on left half of mould

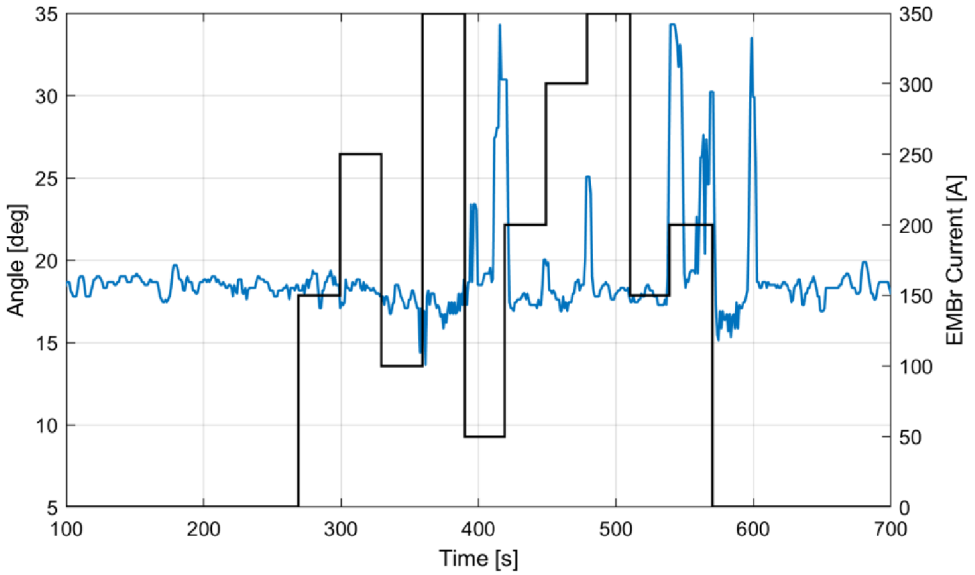

Figure 6.4. Response of jet angle to current changes to the EMBr on right half of mould

6.3. Future Development

The main challenge faced by CIFT in the process of the continuous caster is the applied magnetic field from the EMBr. The EMBr requires large ferromagnetic pole shoes in order to amplify the magnetic field of the brake, which has an effect on the excitation field. Therefore, in order to use the EMBr in a control loop, the magnetic field of the EMBr has to be readjusted accordingly. This can be clearly seen in Figure 6.5 where the author varies the current to the EMBr from 0A to 600A, and then back to 0A for several measurements. The author records the mean value change of the flow induced magnetic field at each current step for sensor 11. The y-axis depicts the starting current value, while the x-axis depicts the end current value. We can see here that going from one current level to another does not result in the same mean value of flow induced magnetic field as in the opposite direction of the current change (going from 0 to 50A results in a different value compared to 50 to 0A).

From these experimental results we can also assume that random current changes would result in larger discrepancies in the flow induced magnetic field. The main reason for this is due to the ferromagnetic parts of the EMBr which results in magnetic hysteresis. Figures 6.3 and 6.4 illustrate partially this issue with the spikes in jet angle occurring at some of the current change. This complicates the process of developing a controller as we would need to compensate for various current level changes in order to avoid constraining our controller to specific current level changes.

In the end, CIFT has the potential to be used in a control loop similarly to UDV. The flow structures in the mould have been successfully reconstructed by solving the linear inverse problem. The challenge occurs with introducing changes to the EMBr current. Therefore, the next step would be to create a model to compensate the effects of the EMBr on the measurements and produce the correct measured flow induced magnetic field. This model with the CIFT setup would be used for controller similarly done in section 5.1 with UDV sensor. The benefit of CIFT is that we are able to obtain even more richer information on the flow structures of the mould and utilise this information for both modelling the process and designing the controller.

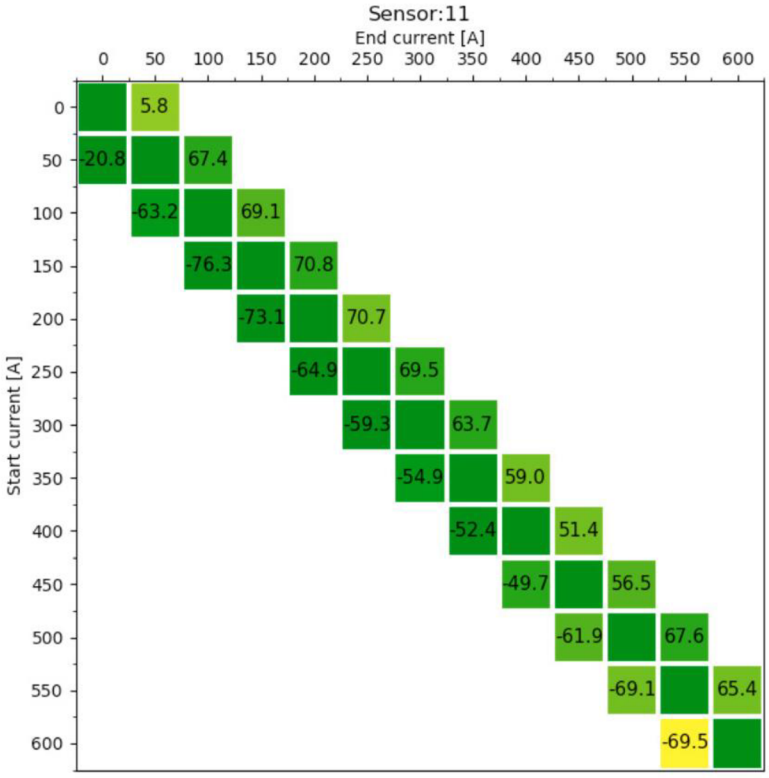

Figure 6.5. Mean value of flow induced magnetic field for transition from one current to another [85]

7. Summary and Conclusion

The general objective of this doctoral thesis was to use two-dimensional flow monitoring in a control loop to improve the control of a continuous caster. This objective was motivated by the fact that many of the quality issues occurring in the end product of the continuous casting process are related to the flow patterns in the mould. By utilizing two-dimensional flow monitoring, we can obtain information on the flow structure in the mould in a non-invasive manner. The control action can then be more direct than in the case of the conventional control based on indirect indicators like the fluctuations of the mould level. This thesis mainly used ultrasound Doppler Velocimetry (UDV) as the two-dimensional flow sensor. In order to create the process model, both computational fluid dynamics (CFD) and system identification were used.

Chapter 4 has shown the difficulty faced with using physical equations to create a model for our controller. Modelling the interaction between the liquid steel in the mould and the EMBr requires a PDE model because of the spatial dependence of the variables. Navier Stokes equation with Lorentz force was implemented using COMSOL to model the effect of the magnetic field of the EMBr on the liquid steel. The complexity of the system, including the turbulent flow in the mould, meant that the number of degrees of freedom of the model could only be decreased to around 50,000. Less than this would not allow for the resolving of the PDE equations. This resulted in a model whose order would be too high to be used for model-based control. Furthermore, due to the limited number of available actuators, the system would end up being highly uncontrollable. For these reasons, the answer to the question of whether the space-discretized CFD model can be used for control is clearly negative in the case of the continuous casting process. Although this modelling approach has been used to build control-oriented models of some simpler processes in the literature, this is definitely not the way to go in the case of the continuous casting process.

For this reason, it was necessary to look for a more viable modelling alternative. This alternative was found in Chapter 5, where the objective of creating a process model was achieved through system identification using data coming from UDV. The Mini-LIMMCAST setup allowed us to obtain experimental data from the sensors and use them to create the models needed for control design and model-based control. However,

multivariable measurements from UDV sensors could not be used directly for identification because they cannot be considered controlled variables for which set points can be specified. It was necessary to find appropriate quantitative flow characteristics that could be used as controlled variables for efficient closed-loop control.

At first, we considered EMBr as a manipulated variable, which means there should be just one controlled variable. The exiting jet angle was proposed as a first quantitative characteristic that could be used as a single controlled variable. Experimental data from the Mini-LIMMCAST setup was used to create a transfer function describing the relationship between the EMBr and the angle of the jet. An MPC was designed to control this angle and keep it within optimum ranges under disturbance. This idea was extended in section 5.1.2. by using experimental data from a clogged SEN to design an algorithm that would detect SEN clogging by analyzing the oscillations of the jet angle. This information was then used to create a switched MPC that could control the system whether there was clogging or not in the SEN.

An alternative characteristic was investigated in section 5.2, where meniscus velocity was used as a variable controllable by the EMBr. In this case, it was found by analyzing the experimental data that the dynamic relationship between EMBr and meniscus velocity is nonlinear. For this reason, a NARX neural network had to be employed to describe the relationship, and adaptive MPC had to be developed instead of standard MPC based on one fixed model. It has turned out that this adaptive MPC can cope with the system's nonlinearities successfully without violating the process constraints.

Lastly, in section 5.3, the control was extended to the multivariable case by introducing the stopper rod position as another manipulated variable besides the EMBr. The investigation has shown that jet impingement point and jet velocity are the most suitable controllable flow characteristics in the case of this two-input, two-output control configuration. Similarly, as in the case of single-input, single-output control configuration, system identification was used to obtain the control-oriented model. A fourth-order discrete state-space model described the deterministic component of the process response with sufficient precision. However, there was also a significant unmodelled stochastic component resulting from the turbulent flow. Despite this, the model was precise enough to be used as a part of the model-based predictive controller, which could track both set-

points without exceeding any constraints. In this way, optimal flow structures in the mould could be achieved.

In the end, it can be stated that several characteristics can be extracted from the UDV measured velocity profiles in the region surrounding the SEN in the mould. These characteristics can be used by model-based controllers in single-variable or two-variable configurations to adjust the flow structure in the mould according to the specified set points. The techniques used for control loop design can be extended to other sensors based on multidimensional measurement data if similar information on the velocity fields of the mould is obtained. In Chapter 6, we attempted to extend these techniques to CIFT, where we used the velocity profile to obtain the exiting jet angle. Although CIFT is able to reconstruct the flow structures in the mould successfully, an issue occurs when introducing changes to the EMBr current. The main reason for this is the effect of the EMBr magnetic field and especially of the magnetic hysteresis associated with the ferromagnetic parts of the EMBr on CIFT measurements. It is possible to build a model of these hysteretic effects and compensate for them. CIFT can then be utilized in a control loop similarly to UDV. However, correct compensation for continuous-valued EMBr current (and not only for one or several discrete values of this current) remains still an open research problem.

Despite these remaining issues, it can be stated in conclusion that it has been shown that two-dimensional flow monitoring can be utilized in a control loop to control the flow structure in the mould of a continuous caster. The first objective of creating a process model was achieved mainly through system identification. Furthermore, by quantifying flow characteristics using the exiting jet, meniscus velocity, jet impingement point, and jet velocity, we could achieve our next objective of identifying characteristics that can be utilized as controlled variables for optimizing the flow in the mould. Lastly, through designing and testing various control strategies, we can achieve our third major objective of developing controllers using the necessary quantitative flow characteristics.

An interesting objective for future work would be to introduce more complex actuators to the process to achieve even better control over the flow in the mould. An example of this can be an electromagnetic stirrer that creates a rotating magnetic induction field and corresponding electromagnetic force applied to the steel liquid. The combined actuators can potentially allow us to optimize the flow patterns on both sides of the mould.

References

[1] D. Schurmann, I. Glavinic, B. Willers, K. Timmel, and S. Eckert, "Impact of the Electromagnetic Brake Position on the Flow Structure in a Slab Continuous Casting Mold: An Experimental Parameter Study," Metall. Mater. Trans. B, vol. 51, Nov. 2019, doi: 10.1007/s11663-019-01721-x.

[2] S. Louhenkilpi, "Chapter 1.8 - Continuous Casting of Steel," in Treatise on Process Metallurgy, S. Seetharaman, Ed. Boston: Elsevier, 2014, pp. 373–434. doi: 10.1016/B978-0-08-096988-6.00007-9.

[3] I. K. Craig, F. R. Camisani-Calzolari, and P. C. Pistorius, "A contemplative stance on the automation of continuous casting in steel processing," Control Eng. Pract., p. 8, 2001.

[4] B. G. Thomas, "Review on Modeling and Simulation of Continuous Casting," Steel Res. Int., vol. 89, no. 1, p. 1700312, Jan. 2018, doi: 10.1002/srin.201700312.

[5] B. G. Thomas, "On-line Detection of Quality Problems in Continuous Casting of Steel," p. 16, 2003.

[6] R. Liu, B. G. Thomas, J. Sengupta, S. D. Chung, and M. Trinh, "Measurements of Molten Steel Surface Velocity and Effect of Stopper-rod Movement on Transient Multiphase Fluid Flow in Continuous Casting," ISIJ Int., vol. 54, no. 10, pp. 2314–2323, Oct. 2014, doi: 10.2355/isijinternational.54.2314.

[7] K. Cukierski and B. G. Thomas, "Flow Control with Local Electromagnetic Braking in Continuous Casting of Steel Slabs," Metall. Mater. Trans. B, vol. 39, no. 1, pp. 94–107, Feb. 2008, doi: 10.1007/s11663-007-9109-3.

[8] H. L. Gerber, "Electromagnetic Processing of Liquid Steel," IEEE Trans. Ind. Appl., vol. 33, no. 3, p. 6, 1997.

[9] P. Gardin, J.-M. Galpin, M.-C. Regnier, and J.-P. Radot, "Liquid steel flow control inside continuous casting mold using a static magnetic field," IEEE Trans. Magn., vol. 31, no. 3, pp. 2088–2091, May 1995, doi: 10.1109/20.376456.

[10] L. Zhang, S. Yang, K. Cai, J. Li, X. Wan, and B. G. Thomas, "Investigation of Fluid Flow and Steel Cleanliness in the Continuous Casting Strand," Metall. Mater. Trans. B, vol. 38, no. 1, pp. 63–83, Apr. 2007, doi: 10.1007/s11663-006-9007-0.

[11] B. G. Thomas, “Modeling of the continuous casting of steel—past, present, and future,” Metall. Mater. Trans. B, vol. 33, no. 6, pp. 795–812, Dec. 2002, doi: 10.1007/s11663-002-0063-9.

[12] Thomas, Brian G, “Application of Mathematical Models to the Continuous Slab Casting Mold,” Iron Steelmak..

[13] H. Kitada, O. Kondo, H. Kusachi, and K. Sasame, “H Control of Molten Steel Level in Continuous Caster,” IEEE Trans. CONTROL Syst. Technol., vol. 6, no. 2, p. 8, 1998.

[14] L. Smutný, R. Farana, A. Víteĉek, and D. Kaĉmář, “MOULD LEVEL CONTROL FOR THE CONTINUOUS STEEL CASTING,” IFAC Proc. Vol., vol. 38, no. 1, pp. 163–168, 2005, doi: 10.3182/20050703-6-CZ-1902.01706.

[15] Graebe, Goodwin, West, and Stepien, “An application of advanced control to steel casting,” 1994, pp. 1533–1538 vol.3. doi: 10.1109/CCA.1994.381488.

[16] M. Dussud, S. Galichet, and L. P. Foulloy, “Application of fuzzy logic control for continuous casting mold level control,” IEEE Trans. Control Syst. Technol., vol. 6, no. 2, pp. 246–256, Mar. 1998, doi: 10.1109/87.664191.

[17] G. G. Yero, M. R. Mendoza, and P. Albertos, “Robust nonlinear adaptive mould level control for steel continuous casting,” IFAC-Pap., vol. 51, no. 25, pp. 164–170, Jan. 2018, doi: 10.1016/j.ifacol.2018.11.099.

[18] C. Furtmüller, P. Colaneri, and L. del Re, “Adaptive robust stabilization of continuous casting,” Automatica, vol. 48, no. 1, pp. 225–232, Jan. 2012, doi: 10.1016/j.automatica.2011.09.049.

[19] J. S. Ha, J. R. Cho, B. Y. Lee, and M. Y. Ha, “Numerical analysis of secondary cooling and bulging in the continuous casting of slabs,” J. Mater. Process. Technol., vol. 113, no. 1, pp. 257–261, Jun. 2001, doi: 10.1016/S0924-0136(01)00654-9.

[20] R. Guan, C. Ji, C. Wu, and M. Zhu, “Numerical modelling of fluid flow and macrosegregation in a continuous casting slab with asymmetrical bulging and mechanical reduction,” Int. J. Heat Mass Transf., vol. 141, pp. 503–516, Oct. 2019, doi: 10.1016/j.ijheatmasstransfer.2019.06.079.

[21] M. Kim, S. Moon, C. Na, D. Lee, Y. Kueon, and J. S. Lee, "Control of mold level in continuous casting based on a disturbance observer," J. Process Control, vol. 21, no. 7, pp. 1022–1029, Aug. 2011, doi: 10.1016/j.jprocont.2011.06.003.

[22] C. Furtmueller and L. del Re, "Disturbance suppression for an industrial level control system with uncertain input delay and uncertain gain," in 2006 IEEE Conference on Computer Aided Control System Design, 2006 IEEE International Conference on Control Applications, 2006 IEEE International Symposium on Intelligent Control, Oct. 2006, pp. 3206–3211. doi: 10.1109/CACSD-CCA-ISIC.2006.4777151.

[23] K. Jabri, E. Godoy, D. Dumur, A. Mouchette, and B. Bèle, "Cancellation of bulging effect on mould level in continuous casting: Experimental validation," J. Process Control, vol. 21, no. 2, pp. 271–278, Feb. 2011, doi: 10.1016/j.jprocont.2010.10.020.

[24] K. Jabri, B. Bele, A. Mouchette, D. Dumur, and E. Godoy, "Suppression of periodic disturbances in the continuous casting process," in 2008 IEEE International Conference on Control Applications, Sep. 2008, pp. 91–96. doi: 10.1109/CCA.2008.4629617.

[25] Y. Feng, M. Wu, X. Chen, L. Chen, and S. Du, "A fuzzy PID controller with nonlinear compensation term for mold level of continuous casting process," Inf. Sci., vol. 539, pp. 487–503, Oct. 2020, doi: 10.1016/j.ins.2020.06.024.

[26] K. Jabri, D. Dumur, E. Godoy, A. Mouchette, and B. Bèle, "Particle swarm optimization based tuning of a modified smith predictor for mould level control in continuous casting," J. Process Control, vol. 21, no. 2, pp. 263–270, Feb. 2011, doi: 10.1016/j.jprocont.2010.10.019.

[27] J. Zhang, D. Chen, S. Wang, and M. Long, "Compensation Control Model of Superheat and Cooling Water Temperature for Secondary Cooling of Continuous Casting," Steel Res. Int., vol. 82, no. 3, pp. 213–221, 2011, doi: 10.1002/srin.201000148.

[28] J. Ma, Z. Xie, and G. Jia, "Applying of Real-time Heat Transfer and Solidification Model on the Dynamic Control System of Billet Continuous Casting," ISIJ Int., vol. 48, no. 12, pp. 1722–1727, 2008, doi: 10.2355/isijinternational.48.1722.

[29] Y. Wang, D. Li, Y. Peng, and L. Zhu, "Computational modeling and control system of continuous casting process," Int. J. Adv. Manuf. Technol., vol. 33, no. 1–2, pp. 1–6, May 2007, doi: 10.1007/s00170-006-0451-4.

[30] C. Belavý, G. Hulkó, L. Bartalský, and M. Kubiš, "Robust Control of Temperature Fields in Steel Casting Mould as Distributed Parameter Systems," IFAC-Pap., vol. 48, no. 14, pp. 408–413, Jan. 2015, doi: 10.1016/j.ifacol.2015.09.491.

[31] G. Hulkó, K. Ondrejkovič, P. Buček, and M. Bartko, "Software sensor as distributed parameter system for the control of secondary cooling in the continuous casting of steel," IFAC-Pap., vol. 49, no. 20, pp. 49–54, 2016, doi: 10.1016/j.ifacol.2016.10.095.

[32] B. Petrus, K. Zheng, X. Zhou, B. G. Thomas, and J. Bentsman, "Real-Time, Model-Based Spray-Cooling Control System for Steel Continuous Casting," Metall. Mater. Trans. B, vol. 42, no. 1, pp. 87–103, Feb. 2011, doi: 10.1007/s11663-010-9452-7.

[33] T. Mauder, C. Sandera, and J. Stetina, "Optimal Control Algorithm for Continuous Casting Process by Using Fuzzy Logic," Steel Res. Int., vol. 86, no. 7, pp. 785–798, 2015, doi: 10.1002/srin.201400213.

[34] A. V. Lotov, G. K. Kamenev, V. E. Berezkin, and K. Miettinen, "Optimal control of cooling process in continuous casting of steel using a visualization-based multi-criteria approach," Appl. Math. Model., vol. 29, no. 7, pp. 653–672, Jul. 2005, doi: 10.1016/j.apm.2004.10.009.

[35] G. W. Song et al., "Temperature Control Optimization in a Steel-Making Continuous Casting Process Using a Multimodal Deep Learning Approach," Steel Res. Int., vol. 90, no. 12, p. 1900321, 2019, doi: 10.1002/srin.201900321.

[36] D. Xie, Z. Huang, H. Ji, and H. Li, "An Online Flow Pattern Identification System for Gas amp;#8211;Oil Two-Phase Flow Using Electrical Capacitance Tomography," IEEE Trans. Instrum. Meas., vol. 55, no. 5, pp. 1833–1838, Oct. 2006, doi: 10.1109/TIM.2006.881558.

[37] T. Dyakowski, L. F. C. Jeanmeure, and A. J. Jaworski, "Applications of electrical tomography for gas–solids and liquid–solids flows — a review," Powder Technol., vol. 112, no. 3, pp. 174–192, Oct. 2000, doi: 10.1016/S0032-5910(00)00292-8.

[38] D. Zhao et al., "The control and maintenance of desired flow patterns in bends of different orientations," Flow Meas. Instrum., vol. 53, pp. 230–242, Mar. 2017, doi: 10.1016/j.flowmeasinst.2016.09.003.

[39] Y. Zhang and X. Ai, "The Identification of Two-Phase Flow Regimes Using HMM Model Based on ERT System and PCA Feature Extraction," in 2014 Fifth

International Conference on Intelligent Systems Design and Engineering Applications, Jun. 2014, pp. 1053–1055. doi: 10.1109/ISDEA.2014.232.

[40] P. D. Christofides, "Control of nonlinear distributed process systems: Recent developments and challenges," AIChE J., vol. 47, no. 3, pp. 514–518, 2001, doi: 10.1002/aic.690470302.

[41] J. A. Villegas, S. R. Duncan, H. G. Wang, W. Q. Yang, and R. S. Raghavan, "Distributed parameter control of a batch fluidised bed dryer," Control Eng. Pract., vol. 17, no. 9, pp. 1096–1106, Sep. 2009, doi: 10.1016/j.conengprac.2009.04.012.

[42] P. V. S. Ponnapalli, D. Benchebra, R. Deloughry, and I. Ibrahim, "Application of an ANN-based Controller for the Control of Pneumatic Conveyed Polypropylene Pellet Flow," p. 6.

[43] A. Seppänen, "State Estimation in Process Tomography PhD thesis."

[44] D. Sbarbaro and S. Vergara, "Design of a control system based on EIT sensors: An optimization based approach," IFAC-Pap., vol. 48, no. 25, pp. 218–222, 2015, doi: 10.1016/j.ifacol.2015.11.089.

[45] M. Soleimani, W. R. B. Lionheart, and A. J. Peyton, "Image Reconstruction for High-Contrast Conductivity Imaging in Mutual Induction Tomography for Industrial Applications," IEEE Trans. Instrum. Meas., vol. 56, no. 5, pp. 2024–2032, Oct. 2007, doi: 10.1109/TIM.2007.895598.

[46] S. F. A. Bukhari, W. Yang, and H. McCann, "A Hybrid Control Strategy for Oil Separators Based on Electrical Capacitance Tomography Images," Meas. Control, vol. 40, no. 7, pp. 211–217, Sep. 2007, doi: 10.1177/002029400704000703.

[47] J. A. Gutierrez-Gnecchi and E. Marroquín-Pineda, "Control of a Pilot-Scale, Solid-Liquid Separation Plant Using Electrical Impedance Tomography Measurements," Part. Part. Syst. Charact., vol. 25, no. 4, pp. 306–313, doi: 10.1002/ppsc.200800034.

[48] B. G. Thomas and S. M. Cho, "Overview of Electromagnetic Forces to Control Flow During Continuous Casting of Steel," IOP Conf. Ser. Mater. Sci. Eng., vol. 424, p. 012027, Oct. 2018, doi: 10.1088/1757-899X/424/1/012027.

[49] B. G. Thomas and R. Chaudhary, "State of the Art in Electromagnetic Flow Control in Continuous Casting of Steel Slabs: Modeling and Plant Validation," p. 6, 2009.

[50] L. B. Trindade, J. E. A. Nadalon, A. C. Contini, and R. C. Barroso, “Modeling of Solidification in Continuous Casting Round Billet with Mold Electromagnetic Stirring (M-EMS),” Steel Res. Int., vol. 88, no. 4, p. 1600319, 2017, doi: 10.1002/srin.201600319.

[51] Y. Haiqi, W. Baofeng, L. Huiqin, and L. Jianchao, “Influence of electromagnetic brake on flow field of liquid steel in the slab continuous casting mold,” J. Mater. Process. Technol., vol. 202, no. 1–3, pp. 179–187, Jun. 2008, doi: 10.1016/j.jmatprotec.2007.08.054.

[52] A. Maurya and P. K. Jha, “Influence of electromagnetic stirrer position on fluid flow and solidification in continuous casting mold,” Appl. Math. Model., vol. 48, pp. 736–748, Aug. 2017, doi: 10.1016/j.apm.2017.02.029.

[53] K. Dekemele, C.-M. Ionescu, M. De Doncker, and R. De Keyser, “Closed loop control of an electromagnetic stirrer in the continuous casting process,” Jun. 2016, pp. 61–66. doi: 10.1109/ECC.2016.7810264.

[54] H. Wang, G. Li, Y. Lei, Y. Zhao, Q. Dai, and J. Wang, “Mathematical Heat Transfer Model Research for the Improvement of Continuous Casting Slab Temperature,” ISIJ Int., vol. 45, no. 9, pp. 1291–1296, 2005, doi: 10.2355/isijinternational.45.1291.

[55] M. Janik and H. Dyja, “Modelling of three-dimensional temperature field inside the mould during continuous casting of steel,” J. Mater. Process. Technol., vol. 157–158, pp. 177–182, Dec. 2004, doi: 10.1016/j.jmatprotec.2004.09.026.

[56] K. Jin, S. P. Vanka, and B. G. Thomas, “Large Eddy Simulations of Electromagnetic Braking Effects on Argon Bubble Transport and Capture in a Steel Continuous Casting Mold,” Metall. Mater. Trans. B, vol. 49, no. 3, pp. 1360–1377, Jun. 2018, doi: 10.1007/s11663-018-1191-1.

[57] B. G. Thomas, Q. Yuan, S. Mahmood, R. Liu, and R. Chaudhary, “Transport and Entrapment of Particles in Steel Continuous Casting,” Metall. Mater. Trans. B, vol. 45, no. 1, pp. 22–35, Feb. 2014, doi: 10.1007/s11663-013-9916-7.

[58] B. G. Thomas, A. Dennisov, and H. Bai, “Behavior of argon bubbles during continuous casting of steel," 80th Steelmaking Conference,” in Iron and Steel Society/AIME, 410 Commonwealth Drive, Warrendale, PA, 1997, pp. 375–384.

[59] C. Pfeiler, M. Wu, and A. Ludwig, “Influence of argon gas bubbles and non-metallic inclusions on the flow behavior in steel continuous casting,” Mater. Sci. Eng. A, vol. 413–414, pp. 115–120, Dec. 2005, doi: 10.1016/j.msea.2005.08.178.

[60] W. Chen, Y. Ren, L. Zhang, and P. R. Scheller, “Numerical Simulation of Steel and Argon Gas Two-Phase Flow in Continuous Casting Using LES + VOF + DPM Model,” JOM, vol. 71, no. 3, pp. 1158–1168, Mar. 2019, doi: 10.1007/s11837-018-3255-8.

[61] N. Kubo, T. Ishii, J. Kubota, and N. Aramaki, “Two-phase Flow Numerical Simulation of Molten Steel and Argon Gas in a Continuous Casting Mold,” ISIJ Int., vol. 42, no. 11, pp. 1251–1258, 2002, doi: 10.2355/isijinternational.42.1251.

[62] H. Yu and M. Zhu, “Numerical Simulation of the Effects of Electromagnetic Brake and Argon Gas Injection on the Three-dimensional Multiphase Flow and Heat Transfer in Slab Continuous Casting Mold,” ISIJ Int., vol. 48, no. 5, pp. 584–591, 2008, doi: 10.2355/isijinternational.48.584.

[63] B. Li and F. Tsukihashi, “Numerical Estimation of the Effect of the Magnetic Field Application on the Motion of Inclusion in Continuous Casting of Steel,” ISIJ Int., vol. 43, no. 6, pp. 923–931, 2003, doi: 10.2355/isijinternational.43.923.

[64] M. Ratajczak, T. Wondrak, and F. Stefani, “A gradiometric version of contactless inductive flow tomography: theory and first applications,” Philos. Trans. R. Soc. Math. Phys. Eng. Sci., vol. 374, no. 2070, p. 20150330, Jun. 2016, doi: 10.1098/rsta.2015.0330.

[65] A. Kaasinen, “Optimal control in process tomography,” University of Eastern Finland, Kuopio, 2013.

[66] A. Blishchik, M. van der Lans, and S. Kenjereš, “An extensive numerical benchmark of the various magnetohydrodynamic flows,” Int. J. Heat Fluid Flow, vol. 90, p. 108800, Aug. 2021, doi: 10.1016/j.ijheatfluidflow.2021.108800.

[67] M. Hosseini, A. Kaasinen, G. Link, T. Lähivaara, and M. Vauhkonen, “LQR Control of Moisture Distribution in Microwave Drying Process Based on a Finite Element Model of Parabolic PDEs,” IFAC-Pap., vol. 53, no. 2, pp. 11470–11476, Jan. 2020, doi: 10.1016/j.ifacol.2020.12.586.

[68] S.-M. Cho et al., “Effect of nozzle clogging on surface flow and vortex formation in the continuous casting mold,” Iron Steel Technol., vol. 9, pp. 85–95, 2012.

[69] X. Deng et al., “Flow pattern control in continuous slab casting moulds: physical modelling and plant trials,” Ironmak. Steelmak., vol. 44, no. 6, pp. 461–471, Jul. 2017, doi: 10.1080/03019233.2016.1215666.

[70] S. Abouelazayem, I. Glavinić, T. Wondrak, and J. Hlava, “Control of Jet Flow Angle in Continuous Casting Process using an Electromagnetic Brake,” IFAC-Pap., vol. 52, no. 14, pp. 88–93, Jan. 2019, doi: 10.1016/j.ifacol.2019.09.169.

[71] S. Abouelazayem, I. Glavinić, T. Wondrak, and J. Hlava, “Switched MPC Based on Clogging Detection in Continuous Casting Process,” IFAC-Pap., vol. 53, no. 2, pp. 11491–11496, Jan. 2020, doi: 10.1016/j.ifacol.2020.12.589.

[72] H. Bai and B. G. Thomas, “Effects of clogging, argon injection, and continuous casting conditions on flow and air aspiration in submerged entry nozzles,” Metall. Mater. Trans. B, vol. 32, no. 4, pp. 707–722, Aug. 2001, doi: 10.1007/s11663-001-0125-4.

[73] R. Isermann and M. Münchhof, “Correlation Analysis with Continuous Time Models,” in Identification of Dynamic Systems: An Introduction with Applications, R. Isermann and M. Münchhof, Eds. Berlin, Heidelberg: Springer, 2011, pp. 149–178. doi: 10.1007/978-3-540-78879-9_6.

[74] “What Is a Process Model? - MATLAB & Simulink - MathWorks United Kingdom.” https://uk.mathworks.com/help/ident/ug/what-is-a-process-model.html (accessed Dec. 06, 2021).

[75] H. Barati, M. Wu, A. Kharicha, and A. Ludwig, “A transient model for nozzle clogging,” Powder Technol., vol. 329, Feb. 2018, doi: 10.1016/j.powtec.2018.01.053.

[76] M. Soliman, O. Malik, and D. Westwick, “Multiple model MIMO predictive control for variable speed variable pitch wind turbines,” Proc. 2010 Am. Control Conf., 2010, doi: 10.1109/ACC.2010.5531355.

[77] A. P. Wiese, M. Blom, C. Manzie, M. Brear, and A. Kitchener, “Model reduction and MIMO model predictive control of gas turbine systems,” 2015, doi: 10.1016/J.CONENGPRAC.2015.09.015.

[78] M. Tanaskovic, L. Fagiano, and V. Gligorovski, “Adaptive model predictive control for linear time varying MIMO systems,” Automatica, vol. 105, pp. 237–245, Jul. 2019, doi: 10.1016/j.automatica.2019.03.030.

[79] “Optimization Problem - MATLAB & Simulink - MathWorks United Kingdom.” https://uk.mathworks.com/help/mpc/ug/optimization-problem.html (accessed Dec. 10, 2021).

[80] R. Aguilera, P. Lezana Illesca, and D. Quevedo, “Switched Model Predictive Control for Improved Transient and Steady-State Performance,” Ind. Inform. IEEE Trans. On, vol. 11, pp. 968–977, Aug. 2015, doi: 10.1109/TII.2015.2449992.

[81] L. Zhang and R. D. Braatz, “On switched MPC of a class of switched linear systems with modal dwell time,” in 52nd IEEE Conference on Decision and Control, Dec. 2013, pp. 91–96. doi: 10.1109/CDC.2013.6759864.

[82] S. Abouelazayem, I. Glavinic, T. Wondrak, and J. Hlava, “Adaptive Control of Meniscus Velocity in Continuous Caster based on NARX Neural Network Model,” IFAC-Pap., vol. 52, pp. 222–227, Jan. 2019, doi: 10.1016/j.ifacol.2019.12.653.

[83] “Recursive Algorithms for Online Parameter Estimation - MATLAB & Simulink - MathWorks United Kingdom.” https://uk.mathworks.com/help/ident/ug/algorithms-for-online-estimation.html#buagqe2-1 (accessed Dec. 15, 2021).

[84] S. Abouelazayem, I. Glavinić, T. Wondrak, and J. Hlava, “Flow Control Based on Feature Extraction in Continuous Casting Process,” Sensors, vol. 20, no. 23, Art. no. 23, Jan. 2020, doi: 10.3390/s20236880.

[85] I. Glavinić, M. Ratajczak, F. Stefani, and T. Wondrak, “Flow monitoring for continuous steel casting using Contactless Inductive Flow Tomography (CIFT),” IFAC-Pap., vol. 53, no. 2, pp. 11477–11482, Jan. 2020, doi: 10.1016/j.ifacol.2020.12.587.

[86] F. Stefani, T. Gundrum, and G. Gerbeth, “Contactless inductive flow tomography.,” Phys. Rev. E Stat. Nonlin. Soft Matter Phys., 2004, doi: 10.1103/PhysRevE.70.056306.

List of Publications

S. Abouelazayem, I. Glavinić, T. Wondrak, and J. Hlava, “Flow Control Based on Feature Extraction in Continuous Casting Process,” Sensors, vol. 20, no. 23, p. 6880, Dec. 2020.

S. Abouelazayem, I. Glavinić, T. Wondrak, and J. Hlava, “Switched MPC based on clogging detection in continuous casting process,” IFAC-PapersOnLine, vol. 53, no. 2, pp. 11491–11496, 2020.

S. Abouelazayem, I. Glavinić, T. Wondrak and J. Hlava, "Adaptive Control of Meniscus Velocity in Continuous Caster based on NARX Neural Network Model", IFAC-PapersOnLine, vol. 52, no. 29, pp. 222-227, 2019.

S. Abouelazayem, I. Glavinić, T. Wondrak and J. Hlava, "Control of Jet Flow Angle in Continuous Casting Process using an Electromagnetic Brake", IFAC-PapersOnLine, vol. 52, no. 14, pp. 88-93, 2019.

J. Hlava and **S. Abouelazayem**, “Control systems with tomographic sensors—a review,” Sensors, vol. 22, no. 8, p. 2847, 2022.

I. Glavinić, I. Muttakin, **S. Abouelazayem**, A. Blishchik, F. Stefani, S. Eckert, M. Soleimani, I. Saidani, J. Hlava, S. Kenjereš, and T. Wondrak, “Laboratory investigation of tomography-controlled continuous steel casting,” Sensors, vol. 22, no. 6, p. 2195, 2022.

I. Glavinić, **S. Abouelazayem**, M. Ratajczak, D. Schurmann, S. Eckert, F. Stefani, J. Hlava, and T. Wondrak, “Flow Control in the Model of a Continuous Caster by Using Contactless Inductive Flow Tomography,” Materials Processing Fundamentals 2019 The Minerals, Metals & Materials Series, pp. 49–58, 2019.

T. Wondrak, U. Hampel, M. Ratajczak, I. Glavinic, F. Stefani, S. Eckert, D. V. D. Plas, P. Pennerstorfer, I. Muttakin, M. Soleimani, **S. Abouelazayem**, J. Hlava, A. Blishchik, and S. Kenjeres, “Real-time control of the mould flow in a model of continuous casting in frame of the TOMOCON project,” IOP Conference Series: Materials Science and Engineering, vol. 424, p. 012003, 2018.

Curriculum Vitae

Shereen Abouelazayem received her BSc in Electronics and Communications Engineering from the American University in Cairo in 2015. She received her MSc in Electrical Engineering in the University of Strathclyde in Glasgow. Her MSc thesis was titled "Multi-Loop PID Tuning for Quadruple Tank System." Before pursuing her PhD, Shereen worked in Vodafone Egypt as a Network Engineer from 2017 to 2018.

In 2018, Shereen was accepted to a European Training Network under the Marie-Curie Actions. The project is under the name "Smart tomographic sensors for advanced industrial process control (TOMOCON)". Shereen's PhD concentrated on the control of the continuous casting process using two-dimensional flow field measurements. As part of her PhD program, Shereen has undergone training in the following universities and companies: Chalmers University of Technology, Primetals Technologies, University of East Finland, and Tata Steel. Shereen is the author of six papers in SCOPUS indexed conference proceedings and three journal paper indexed in ISI Web of Science.